SYSTEM IDENTIFICATION AND CONTROL OF MAGNETIC BEARING SYSTEMS

by

Fitriah Abdul Somad

A thesis submitted in fulfillment of
the requirement for the degree of

Master of Engineering
(by Research)

2007

School of Electrical Engineering
Victoria University

ABSTRACT

This thesis presents investigations aimed at obtaining a system model for the stabilisation of an Active Magnetic Bearing (AMB) System. Furthermore, the study reported here set out to design both conventional and advanced controllers based on the system model.

This research report demonstrates that the literature on AMBs shows that AMBs are making their mark in the industry; they are increasingly being used in applications including jet engines, compressors, pumps and flywheel systems. In this study, it has also been observed that the basic design of AMBs is an arrangement of electromagnets placed equidistant in a ring round a rotor. The point of departure for this study is that AMBs are highly nonlinear and inherently unstable. Hence, the need for an automatic control to keep the system stabilized.

The first step of the research was to determine the transfer function of the MBC 500 magnetic bearing system both analytically and experimentally. An analytical model has been derived based on principle of physics. As the AMB system under analysis is inherently unstable, it was necessary to identify the model using a closed-loop system identification. Frequency response data has been collected using the two-step closed-loop system identification. As there are resonant modes in the MBC 500 magnetic bearing system, the system identification approach has identified the corresponding resonant frequencies. Subsequent to obtaining the model, a conventional controller was designed to stabilise the AMB system. Two notch filters were designed to deal with the magnitude and phase fluctuations around the two dominant resonant frequencies. The

designed conventional controller and notch filters have been implemented using MATLAB, SIMULINK and dSPACE DS1102 digital signal processing (DSP) card. Both the step response and robustness tests have demonstrated the effectiveness of the conventional controller and notch filters designed.

A significant conclusion has been drawn when designing the conventional controller. It was found that a controller that had a large positive phase angle had a negative effect on the system. This finding was very significant because it restricted the controller specifications and yielded an optimum lead angle for the conventional controller.

The advanced PD-like Fuzzy Logic Controller (FLC) has also been designed for AMB system stabilisation. The designed FLC can deal with the magnitude and phase fluctuations around resonant frequencies without using notch filters. The performance of the designed FLC has been evaluated via simulation. Simulation results show that the FLC designed leads to a reliable system performance. Comparison studies of the FLC performances with two different sets of rules, two different inference methods, different membership functions, different *t*-norm and *s*-norm operations, and different defuzzification were investigated. To further improve system performance, scaling factors were tuned. Again, simulations showed highly promising results.

Comparative studies between the conventional and advanced fuzzy control methods were also carried out. Advantages and disadvantages of both approaches have been summarised. The thesis has also suggested further research work in the control of AMBs.

DECLARATION

"I, Fitriah Abdul Somad, declare that the Master by Research thesis entitled **System Identification and Control of Magnetic Bearing Systems** is no more than 60,000 words in length, exclusive of tables, figures, appendices, references and footnotes. This thesis contains no material that has been submitted previously, in whole or in part, for the award of any other academic degree or diploma. Except where otherwise indicated, this thesis is my own work."

Fitriah Abdul Somad 19 August 2007

ACKNOWLEDGMENTS

Although there is only one author credited on the title page of this thesis, it would never have been completed without the support of many people I have been fortunate to know. The number of years spent at Victoria University in particular in the School of Electrical Engineering has had their low and high points and have been a blessing to have been surrounded by great people with whom to share the moments.

The goal of the master by research program is not only to accomplish research but also to train one as a scientist. In this regard, I give special thanks to Dr Juan Shi whose supervision style and patience have given me the support that has contributed to this goal. She was generous with her time, and I am grateful to her for constantly encouraging me through the research. In addition, she is always approachable.

I also owe a huge debt to the former Head of School of Electrical Engineering, Associate Professor Aladin Zayegh, who introduced me to this research. He was also very helpful when I had a problem regarding my research. Furthermore, I thank Mr Robert Ives and Dr Wee Sit Lee for allowing me to attend their lectures and share their knowledge in control engineering with me.

On the whole, the School of Electrical Engineering has been a very warm and friendly place. I thank Elizabeth Smith and Puspha Richards from the Faculty of Health, Engineering and Science who always helped me when I needed assistance.

I should point out also that I have been fortunate to have benefited from the AusAID scholarship program. I thank Kerry Wright and Esther Newcastle for the patience in helping me cope with my time to study at Victoria University from the beginning stage until I return to my home country. Last but not least, I cannot adequately thank: my parents, H. Abdul Somad and Hj. Andi Aryani; my parents in law, Andi Burhanuddin and Hj. Hamsinah Wahid; my husband, Andi Palantei; all my siblings Meutia Farida-Arul Afandy, Firmansyah-Dewi-Rendra-Erlang and Faiqa Sari Dewi, and all my siblings in law Andi Pattiroi, Andi Tenri Ola and Andi Baso Palinrungi who provided me with their unfailing support and belief in me through the many stages of this candidature process. Their love has been the source and the strength of my life. Palantei has been patient with me in many moments of self-doubt and has spent countless hours during my time in Melbourne. His unfailing love and cheerfulness never failed to brighten up even the most difficult time of thesis-writing days. Words cannot adequately express my gratitude to nor my love for him.

Fitriah Abdul Somad

TABLE OF CONTENTS

LIST OF FIGURES

LIST OF TABLES

LIST OF SYMBOLS

A, B, C and D	State space system matrices
A_{base}	Average magnitude of the resonance response curve
acont, bcont, ccont and dcont	State space system matrices of on-board controllers
A_{peak}	Magnitude at the peak of the resonance response curve
A_r, B_r and C_r	State space system matrices for the rigid body model
C	Magnetic bearing feedback controller
C_{lead1} (s)	Transfer function of the lead compensator
F	Force of horseshoe electromagnets
F_i	Bearing force on the rotor
f_n	Resonant peak frequency
F_x	Net force generated by opposing electromagnets
F_1 and F_2	Forces exerted on the rotor by left and right bearings, respectively
G	Magnetic bearing system model
I	Rotational moment of inertia of the system
$i_{control}$	Control current supplied by the current amplifier
I_0	Moment of inertia of the rotor with respect to rotation about an axis in the y direction
K	*S*tiffness of the rotor
LPF	Low Pass Filter
l	Distance from each bearing to the end of the rotor
L	Total length of the rotor

l_2	Distance from Hall-effect sensor to the end of the rotor
M	Mass of the rotor
N(s)	Notch filter transfer function
n	Noise of magnetic bearing system model
P	Vector forcing function of the rotor
Q	Quality factor of the notch filter
T_{ur}	Transfer function from input r to output u
T_{yr}	Transfer function from input r to output y
u	System input vector
$V_{control}$	Output voltage of the controller
V_{sense}	Output voltage of the sensor
x	System state vector
x_f	System state vector of the flexible body system model
x_0	Horizontal displacements of the centre of mass of the rotor
x_1	Displacement of the shaft of the left bearing
x_1 and x_2	Horizontal displacements of the rotor at left and right bearing positions, respectively
X_1 and X_2	Horizontal displacements of the rotor at left and right Hall-effect sensor positions, respectively
y	System output
y_1 and y_2	Vertical displacements of the rotor at bearing positions

ω_{max}	Frequency at which the phase angle is at its maximum
ω_0	Resonant frequency in radians per second
θ	Angle that the long axis of the rotor makes with the z axis
$\sum \vec{F}$	Summation of all external forces applied to the system
$\vec{a}$	Acceleration of the centre of gravity of the system
$\sum \vec{M}$	Summation of all moments applied externally to the system
$\vec{\alpha}$	Angular acceleration of the system
$\vec{r}$	Vector perpendicular to the line of application of the force
ϕ_{max}	Maximum phase angle of lead compensator

1 Introduction

1.1 Overview

This chapter provides an overview of the study. It begins by introducing the research problem and then proceeds to the aims and objectives of this research. The organisation of the thesis is also outlined in this chapter.

1.2 Problem Motivation

Active Magnetic Bearings (AMBs) have been used in a rapidly growing number of applications such as jet engines, compressors, pumps, and flywheel systems that are required to meet high speed, low vibration, zero friction wear and clean environment specifications (Polajzer, Dolinar et al. 1999; Motee and Queiroz 2002). However, AMBs are highly nonlinear and inherently unstable. Therefore, it is necessary to use automatic control to keep the system stabilised. Conventional control methods ranging from Proportional-Derivative (PD) and Proportional-Integral-Derivative (PID) to advanced control methods such as Q-parameterisation (Mohamed and Busch-Vishniac 1995); μ synthesis (Nonami and Ito 1996); adaptive control (Lun, Coppola et al. 1996); H ∞ control (Shiau, Sheu et al. 1997); LMI Control (Hong, Langari et al. 1997); neural network control (Komori, Kumamoto et al. 1998) and hybrid neural fuzzy control (Hajjaji and Ouladsine 2001) have been employed to control the natural instability of these bearings. However, the nonlinearities limit control effectiveness and the region of stable performance (Hung 1995). Much of the control of magnetic bearings literature (Humphris, Kelm et al. 1986; Fujita, Matsumura et al. 1990) concentrates on techniques

based on the linearised dynamic model obtained at its equilibrium point, while other approaches using nonlinear control techniques, such as sliding mode and feedback linearisation, have also been proposed (Rundell, Drakunov et al. 1996; Torres, Ramirez et al. 1999; Lindlau and Knospe 2002; Chen and Knospe 2005). The nonlinear control approaches provide better performance than the controllers which are designed based on the linearised model.

1.3 Problem Statement

This study investigated both conventional and advanced control methods for AMB system stabilisation. The intent of this research study was twofold and was intimately connected to continuing the approach of the AMB system control. Firstly, this research was designed to identify dynamic AMB system models. The second intent of this work was to design both conventional and advanced controllers for magnetic bearing systems. As the active magnetic bearings are highly nonlinear and inherently unstable, a controller has to be designed to keep the AMB system stable. Motivated by the capabilities to overcome the nonlinearities problem, fuzzy logic has been introduced to control magnetic bearing system (Shuliang 2001). Fuzzy logic theory was firstly introduced by Zadeh (1965). Fuzzy logic has been used in many areas and has been proved to be very effective in many control applications in this research. The nonlinear fuzzy logic controller was designed for the AMB system stabilisation. The fuzzy logic approach was chosen to compensate for magnetic nonlinearities and to enhance the performance of the magnetic bearing control system.

1.4 The Objectives of the Research

The aim of this research was to identify a system model and design both the conventional and advanced controllers for an AMB system in order to stabilise the system and to maximise the capabilities of the magnetic bearing system. The first phase of this research involved identifying the AMB system model using both the analytical method and the system identification approach. The second phase involved the implementation of the designed conventional controller. The last phase involved fuzzy logic controller design and simulation. Comparative studies of the conventional and advanced fuzzy logic controller for AMB system by evaluating controller performance via simulation were also done.

1.5 The Structure of the Thesis

This thesis consists of seven chapters. The other six chapters are organised as follows.

In chapter 2, some background materials that are directly related to this research are reviewed. Firstly, the active magnetic bearings are described and their advantages and disadvantages are discussed. Different control methods for stabilising AMB systems are then summarised. Finally, the three main steps in model identification: data acquisition, parameter estimation, and model validation are explained at the end of this chapter.

A detailed description of the model identification is presented in Chapter 3. An analytical model derivation is firstly reviewed. This provides basic knowledge on the AMB system rigid body model and bending body model. This is then followed by system identification which includes data acquisition and parameter estimation.

In chapter 4 an account of the design of notch filters based on the resonant frequencies identified in the previous chapter is provided. Furthermore, here the design and implementation of the conventional controller based on the model derived in chapter 3 is reported.

Fuzzy Logic theory and Fuzzy Logic Controller (FLC) structures with two different fuzzy inference methods are introduced at the beginning of chapter 5. These inference methods are Mamdani and Sugeno-Type fuzzy inference methods. PD-like FLC is then designed for the AMB system stabilisation. The performance of the designed PD-like FLC has been evaluated via simulation. Different fuzzy inference methods, different membership functions, different AND methods, different OR methods, and different implication methods have been investigated in order to find the best FLC. Comparative studies of the designed conventional and the advanced PD-like FLC for AMB system stabilisation evaluated via controller performance simulation are reported in Chapter 6. Finally, Chapter 7 presents the general conclusions by bringing together the preceding chapters. This chapter also examines the extent to which the objectives have been achieved; presents some directions for future research and development and other related work. In regards to appendices, Appendix A shows the program used for preparing data for system identification, while Appendix B provides the frequency response data collected for channel 2 of the MBC 500 magnetic bearing system for the purposes of system identification. Appendix C describes the 'c2dm' function, which converts continuous linear time-invariant systems to discrete time.

2 A Review on Active Magnetic Bearings and Control Techniques

2.1 Overview

This chapter provides a brief description of active magnetic bearing (AMB) system and its advantages. This is followed by a review of the control methods for stabilising the magnetic bearing system.

2.2 Active Magnetic Bearing

AMBs have been used in a rapidly growing number of applications in industry as an alternative to conventional mechanical bearings. AMBs offer several significant advantages over conventional bearings due to their non-contact operation, which can reduce the losses. AMB systems have other unique abilities such as: high rotor speed, non friction motion, weight reduction, precise position control, active damping and ability to operate under environmental constraints that prohibit the use of lubricants (Polajzer, Dolinar et al. 1999; Motee and Queiroz 2002).

AMBs are required to meet high speed, low vibration, zero friction, and clean environment specifications. The system has to have good transient response in terms of settling time, rise time, overshoot and steady state error. A controller with robustness to uncertainty and capable of adjusting itself according to the rotor speed is essential (Zhang, Lin et al. 2002).

However, unlike conventional bearings, magnetic bearings are highly nonlinear and inherently unstable. The non-linearity of the active magnetic bearing system is due to the relationship between forces that are generated in the electromagnetic actuator, the coil's current and the air gap between the rotor and the stator. These nonlinearities limit control effectiveness and the region of stable performance (Hung 1995). The open loop unstable characteristic of the magnetic bearings requires feedback control to ensure the normal operation of AMB systems (Habib and Hussain 2003).

2.3 Control Methods for Active Magnetic Bearings

As mentioned in the previous section, magnetic bearings require feedback control in order to overcome their instability. Both conventional control methods and advanced control methods have been applied to designing control systems for magnetic bearings. These design techniques are reviewed below.

- *PD and PID Control*

PD control for magnetic bearing is natural because the proportional feedback manifests itself simply as mechanical stiffness and the differential feedback coefficient as mechanical damping (Bleuler, Gahler et al. 1994). There is a sharp rise in the stiffness to static load change when adding an integral (I) term. Several PD control algorithms for controlling magnetic bearings have also been applied by some researchers (Allaire, Lewis et al. 1983; Humphris, Kelm et al. 1986; Keith, Williams et al. 1988). It has been presented by the above researchers that proportional feedback control can increase the critical speed or resonant frequency of the system of a single mass rotor on rigid support while reducing the damping ratio. Furthermore, derivative feedback control of the

system can reduce vibration amplitudes and flatten the response peaks at its critical speeds (Allaire, Lewis et al. 1981). Other experts have also obtained similar results for rotors on flexible supports with the control forces exerted at the bearing locations rather than at the rotor mass location (Allaire, Lewis et al. 1983). It is doubtless that the PD type controller is simple to implement, nevertheless magnetic bearing system's uncertainties and nonlinearities can result in difficulties of restricting the performance of AMBs to a small region and limiting the control effectiveness (Hartavi, Ustun et al. 2003).

A Proportional-Integral-Derivative (PID) controller offers a better solution to this problem as the PID controller has a simple structure and provides robust performance in a wide range of system operating conditions (Petrov, Ganchev et al. 2002). Hartavi, Ustun & Tuncay (2003) have employed the PID type controller technique and they have found that this method can overcome instability problems of the AMB system. However, magnetic bearings have electric power loss due to the direct current flow in the exciting coil. To reduce these losses, Sato & Tanno (1993) adopted the pulse width modulation (PWM) types of amplifiers with decreased switching frequency of the control voltage. Sato & Tanno (1993) have derived the transfer function of the magnetic bearing model and designed a PID controller to stabilise the rotor. A discontinuous controller with a hysteresis band was introduced in order to reduce the switching times and reduce the switching power. However, Williams, Joseph & Allaire (1990) have found that the resultant PID controller presents very poor damping at low frequencies. These controllers do not work well for nonlinear systems, namely, higher order and/or time delayed linear systems and particularly complex or vague systems that

have no precise mathematical models (Tokat, Eksin et al. 2003). Habib & Hussain (2004) have also discovered that PID controllers become ineffective when the machine is operated in highly nonlinear regions.

- *Q-parameterisation method*

The Q-parameterisation theory was used to design a controller for magnetic bearings with radials and thrust controls to stabilise the bearings and achieve the desired robustness and performance goals.

Design requirements for the Q-parameterisation method were described and then formulated as constraints on the controller which was parameterised by a dynamic system Q. In addition, the design problem was satisfied by selecting controller parameters so that all design requirements were met. This design problem was solved using Console, a CAD tandem for optimisation-based design developed at the University of Maryland in 1987. Digital simulation was implemented to verify the proposed methods (Mohamed and Emad 1992).

The Q-parameterisation theory has also been utilised to design controllers in order to solve the imbalance problem in the magnetic bearing system. The imbalance problem can be solved with two methods utilising feedback control. The first method is by compensating for the unbalanced forces with generated electromagnetic forces which cancel the unbalanced forces. The second method is by making the rotor spin around its axis of inertia or automatic balancing without generating unbalanced forces. The Q-

parameterisation is simply a solution with a set of linear equations. In addition, the controller Q-parameter was chosen by considering performance specifications and robustness to model uncertainties. Both the imbalance compensation and automatic balancing can be done at certain rotational speed. If the rotational speed changes then the controller parameters must be varied (Mohamed and Busch-Vishniac 1995).

- *H∞ control using closed loop shaping*

Another control design technique that has been applied for the magnetic bearing system is the H∞ control theory using closed loop shaping. The important requirement in practical magnetic bearing systems is to keep the stiffness of the controlled mechanical parts not below a given value for all relevant frequencies. The requirement is a wide-band disturbance attenuation problem in an H∞ setting. This approach is especially appropriate for applications with the worst case exciting frequency of disturbance forces. Rutland, Keogh & Burrows (1995) implemented the H∞ optimisation method for a magnetic bearing system with a flexible rotor by designing robust controllers. The important goal in the design was to prevent actuator saturation in the presence of disturbances and mass loss of the rotor. By selecting input and output weightings appropriately, a compromise is achieved between transient control forces and vibration levels. The mass loss simulation result showed the avoidance of saturation during transient condition. This transient condition is important in order to ensure the system remains linear. Another important point in the design is that the weighting function must be normalised in order to enable the optimisation problem to achieve desired performance level. If the mass loss is greater than the levels accounted for in this design, then bearing saturation may still occur (Rutland, Keogh et al. 1995).

Jiang & Zmood (1995) have also examined the application of H∞ control theory to ensure both system and external periodic disturbance rejection robustness for magnetic bearing systems.

- *H∞ control using open loop shaping and normalised left coprime factorisation description*

Another type of H∞ control method for magnetic bearing control utilises loop shaping and normalised left coprime factorisation description. McFarland & Glover (1998) have developed the unique H∞ optimisation method using what is called the normalised left coprime factorisation (LCF) plant description. An optimal solution without repetition has been obtained by using the normalised LCF robust stabilisation. This iteration process is essential in common H∞ optimisation problems.

Continuing the earlier experiment, McFarland & Glover then recommended a controller design procedure using open loop shaping particularly the loop shaping design procedure (LSDP) (McFarlane and Glover 1992). Fujita, Hatake & Matsumura (1993) then implemented this method to control the magnetic bearing system. Based on shaping the open loop properly, robust stability and good performance are achieved. The experiment results showed that LSDP provide a practical H∞ design methodology.

The LSDP H∞ controller result consists of two parts: a central controller and a free dynamic parameter Φ. An expert explored thoroughly the free parameter so that synchronous disturbances within some bandwidth can be actively rejected. Therefore,

The LSDP H∞ contaroller can guarantee robust stability and other system performances. Gain scheduling was also implemented in order to reject synchronous disturbances at various frequencies (Matsumura, Namerikawa et al. 1996).

- *μ-synthesis*

μ-synthesis controller design method deals with structured uncertainties. It is likely that the resultant controller is less conservative than H∞ controllers. The reason for this is that μ-synthesis control considers structured uncertainties. Nanomi & Ito (1996) designed and implemented the μ-synthesis controller for magnetic bearing systems with a flexible rotor. The result of the experiments showed that the μ- synthesis controller exhibits significantly greater robustness of mass variations than that of H∞ controllers. However, Fujita, Matsumura & Namerikawa (1992) observed that the performance of the μ-synthesis and the H∞ controller were almost the same. Furthermore, Losch, Gahler & Herzog (1998) have also designed a μ-synthesis controller with a 3 MW pump for the magnetic bearing system. For purposes of determining a suitable weighting function, a new theorem was introduced. The theorem expressed the important point in designing the μ-synthesis controllers, that is, there are three important points: size of the model uncertainty, system limitations, and performance goals. Moreover, the MATLAB D-K iteration script dkit.m was implemented in order to calculate the controller parameters (Balas, Doyle et al. 1995). It is obvious that in order to ensure the resultant μ-synthesis controller has good performance, the structured uncertainty model needs to be constructed carefully.

Namerikawa, Fujita & Matrumura (1998) have investigated three problems for magnetic

bearing systems. The problems are in the areas of the parameter uncertainties, unmodeled dynamics, and linearisation error. The uncertainties structure was described by real/complex numbers/matrices. The results showed good performance of proposed μ-synthesis design using the uncertainty model. Lastly, Fittro & Knospe (1998) have implemented a multivariable μ-synthesis controller for a 32000 rpm, 67.1 kW machine spindle with magnetic bearings. Furthermore, Fittro & Knospe (1998) also designed and implemented an optimal decentralised PID controller. Both theoretical and experimental results exhibited significant improvements in the μ-synthesis control design performance.

- *Sliding mode control*

The sliding mode control is one of the nonlinear methods for controlling magnetic bearing in order to overcome parameter uncertainties and reject disturbances to achieve robust performance.

Tian & Nonami (1994) have experimented with this design. They applied the discrete time sliding mode control on the magnetic bearing system with a flexible rotor. The experiments exhibited that the sliding mode control method implemented could increase the rotor speed up to 40,000 rpm without unstable vibrations. This experiment could not be achieved by implementing the PID controller. For the sliding mode control experimental implementation, a TMS320c30 based DSP controller was used.

Rundell, Drakunov & Decarlo (1996) designed and implemented a continuous time sliding mode observer and controller for magnetic bearings by stabilising the rotational motion of its vertical shaft. In this technique, a sliding mode observer was designed for

state and disturbance estimation, and a sliding mode controller was constructed for driving the system to a specified manifold and maintaining it there. The simulation results showed that the proposed technique enables the system to achieve good robustness.

- *Feedback Linearisation*

Research on nonlinear systems demonstrates that under certain conditions the nonlinear system can be linearised with feedback. This is an important point for designing magnetic bearing control systems as stabilisation is required for a wide range of operating conditions. However, the robust performance of the control system is guaranteed only for small rotor displacements (Ishidori 1987).

The feedback linearisation method has been used for designing nonlinear controllers for a number of magnetic bearing systems (Hung 1991; Lin and Gau 1997; Trumper, Olson et al. 1997; Namerikawa, Fujita et al. 1998).

- *Backstepping approach*

The integrator backstepping (IB) control method has received a great deal of attention in the last decade as this method provides the framework for attacking many electromechanical control problems including AMB (Krstic, Kanellakopoulos et al. 1995).

One of the main benefits of the IB design method is the proviso for systematic desirable modifications of control structures such as compensation for parametric uncertainty or eliminating state measurements. Furthermore, an adaptive controller designed using IB technique for a simplified magnetic bearing control was introduced by Krstic,

Kanellakopoulos & Kokotovic (1995). However, what enabled the use of an IB approach was the structure of the magnetic bearing dynamics (Krstic, Kanellakopoulos et al. 1995). De Queiroz & Dawson (1996) have implemented a backstepping-type controller for magnetic bearing systems utilising a nonlinear model of the planar rotor disk AMB. The magnetic bearing depended on a general flux linkage model. The controller requires the measurement of the rotor position, rotor velocity, and stator current for purposes of achieving global exponential rotor position tracking. Simulation is used to illustrate the performance of the controller.

- *Neural network control*

There are a few research reports on the neural network application in designing controllers for magnetic bearing systems. Bleuler, Diez, Lauber, Meyer & Zlatnik (1990) have designed and implemented a neural network controller for controlling an electromagnet that was used to levitate an iron ball. The experiment showed that a nonlinear ANN (Artificial Neural Networks) controller's performance was much better than that of linear controllers for a typical unstable plant with strong nonlinearities.

In 1998, Paul, Hofmann & Steffani (1998) did some investigations using MLP-network to compensate unbalances at magnetic bearings. The TMS 320c40 DSP was used for controller implementation.

- *Fuzzy Logic Control (FLC)*

Fuzzy logic was first introduced in 1965 by Professor L.A. Zadeh, University of California Berkeley, US, in his paper "Fuzzy Sets" which was published in an academic

journal "Information and Control" (Liu and Lewis 1993). Although Zadeh initially expected his fuzzy logic idea to be applied in large organisational system design and social sciences, most of the applications have been developed in engineering and system control. Even though the fuzzy logic theory was firstly introduced in the USA, it has developed more rapidly in terms of technology and applications in Japan. For example, OMRON, one of Japan's industrial pioneers in this area, began to study about fuzzy theory and its application in 1984 and then many kinds of fuzzy control-based products have been developed and many patents have been granted (more than 1000 in Japan and over 40 in USA) (Reznik 1997).

Since Zadeh's innovation, fuzzy theory has been applied to various fields. The early applications were mainly in the engineering fields (Mukaidono 2001). According to (Passino and Yurkovich 1998; Mukaidono 2001), the application of fuzzy logic has been in the following.:

- Aircraft/spacecraft: flight control, engine control, avionic systems, failure diagnosis, navigation and satellite attitude control.
- Automated highway systems: automatic steering, braking, and throttle control for vehicles, traffic control, elevator, trains and cranes.
- Automobiles: brakes, transmission, suspension and engine control.
- Autonomous vehicles: ground and underwater.
- Manufacturing systems: scheduling and deposition process control.
- Power industry: motor control, power control/distribution and load estimation.
- Process control: temperature, pressure and level control, failure diagnosis, distillation column control, and desalination process.

- Robotics: position control and path planning.
- Consumer products: washing machines, microwave ovens, rice cookers, vacuum cleaners, camcoders, TVs and VCRs, thermal rugs and word translators.
- Software: medical diagnosis, security, data compression.

Fuzzy logic controllers have been designed and implemented for active magnetic bearing systems for modelling and control purposes.

Hung (Hung 1995) used the principles of fuzzy theory to compensate the magnetic nonlinearities in order to improve the system performance. Kosaki, Sano & Tanaka (1997) have designed a model-based fuzzy controller for magnetic bearing systems. The performance of the fuzzy logic controller was verified via simulation. Furthermore, Hong, Langari & Joh (1997) implemented Sugeno-Kang (TSK) fuzzy model for modelling magnetic bearings. Based on the TSK fuzzy model, nonlinear fuzzy controllers were derived by means of a systematic synthesis approach. Finally, simulation was used to illustrate that the implementation of a fuzzy controller not only maximised the stability boundary but also achieved better performance than a linear controller, a simulation was used.

In 1995, Yang used the fuzzy logic approach to the synthesis of synchronisation control for a suspended rotor system. The synchronisation control enables a whirling rotor to experience the synchronous motion along the magnetic bearing axes, thereby avoiding the gyroscopic effects that degrade the stability of the rotor system when spinning at high speed. Simulation results demonstrated the performance of the fuzzy logic

controller.

Based on all the control techniques reviewed above, much of the literature concerns the control of magnetic bearings concentrates on techniques based on the linearised dynamic model of the magnetic bearing system (Humphris, Kelm et al. 1986; Fujita, Matsumura et al. 1990). However, these methods are only effective in limited nominal design conditions. The linear control performs well when the position of the rotor is close to the designed operating condition, but it drops quickly outside of the operating point (Hung 1995). Furthermore, linear optimal control techniques also focus on linearising the dynamics of the magnetic bearing systems about the bearing centre at nominal speed, which affords opportunities for the linear quadratic Gaussian optimal control (Smith and Weldon 1995). Meanwhile, approaches using nonlinear control techniques provide better performance than the controllers designed based on the linearised model. However, the nonlinear control theory is generally complicated compared to the linear control. Finding solutions to nonlinear equations is quite daunting. Even though the system can be precisely described, it is not always possible to find a nonlinear solution that enables achieving a stable closed loop system.

Drawing on the various studies, both conventional PD controllers and fuzzy logic controllers have been considered as potential solutions for stabilising the active magnetic bearing in this research.

2.4 Summary

This chapter has provided a brief description of the active magnetic bearing (AMB) system and its advantages. The description has been followed by a review of the literature on control methods for stabilising the magnetic bearing system. Modeling and system identification of the MBC500 will be described in the next chapter.

3 Modeling and System Identification of the MBC 500 Magnetic Bearing System

3.1 Overview

This chapter firstly provides information on the MBC 500 magnetic bearing system parameters. The analytical model of the MBC 500 magnetic bearing system draws on principles of physics. Both the rigid body model and bending body model are described. Finally, system identification which includes data acquisition and parameter estimation is presented.

3.2 The MBC 500 System Parameters

The device for this research is the MBC 500 magnetic bearing system. The MBC 500 consists of two active radial magnetic bearings and a supported rotor mounted on top of an anodized aluminium case (Magnetic Moments 1995). See Figure 3.1 below.

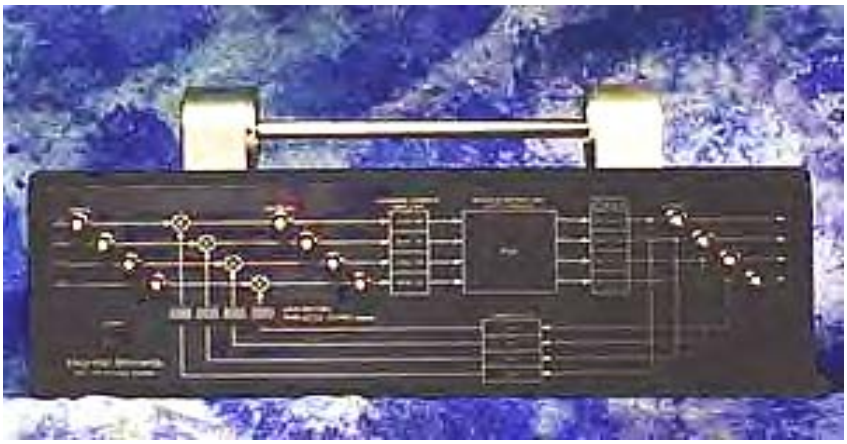

Figure 3.1 MBC 500 magnetic bearing research experiment
Source: (Magnetic Moments 1995)

The shaft is actively positioned in the radial directions at the shaft ends. It has 4 degrees of freedom and it is passively centered in the axial direction. Moreover, it freely rotates about its axis. The magnetic bearing system includes four linear current amplifier pairs and one pair for each radial bearing axis. In addition, it also includes four internal lead-lag compensators which independently control the radial bearing axis (Magnetic Moments 1995).

In addition, the front panel of the MBC 500 magnetic bearing system (shown in Figure 3.2) is a graphical representation of the system dynamics of the MBC 500. The panel contains 12 BNC connections for easy access to the systems with four inputs and eight outputs. Moreover, there are four switches in the feedback loops. These switches allow the user to open the loop for the internal controllers independently. If only one loop is switched off, the user can perform single-input single-output (SISO) control design experiments (Magnetic Moments 1995).

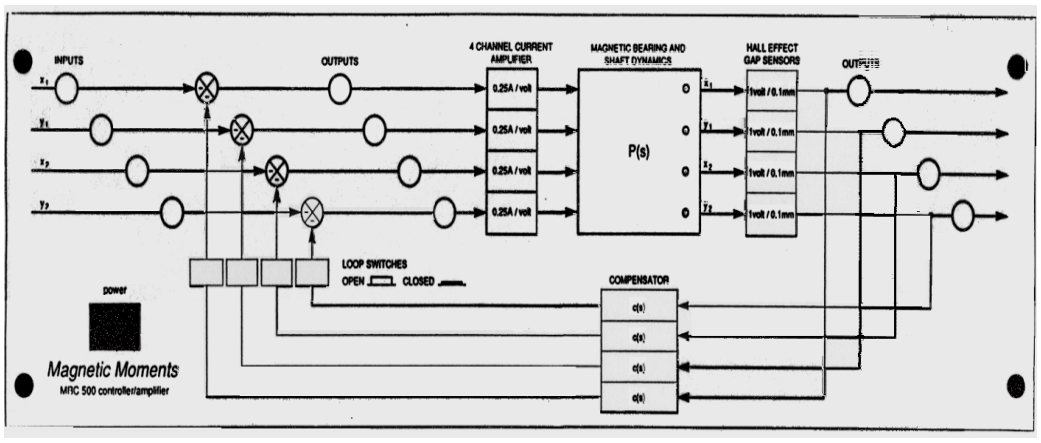

Figure 3.2 Front panel block diagram of MBC 500
Source: (Magnetic Moments 1995)

All the information in this section about the MBC 500 system parameters has been directly taken from the MBC 500 Magnetic Bearing System Operating Instruction Manual (Magnetic Moments 1995). This section describes the blocks given on the front panel of the MBC 500 magnetic bearing system in greater detail. These models given below are nominal and serve as a guide only. The shaft's schematic showing electromagnets and Hall-effect sensors, is provided in Figure 3.3 below.

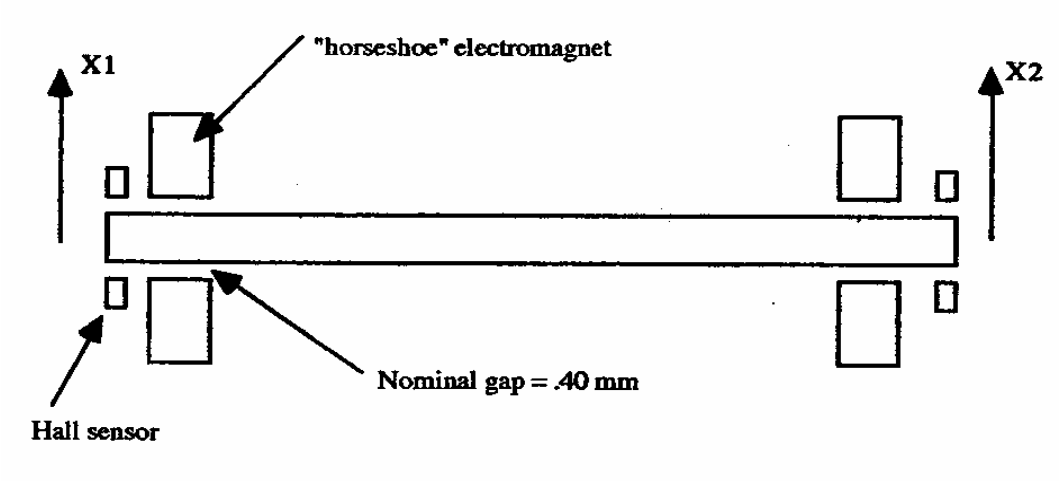

Figure 3.3 Shaft schematic showing electromagnets and Hall-effect sensors
Source: (Magnetic Moments 1995)

- **Shaft parameters**

The shaft on the MBC 500 is made from non-magnetic 303 stainless steel with a modulus of elasticity 28 x 106 psi, density 0.29 lb/in3, diameter 0.490 inches (1.2446cm), and length 10.6 inches (26.924 cm). The bearings are centred 0.95 inches (2.413 cm) from the shaft ends, and the Hall sensors are centred 0.11 inches (0.2794 cm) from the shaft ends (Magnetic Moments 1995).

- **Bearing parameters**

The bearing coils have a 0.5 Amp bias upon which a control signal is superimposed. The force applied by a single horseshoe electromagnet can be determined by the formula:

$F = k(i_{control} + 0.5)^2/g^2$ (Magnetic Moments 1995)..... 3.1

Where k = 2.8 x 10^{-7} Nm^2/A^2, $i_{control}$ is the control current supplied by the current amplifier in addition to the 0.5A bias current, and g is the air gap in meters. The bias current in opposing electromagnets has an opposite sign and when the control current is added to both coils, the net force generated by opposing electromagnets can be calculated as (Magnetic Moments 1995):

$$F_x = k\frac{(i_{control} + 0.5)^2}{(x_1 - 0.0004)^2} - k\frac{(i_{control} - 0.5)^2}{(x_1 - 0.0004)^2} \quad \text{..... 3.2}$$

Where x_1 is the displacement of the shaft inside the left bearing of Figure 3.3. The same expression holds for bearing 2 and the y forces as well.

- **Amplifier Model**

The current amplifier model has a simple first order response. Each of the four current amps is described by the formula(Magnetic Moments 1995) :

$$i_{control} = \frac{0.25}{(1+2.2\times10^{-4}s)} A/volt \times V_{control} \quad \text{..... 3.3}$$

- **Compensator Model**

The nominal compensator model is derived from the circuit schematic and relates $V_{control}$ to V_{sense} by the following transfer function (Magnetic Moments 1995):

$$V_{control} = \frac{1.41(1+8.9\times10^{-4}\,s)}{(1+3.3\times10^{-4}\,s)(1+2.2\times10^{-5}\,s)} V_{sense} \quad \text{..... 3.4}$$

This compensator can be implemented in an external controller, but time needs to be considered in tuning the controller due to the nonlinear unstable system.

- **Sensor Nonlinearity**

The displacements sensed by the two opposing Hall-effect sensors shown in Figure 3.3 are combined electronically to yield the following relationship between shaft end displacements X_1, X_2, Y_1, or Y_2. Expressed in terms of X_1, we approximately have:

V_{sense} = 5 Volts/mmX_1 + 24 Volts/mm^3 X_1^3 ± 1 Volt offset.

V_{sense} is available on the front panel via the sensor output BNC connector.

Since the magnetic bearing system is inherently unstable, it is necessary to use automatic control to keep the system stabilised. To stabilise the system, the position of the rotor needs to be sensed and the controller must control the amount of current onto the magnets.

3.3 Analytical Model of the Magnetic Bearing System

Morse, Smith & Paden (1996) provide the details for the derivation of the analytical model of the MBC 500 magnetic system. This section provides a brief review of the analytical model found based on the physical laws of active magnetic bearing.

Analytical Model Derivation

An analytical model is needed in model based control system design. The physics governing the AMB can be described by differential equations, which represent the motion of the AMB in response to certain input signals. This will be in the form of a state space model. A "state-space" model of the system keeps the form of:

$$\chi = Ax + Bu \quad \text{.....} \quad 3.5$$
$$y = Cx + Du \quad \text{.....} \quad 3.6$$

Where x is the state vector, u is the system input vector and y is the system output. The A, B, C and D matrices describe the system mathematically.

For the MBC 500 system, the analytical derivation is broken into two parts: 'Rigid Body' and "Bending Body'. When the system acts as a 'Rigid Body' it means that it remains completely inflexible. When the system acts as a 'Bending Body' it means that it is flexible in rotor motion. Then, MATLAB will be used to compile the models and determine the characteristics (Morse, Smith et al. 1995). A diagram of the MBC 500 system configuration is shown in Figure 3.4.

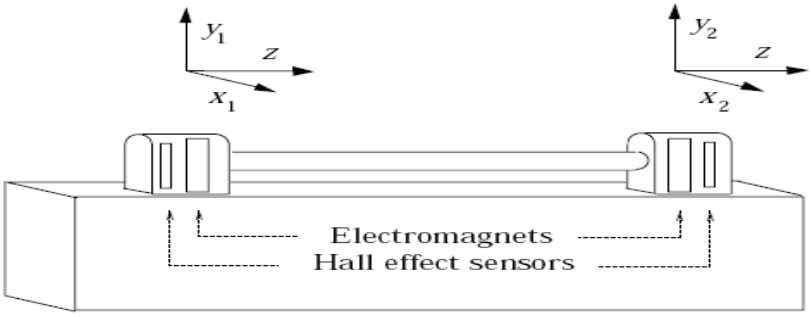

Figure 3.4 MBC 500 system configuration
Source: (Morse, Smith et al. 1995)

This MBC 500 system contains a stainless steel shaft or rotor. The rotor or a stainless steel shaft can levitate using eight "horseshoe" electromagnets with four at each of the rotor. Hall effect sensors placed just outside of the electromagnets at each end of the rotor measure the rotor end displacement. The rotor movement is controlled in four degrees of freedom. This four degrees of freedom are broken into two translational degrees, including translation in the horizontal direction, x_1 and x_2, perpendicular to the z axis, and translation in the vertical direction, y_1 and y_2. Also included in the MBC 500 are four on-board controllers which levitate the bearing when the controllers are connected in feedback. There are also four switches on the front panel of the MBC 500 to disconnect each of the controllers so that any one or all of them can be replaced by an external controller (Morse, Smith et al. 1995).

Rigid Body Model

The first analysis of the system assumes that the rotor acts as a rigid body. The definition of a rigid body is that the rotor does not change shape, which implies that the rotor does not bend but experiences only transitional or rotational motion. Moreover, the horizontal and vertical dynamics, i.e. the x and y directions, are uncoupled. The

effects of coupling cannot be ignored if the rotor were spinning or if the actuators or sensors were misaligned. Theoretically, the system operates identically in the *x* and *y* directions if their dynamics are uncoupled. However, the additional constant force of gravity acts in the *y* direction. The force is non-linear, consequently it cannot be modeled by a linear system model. For this reason, the analysis of the gravity effect in the linear *y* direction is neglected. As mentioned earlier, that the *x* and *y* directions are identical, the derivation is focused on the horizontal or *x* direction motion. The system configuration is shown in Figure 3.5, while the parameters are defined in Table 3.1 and the system variables are described in Table 3.2 (Morse, Smith et al. 1995).

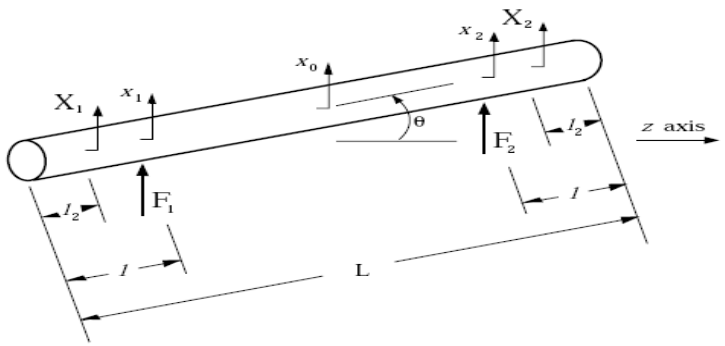

Figure 3.5 Rotor configuration

Source: (Magnetic Moments 1995)

Symbol	***Description***
x_0	The horizontal displacements of the centre of mass of the rotor
x_1 and x_2	The horizontal displacements of the rotor at left and right bearing positions, respectively
X_1 and X_2	The horizontal displacements of the rotor at left and right Hall-effect sensor positions, respectively
θ	The angle that the long axis of the rotor makes with the z axis
F_1 and F_2	The forces exerted on the rotor by left and right bearings, respectively

Table 3.1 System variables

Source: (Magnetic Moments 1995)

Symbol	***Description***	***Value***
L	Total length of the rotor	0.269 m
l	Distance from each bearing to the end of the rotor	0.024 m
l_2	Distance from Hall-effect sensor to the end of the rotor	0.0028 m
I_0	Moment of inertia of the rotor with respect to rotation about an axis in the y direction $I_0 = \frac{1}{12} mL^2$	1.5884×10^{-3} kgm^2
M	Mass of the rotor	0.269 kg

Table 3.2 System parameters

Source: (Magnetic Moments 1995)

To translate the rotor nominal position, that is, the desired rotor position corresponds to $x_1 = 0$ and $x_2 = 0$ or equivalently $X_1 = 0$ and $X_2 = 0$ or $x_0 = 0$ and $\theta = 0$. The rotor will be centered horizontally with respect to the front and back electromagnets on each end, and its long axis is parallel to the z axis. In addition, the rotor end displacements are expressed as shown below (Morse, Smith et al. 1995):

$x_1 = x_0 - (\frac{L}{2} - l)\sin\theta$ 3.7

$x_2 = x_0 + (\frac{L}{2} - l)\sin\theta$ 3.8

$X_1 = x_0 - (\frac{L}{2} - l_2)\sin\theta$ 3.9

$X_2 = x_0 + (\frac{L}{2} - l_2)\sin\theta$ 3.10

Assume that θ is small, this is a valid assumption considering the physical dimension of the system. The first order approximations are: $\sin\theta \cong \theta$ and $\cos\theta \cong 1$.

Newton's law is used to find the equations of motion for rigid body mechanical systems. In addition, the force balance equation is used for the rotor analysis as shown

below (Morse, Smith et al. 1995):

$$\sum \vec{F} = m\vec{a} \quad \text{..... 3.11}$$

where $\sum \vec{F}$ is the summation of all external forces applied to the system, m is the rotor mass, and $\vec{a}$ is the acceleration of the centre of gravity of the system.

The moment balance can be expressed as:

$$\sum \vec{M} = I\vec{\alpha} \quad \text{..... 3.12}$$

where $\sum \vec{M}$ is the summation of all moments applied externally to the system, I is the rotational moment of inertia of the system about the axis through the centre of gravity and in the direction of rotation, and $\vec{\alpha}$ is the angular acceleration of the system.

The moments and forces are interrelated as shown in the following equation:

$$\vec{M} = \vec{r}\, x\, \vec{F} \quad \text{..... 3.13}$$

where $\vec{r}$ is any vector pointing from point 0 to the line of application of the force $\vec{F}$. This relationship is shown pictorially in Figure 3.6a below.

However, if the vector $\vec{r}$ is chosen to be perpendicular to the line of application of the force $\vec{F}$ as shown in Figure 3.6b, then the above equation reduces to

$$M=rF \quad \text{..... 3.14}$$

As can be seen in Figure 3.6, the sense of the moment is counter-clockwise. From the force and moment balance equations above, the non-linear differential equations can be derived governing the rigid body motion as shown in Figure 3.5 above. The motion is only in one plane which is the x direction. The equations of motion are shown below:

$$\sum F = m\ddot{x}_0 = F_1 + F_2 \quad \text{..... 3.15}$$

$$\sum M = I_0\ddot{\theta} = F_2(\tfrac{L}{2} - l)\cos\theta - F_1(\tfrac{L}{2} - l)\cos\theta \quad \text{..... 3.16}$$

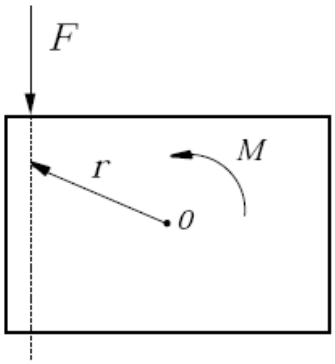

Figure 3.6a

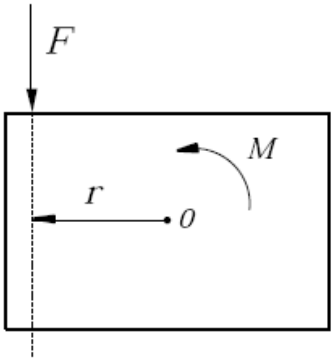

Figure 3.6b

Figure 3.6 Force/Moment relationships
Source: (Morse, Smith et al. 1995)

All the above differential equations, system parameters and variables have been used in order to determine a suitable model for the rigid body system. This useful information was obtained through doing a series of exercises set in the MBC500 manual. The final result took the form of a two-input, two-output state space representation in the form:

$$\begin{bmatrix} \dot{x}_0 \\ \ddot{x}_0 \\ \dot{\theta} \\ \ddot{\theta} \\ \dot{i}_{control1} \\ \dot{i}_{control2} \end{bmatrix} = A_r \begin{bmatrix} x_0 \\ \dot{x}_0 \\ \theta \\ \dot{\theta} \\ i_{control1} \\ i_{control2} \end{bmatrix} + B_r \begin{bmatrix} V_{control_1} \\ V_{control_2} \end{bmatrix} \quad \text{..... 3.17}$$

$$\begin{bmatrix} V_{sense1} \\ V_{sense2} \end{bmatrix} = C_r \begin{bmatrix} x_0 \\ \dot{x}_0 \\ \theta \\ \dot{\theta} \\ i_{control1} \\ i_{control2} \end{bmatrix} \quad \text{..... 3.18}$$

where A_r, B_r and C_r are the state space matrices for the rigid body case. From this result, the system response has been determined.

The manual of MBC 500 provides the following nominal transfer function for each of the on-board controllers:

$$V_{control_i} = \frac{1.41(1+8.9\times10^{-4}s)}{(1+3.3\times10^{-4}s)(1+2.2\times10^{-5}s)} V_{sense_i} = C(s)V_{sense_i} \quad \text{..... 3.19}$$

For the controller design, the controller $C_{x1}(s)$ is replaced by mapping V_{sense1} to $V_{control1}$. The system seen by the controller is as shown in Figure3.7. However, because of the rigid body is a simplified version in that the x and y rotor motion are uncoupled, an equivalent system configuration is shown in Figure 3.8.

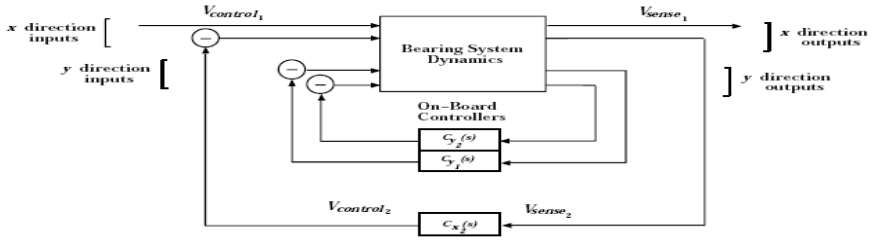

Figure 3.7 Bearing system seen by controller $C_{x1} - x$ and y directions coupled
Source: (Morse, Smith et al. 1995)

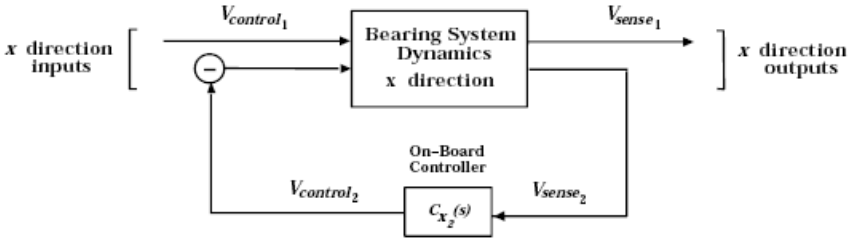

Figure 3.8 Bearing system seen by controller $C_{x1} - x$ and y directions uncoupled
Source: (Morse, Smith et al. 1995)

In order to obtain the analytical model for the rigid body system to be controlled, the controllers $C_{x2}(s)$, $C_{y1}(s)$ and $C_{y2}(s)$ must be included in the feedback as shown in Figure 3.7. Specific commands in MATLAB can convert the controller model C(s) to a state space model. This state space model has controller matrices *acont*, *bcont*, *ccont* and *dcont* representing the on-board controllers.

From the equation 3.15, it can be obtained that:

$$\ddot{\chi}_0 = \frac{F_1}{m} + \frac{F_2}{m} \quad \text{..... 3.20}$$

Since θ is small so $\cos\theta \approx 1$ and θ becomes:

$$\ddot{\theta} = \frac{F_2(\frac{L}{2}-l)}{I_0} - \frac{F_1(\frac{L}{2}-l)}{I_0} = -\frac{1}{I_0}(\frac{L}{2}-l)F_1 + \frac{1}{I_0}(\frac{L}{2}-l)F_2 \quad \text{..... 3.21}$$

Meanwhile, assuming θ is small so X_1 and X_2 can be simplified as follows by using the equations 3.5 and 3.6:

$$X_1 = x_0 - (\tfrac{L}{2}-l_2)\theta \quad \text{..... 3.22}$$
$$X_2 = x_0 + (\tfrac{L}{2}-l_2)\theta \quad \text{..... 3.23}$$

All the equations above can be written in state space form with the state vector:

$$x = x_r = \begin{bmatrix} x_0 \\ \dot{x}_0 \\ \theta \\ \dot{\theta} \end{bmatrix}$$

where *r* means rigid body. In addition, F_1 and F_2 represent input variables and X_1 and X_2 are output variables, the state space equations can be written as follows:

$$\begin{bmatrix} \dot{x}_0 \\ \ddot{x}_0 \\ \dot{\theta} \\ \ddot{\theta} \end{bmatrix} = \begin{bmatrix} 0 & 1 & 0 & 0 \\ 0 & 0 & 0 & 0 \\ 0 & 0 & 0 & 1 \\ 0 & 0 & 0 & 0 \end{bmatrix} \begin{bmatrix} x_0 \\ \dot{x}_0 \\ \theta \\ \dot{\theta} \end{bmatrix} + \begin{bmatrix} 0 & 0 \\ \frac{1}{m} & \frac{1}{m} \\ 0 & 0 \\ -\frac{1}{I_0(\frac{L}{2}-l)} & \frac{1}{I_0(\frac{L}{2}-l)} \end{bmatrix} \begin{bmatrix} F_1 \\ F_2 \end{bmatrix} \quad \text{..... 3.24}$$

$$\begin{bmatrix} X_1 \\ X_2 \end{bmatrix} = \begin{bmatrix} 1 & 0 & -(\frac{l}{2}-l_2) & 0 \\ 1 & 0 & (\frac{l}{2}-l_2) & 0 \end{bmatrix} \begin{bmatrix} x_0 \\ \dot{x}_0 \\ \theta \\ \dot{\theta} \end{bmatrix} \quad \text{..... 3.25}$$

Clearly, it can be seen that all four eigenvalues are 0 for the state matrix.

By implementing the first order approximation at the point (0,0) to describe the bearing force on the rotor:

$$F_i(x_i, i_{controli}) = F_i(0,0) + \left[\frac{\partial F_i}{\partial x_i}(0,0)\right](x_i - 0) + \left[\frac{\partial F_i}{\partial i_{controli}}(0,0)\right](i_{controli} - 0) \quad \text{..... 3.26}$$

The *i*th non-linear be

Bearing force can be expressed as (Magnetic Moments 1995):

$$F_i = k\frac{(i_{control_i} + 0.5)^2}{(x_i - 0.0004)^2} - k\frac{(i_{control_i} - 0.5)^2}{(x_i + 0.0004)^2} \quad \text{..... 3.27}$$

where k=2.8 x 10^{-7} Nm^2/Amp^2.

$\frac{\partial F_i}{\partial x_i}$ can be found as follows:

$$\frac{\partial F_i}{\partial x_i} = k\left(\frac{-2(i_{controli} + 0.5)^2}{(x_i - 0.0004)^3} - \frac{-2(i_{controli} - 0.5)^2}{(x_i + 0.0004)^3}\right) \quad \text{..... 3.28}$$

and

$$\left.\frac{\partial F_i}{\partial x_i}\right|_{(0,0)} = 4375 \quad \text{..... 3.29}$$

$\frac{\partial F_i}{\partial i_{controli}}$ can be derived as:

$$\frac{\partial F_i}{\partial i_{controli}} = k\left(\frac{2(i_{controli} + 0.5)}{(x_i - 0.0004)^2} - \frac{2(i_{controli} - 0.5)}{(x_i + 0.0004)^2}\right) \quad \text{..... 3.30}$$

and

$$\left.\frac{\partial F_i}{\partial i_{controli}}\right|_{(0,0)} = 3.5 \quad \text{..... 3.31}$$

F_1 and F_2 can thus be expressed as:

$$F_1 = 4375x_1 + 3.5i_{control1} \quad \text{..... 3.32}$$

$$F_2 = 4375x_2 + 3.5i_{control2} \quad \text{..... 3.33}$$

Combining equation 3.7 with equation 3.32, F_1 and F_2 can be expressed as follows:

$$F_1 = 4375x_0 - 4375(\tfrac{L}{2} - l)\theta + 3.5i_{control1} \quad \text{..... 3.34}$$

Combining equation 3.8 with equation 3.33, F_1 and F_2 can be expressed as follows:

$$F_2 = 4375x_0 + 4375(\tfrac{L}{2} - l)\theta + 3.5i_{control2} \quad \text{..... 3.35}$$

$\ddot{x}_0$ can be written as:

$$\ddot{x}_0 = \frac{4375x_0 - 4375(\frac{L}{2} - l)\theta + 3.5i_{control1}}{m} + \frac{4375x_0 + 4375(\frac{L}{2} - l)\theta + 3.5i_{control2}}{m}$$

$$\ddot{x}_0 = \frac{8750}{m}x_0 + \frac{3.5i_{control1}}{m} + \frac{3.5i_{control2}}{m} \quad \text{..... 3.36}$$

Meanwhile, $\ddot{\theta}$ can be expressed as:

$$\ddot{\theta} = -\frac{1}{I_0}(\frac{L}{2} - l)\left(4375x_0 - 4375(\tfrac{L}{2} - l)\theta + 3.5i_{control1}\right) + \frac{1}{I_0}(\frac{L}{2} - l)\left(4375x_0 + 4375(\tfrac{L}{2} - l)\theta + 3.5i_{control2}\right)$$

$$\ddot{\theta} = 8750\frac{(\frac{L}{2} - l)^2\theta}{I_0} - 3.5\frac{(\frac{L}{2} - l)\theta}{I_0}i_{control1} + 3.5\frac{(\frac{L}{2} - l)\theta}{I_0}i_{control2} \quad \text{..... 3.37}$$

Therefore, the new state space rigid body system model including the actuator dynamics with $i_{control1}$ and $i_{control2}$ as input variables can be expressed below:

$$\begin{bmatrix} \dot{x}_0 \\ \ddot{x}_0 \\ \dot{\theta} \\ \ddot{\theta} \end{bmatrix} = \begin{bmatrix} 0 & 1 & 0 & 0 \\ \frac{8750}{m} & 0 & 0 & 0 \\ 0 & 0 & 0 & 1 \\ 0 & 0 & \frac{8750(\frac{L}{2}-l)^2}{I_0} & 0 \end{bmatrix} \begin{bmatrix} x_0 \\ \dot{x}_0 \\ \theta \\ \dot{\theta} \end{bmatrix} + \begin{bmatrix} 0 & 0 \\ \frac{3.5}{m} & \frac{3.5}{m} \\ 0 & 0 \\ -\frac{3.5}{I_0}(\frac{L}{2}-l) & \frac{3.5}{I_0}(\frac{L}{2}-l) \end{bmatrix} \begin{bmatrix} i_{control1} \\ i_{control2} \end{bmatrix} \quad \text{..... 3.38}$$

$$\begin{bmatrix} X_1 \\ X_2 \end{bmatrix} = \begin{bmatrix} 1 & 0 & -(\frac{L}{2}-l_2) & 0 \\ 1 & 0 & (\frac{L}{2}-l_2) & 0 \end{bmatrix} \begin{bmatrix} x_0 \\ \dot{x}_0 \\ \theta \\ \dot{\theta} \end{bmatrix} \quad \text{..... 3.39}$$

Using the system parameters given in Table 3.2, the eigenvalues of the state matrix are:

$$\pm\sqrt{\frac{8750}{m}} = \pm\sqrt{\frac{8750}{0.2629}} = \pm 182.4 \frac{rad}{\sec};$$

$$\pm\sqrt{\frac{8750\times(\frac{L}{2}-l)^2}{I_0}} = \pm\sqrt{\frac{8750\times 0.1105^2}{1.5884*10^{-3}}} = \pm 259.4 \frac{rad}{\sec}$$

As can be seen, the system is unstable because there are two positive eigenvalues.

Another implementation of Taylor series approximation at the $x_i = 0$ can be used to linearise the sensor non-linearity:

$$V_{sensei}(X_i) = V_{sensei}(0) + \left[\frac{\partial V_{sensei}}{\partial X_i}(0)\right](X_i - 0) \quad \text{..... 3.40}$$

Where the relationship between the voltage sensed and the rotor displacement is given below (Magnetic Moments, 1995):

$$V_{sense_i} = 5000X_i + (25\times 10^9)X_i^{\,3} \quad \text{..... 3.41}$$

$\frac{\partial V_{sensei}}{\partial X_i}$ can be calculated as:

$$\frac{\partial V_{sensei}}{\partial X_i} = 5000 + 3(25\times 10^9)X_i^{\,2} \quad \text{..... 3.42}$$

$$\left.\frac{\partial V_{sensei}}{\partial X_i}\right|_{(0)} = 5000 \quad \text{..... 3.43}$$

As the result: $V_{sensei} = 5000X_i$ 3.44

The output equation becomes:

$$\begin{bmatrix} V_{sense1} \\ V_{sense2} \end{bmatrix} = 5000\begin{bmatrix} 1 & 0 & -(\frac{L}{2}-l_2) & 0 \\ 1 & 0 & (\frac{L}{2}-l_2) & 0 \end{bmatrix} x_r \quad \text{..... 3.45}$$

Since the sensor transfer function is purely a gain, the eigenvalues of the system are not affected. Furthermore, the magnetic bearing manual gives the dynamic characteristics of current amplifiers:

$$\frac{d}{dt}(i_{controli}) = -\frac{1}{2.2\times 10^{-4}} i_{controli} + \frac{0.25}{2.2\times 10^{-4}} V_{controli}$$

The amplifier input is $V_{controli}$ and its output is $i_{controli}$. $V_{control1}$ and $V_{control2}$ are the voltages that the controller produces to control the bearing. The current amplifier is a low pass filter, the range of frequencies passed by the current amplifier is from 0 to 4545 $\frac{rad}{\sec}$.

By adding the current amplifier dynamics to the rigid body model obtained above, let $V_{control1}$ and $V_{control2}$ as input variables and V_{sense1} and V_{sense2} as output variables.

The new state vector becomes:

$$\dot{x}_r = \begin{bmatrix} \dot{x}_0 \\ \ddot{x}_0 \\ \dot{\theta} \\ \ddot{\theta} \\ i_{control1} \\ i_{control2} \end{bmatrix} \text{ and } x_r = \begin{bmatrix} x_0 \\ \dot{x}_0 \\ \theta \\ \dot{\theta} \\ i_{control1} \\ i_{control2} \end{bmatrix}$$

The new state space rigid body model can be written as follows:

$$\dot{x}_r = \begin{bmatrix} 0 & 1 & 0 & 0 & 0 & 0 \\ \frac{8750}{m} & 0 & 0 & 0 & \frac{3.5}{m} & \frac{3.5}{m} \\ 0 & 0 & 0 & 1 & 0 & 0 \\ 0 & 0 & \frac{8750(\frac{L}{2}-l)^2}{I_o} & 0 & -\frac{3.5}{I_0}(\frac{L}{2}-l) & \frac{3.5}{I_0}(\frac{L}{2}-l) \\ 0 & 0 & 0 & 0 & \frac{-1}{2.2\times10^{-4}} & 0 \\ 0 & 0 & 0 & 0 & 0 & \frac{-1}{2.2\times10^{-4}} \end{bmatrix} x_r + \begin{bmatrix} 0 & 0 \\ 0 & 0 \\ 0 & 0 \\ 0 & 0 \\ \frac{0.25}{2.2\times10^{-4}} & 0 \\ 0 & \frac{0.25}{2.2\times10^{-4}} \end{bmatrix} \begin{bmatrix} V_{control1} \\ V_{control2} \end{bmatrix} \quad \text{..... 3.46}$$

And the new output equation can be expressed as:

$$\begin{bmatrix} V_{sense1} \\ V_{sense2} \end{bmatrix} = 5000 \begin{bmatrix} 1 & 0 & -(\frac{L}{2}-l_2) & 0 & 0 & 0 \\ 1 & 0 & (\frac{L}{2}-l_2) & 0 & 0 & 0 \end{bmatrix} x_r \quad \text{..... 3.47}$$

The A, B, C and D matrices can thus be written as follow:

$$A = \begin{bmatrix} 0 & 1 & 0 & 0 & 0 & 0 \\ \frac{8750}{m} & 0 & 0 & 0 & \frac{3.5}{m} & \frac{3.5}{m} \\ 0 & 0 & 0 & 1 & 0 & 0 \\ 0 & 0 & \frac{8750(\frac{L}{2}-l)^2}{I_o} & 0 & -\frac{3.5}{I_0}(\frac{L}{2}-l) & \frac{3.5}{I_0}(\frac{L}{2}-l) \\ 0 & 0 & 0 & 0 & \frac{-1}{2.2\times10^{-4}} & 0 \\ 0 & 0 & 0 & 0 & 0 & \frac{-1}{2.2\times10^{-4}} \end{bmatrix}$$

$$B = \begin{bmatrix} 0 & 0 \\ 0 & 0 \\ 0 & 0 \\ 0 & 0 \\ \frac{0.25}{2.2\times10^{-4}} & 0 \\ 0 & \frac{0.25}{2.2\times10^{-4}} \end{bmatrix},\quad C = 5000\begin{bmatrix} 1 & 0 & -(\frac{L}{2}-l_2) & 0 & 0 & 0 \\ 1 & 0 & (\frac{L}{2}-l_2) & 0 & 0 & 0 \end{bmatrix} \text{ and } D = \begin{bmatrix} 0 & 0 \\ 0 & 0 \end{bmatrix}$$

The eigenvalues of the A matrix of the model obtained above correspond to the rigid body rotor modes and the current amplifier dynamics. These eigenvalues are the poles of the system. Table 3.3 gives the eigenvalues and their corresponding pole location on the s-plane.

Mode/Dynamic	**Eigenvalues**
Rigid body rotor	182.4
Rigid body rotor	-182.4
Rigid body rotor	259.4
Rigid body rotor	-259.4
Current amplifier	-4545.5
Current amplifier	-4545.5

Table 3.3 Pole locations of the Rigid Body model

From the magnetic bearing manual, the nominal transfer function for each of the on-board controllers is:

$$V_{controli} = \frac{1.41(1+8.9\times10^{-4}s)}{(1+3.3\times10^{-4}s)(1+2.2\times10^{-5}s)}V_{sensei} = C(s)V_{sensei}.$$

Finally, the specific commands in MATLAB convert the controller model C(s) to a state space model. This state space model has controller matrices acont, bcont, ccont and dcont representing the on-board controllers.

The MATLAB commands below are the rigid body analytical model for the system and it will be referred to as the "rigid body model" hereafter.

```
num=A;
den=[7.26e-09 3.52e-04 1];
 [acont,bcont,ccont,dcont]=tf2ss(num,den);
cont=pck(acont,bcont,-ccont,dcont);
sys=pck(A,B,C,D);
sysbar=starp(sys,cont);
[abar,bbar,cbar,dbar]=unpck(sysbar);
freq=logspace(1,5,200);
bode(abar,bbar,cbar,dbar,1,freq);
```

The Bode diagram of the rigid body analytical model in open loop is shown in Figure 3.9. Figure 3.10 shows the significant poles of the open loop rigid body analytical model.

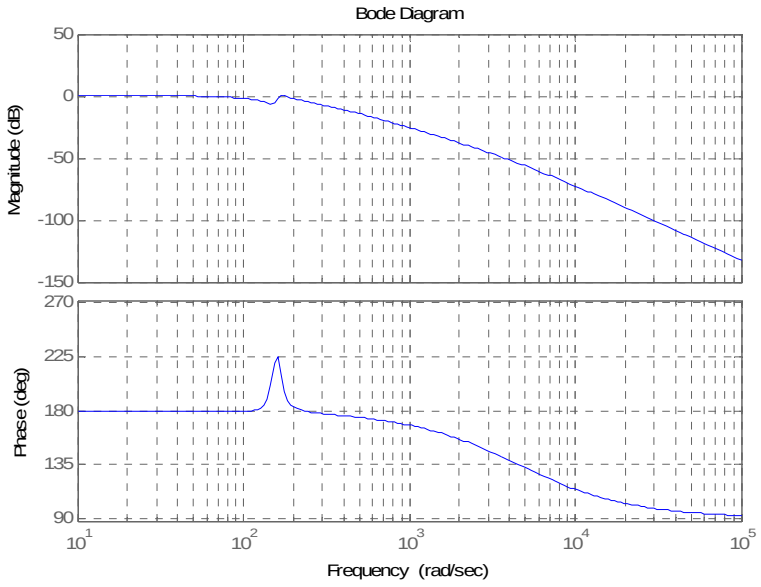

Figure 3.9 Bode diagram of the open loop rigid body analytical model

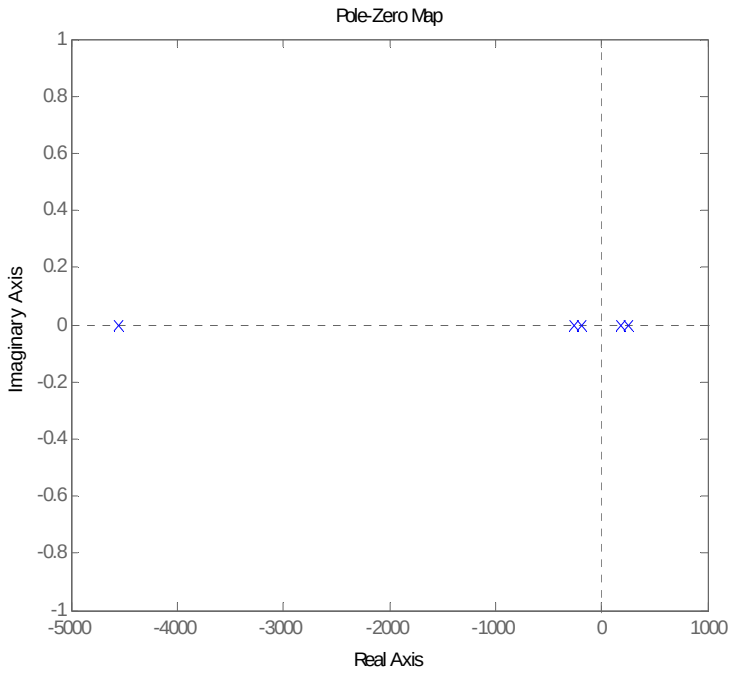

Figure 3.10 Significant poles of the open loop rigid body analytical model

Bending Body Model

In the previous analysis, it was assumed that the rotor is a rigid body. However, during levitation, the rotor does experience some bending. In this section, only two modes of the lowest frequency of bending mode will be modeled. These bending modes are described in Figure 3.11.

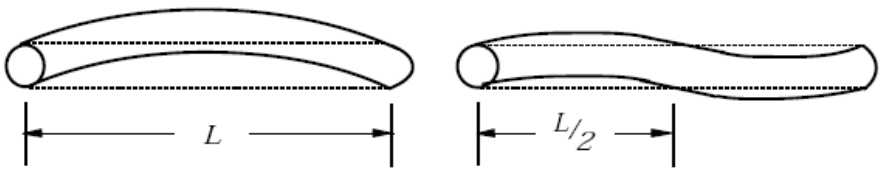

Figure 3.11 Two bending modes taken into account
Source: (Morse, Smith et al. 1995)

The bending model assumes that no rigid body motion is excited in the system; hence an equation of motion can be obtained by describing the system motion strictly due to the rotor bending. To achieve this equation, some matrices must be defined (Morse, Smith et al. 1995).

A vector of amplitude variables is defined by:

$$a \equiv \begin{bmatrix} a_1 \\ a_2 \end{bmatrix} \quad \text{..... 3.48}$$

Rotor displacements are defined by:

$$\begin{bmatrix} X_1 \\ X_2 \end{bmatrix} = \begin{bmatrix} -1.93745e+00 & -1.83546e+00 \\ -1.93745e+00 & 1.83546e+00 \end{bmatrix} \text{a} \quad \text{..... 3.49}$$

$$\begin{bmatrix} x_1 \\ x_2 \end{bmatrix} = \begin{bmatrix} -1.19029e+00 & -6.08354e-01 \\ -1.19029e+00 & -6.08354e-01 \end{bmatrix} \text{a} \quad \text{..... 3.50}$$

Mass matrix is defined by:

$$M = \begin{bmatrix} 2.72146e-01 & 0 \\ 0 & 2.62297e-01 \end{bmatrix} \quad \text{..... 3.51}$$

Stiffness matrix is defined by:

$$K = \begin{bmatrix} 6.05762e+06 & 0 \\ 0 & 4.4363e+07 \end{bmatrix} \quad \text{..... 3.52}$$

A vector forcing function is defined by:

$$P = \begin{bmatrix} -1.19029e+00 & -1.19029e+00 \\ -6.08354e-01 & 6.08354e-01 \end{bmatrix} \begin{bmatrix} F_1 \\ F_2 \end{bmatrix} \quad \text{..... 3.53}$$

The following differential equation describes the bending motion of the rotor:

$$M\ddot{a} + Ka = P \quad \text{..... 3.54}$$

There are similarities between the differential equation given above and the standard differential equation of motion for a spring/mass system. Hence, the rotor behaves much like an interconnection of springs and masses in bending mode (Morse, Smith et al. 1995).

From the differential equations described above, a state vector for the flexible body is defined as; $\dot{x}_f = \begin{bmatrix} \dot{a}_1 \\ \dot{a}_2 \\ \ddot{a}_1 \\ \ddot{a}_2 \end{bmatrix}$

As in the case of the rigid body, F_1 and F_2 are the input variables and X_1 and X_2 are the output variables. The bending mode equations expressed in state space form are as below:

$$\dot{x}_f = \begin{bmatrix} 0 & 0 & 1 & 0 \\ 0 & 0 & 0 & 1 \\ \frac{-6.05762e6}{0.272146} & 0 & 0 & 0 \\ 0 & \frac{-4.4363e7}{0.262297} & 0 & 0 \end{bmatrix} x_f + \begin{bmatrix} 0 & 0 \\ 0 & 0 \\ \frac{-1.19029}{0.272146} & \frac{-1.19029}{0.272146} \\ \frac{-0.608354}{0.262297} & \frac{0.608354}{0.262297} \end{bmatrix} \begin{bmatrix} F_1 \\ F_2 \end{bmatrix} \quad \text{..... 3.55}$$

$$\begin{bmatrix} X_1 \\ X_2 \end{bmatrix} = \begin{bmatrix} -1.93745 & -1.83546 & 0 & 0 \\ -1.93745 & 1.83546 & 0 & 0 \end{bmatrix} x_f \quad \text{..... 3.56}$$

The frequencies of oscillation are: $\pm\sqrt{\frac{-4.4363\times10^7}{0.262297}} = \pm 13005\, j\, \frac{rad}{\sec}$ and

$\pm\sqrt{\frac{-6.05762\times10^6}{0.272146}} = \pm 4718\, j\, \frac{rad}{\sec}$.

The equations of motion for the rotor have been derived in rigid body alone and bending motion alone. The rotor displacement can be expressed as a sum of the displacements due to rigid body motion and bending motion. Let F_1 and F_2 be the input variables; X_1 and X_2 be the output variables. The combined model is:

$$X_i = X_{r\_i} + X_{f\_i} \text{ and } X = \begin{bmatrix} X_1 \\ X_2 \end{bmatrix} = X_{total}.$$

Hence: $X_{total} = C_r x_r + C_f x_f$.

With the new state vector $x_{total} = \begin{bmatrix} x_0 \\ \dot{x}_0 \\ \theta \\ \dot{\theta} \\ a_1 \\ a_2 \\ \dot{a}_1 \\ \dot{a}_2 \end{bmatrix}$

The combined state space model is:

$$\dot{x}_{total} = \begin{bmatrix} 0 & 1 & 0 & 0 & 0 & 0 & 0 & 0 \\ 0 & 0 & 0 & 0 & 0 & 0 & 0 & 0 \\ 0 & 0 & 0 & 1 & 0 & 0 & 0 & 0 \\ 0 & 0 & 0 & 0 & 0 & 0 & 0 & 0 \\ 0 & 0 & 0 & 0 & 0 & 0 & 1 & 0 \\ 0 & 0 & 0 & 0 & 0 & 0 & 0 & 1 \\ 0 & 0 & 0 & 0 & -2.226e7 & 0 & 0 & 0 \\ 0 & 0 & 0 & 0 & 0 & -1.6913e8 & 0 & 0 \end{bmatrix} x_{total} + \begin{bmatrix} 0 & 0 \\ 3.8037 & 3.8037 \\ 0 & 0 \\ -69.5669 & 69.5669 \\ 0 & 0 \\ 0 & 0 \\ -4.3737 & -4.3737 \\ -2.3193 & 2.3193 \end{bmatrix} \begin{bmatrix} F_1 \\ F_2 \end{bmatrix} \quad \text{..... 3.57}$$

and the output equation is:

$$X_{total} = \begin{bmatrix} 1 & 0 & -0.1317 & 0 & -1.93745 & -1.83546 & 0 & 0 \\ 1 & 0 & 0.1317 & 0 & -1.93745 & 1.83546 & 0 & 0 \end{bmatrix} x_{total}. \quad \text{..... 3.58}$$

Using the linear approximations to the input and output non-linearities obtained previously and adding the actuator and sensor dynamics to the combined model described in equations 3.52 and 3.53, the new state space equation can be written as follows with $i_{control1}$ and $i_{control2}$ as input variables, and v_{sense1} and v_{sense2} as output variables:

$$\dot{x}_{total} = A_{total}x_{total} + \begin{bmatrix} 0 & 0 \\ \frac{3.5}{m} & \frac{3.5}{m} \\ 0 & 0 \\ -\frac{3.5}{I_0}(\frac{L}{2}-l) & \frac{3.5}{I_0}(\frac{L}{2}-l) \\ 0 & 0 \\ 0 & 0 \\ \frac{-3.5\times1.19029}{0.272146} & \frac{-3.5\times1.19029}{0.272146} \\ \frac{-3.5\times0.608354}{0.262297} & \frac{3.5\times0.608354}{0.262297} \end{bmatrix} \begin{bmatrix} i_{control1} \\ i_{control2} \end{bmatrix} \text{with} \quad \text{..... 3.59}$$

$$A_{total} = \begin{bmatrix} 0 & 1 & 0 & 0 & 0 & 0 & 0 & 0 \\ \frac{8750}{m} & 0 & 0 & 0 & \frac{-8750\times1.19029}{m} & 0 & 0 & 0 \\ 0 & 0 & 0 & 1 & 0 & 0 & 0 & 0 \\ 0 & 0 & \frac{1}{I_0}(\frac{L}{2}-l)^2\times8750 & 0 & 0 & \frac{1}{I_0}(\frac{L}{2}-l)\times8750\times0.608354 & 0 & 0 \\ 0 & 0 & 0 & 0 & 0 & 0 & 1 & 0 \\ 0 & 0 & 0 & 0 & 0 & 0 & 0 & 1 \\ \frac{-8750\times1.19029}{0.272146} & 0 & 0 & 0 & \frac{-6.05762e6+8750\times1.19029^2}{0.272146} & 0 & 0 & 0 \\ 0 & 0 & \frac{(\frac{L}{2}-l)*8750\times0.608354}{0.262297} & 0 & 0 & \frac{-4.4363e7+8750*0.608354^2}{0.262297} & 0 & 0 \end{bmatrix} \quad \text{..... 3.60}$$

The sensor dynamic only changes the output equation with the gain of 5000:

$$\begin{bmatrix} V_{sense1} \\ V_{sense2} \end{bmatrix} = 5000 \begin{bmatrix} 1 & 0 & -(\frac{L}{2}-l_2) & 0 & -1.93745 & -1.83546 & 0 & 0 \\ 1 & 0 & (\frac{L}{2}-l_2) & 0 & -1.93745 & 1.83546 & 0 & 0 \end{bmatrix} x_{total}$$

Adding the current amplifier dynamics described previously and letting $V_{control1}$ and $V_{control2}$ be input variables; and V_{sense1} and V_{sense2} output variables, with the new state vector can be expressed as:

$$x_{total} = \begin{bmatrix} x_0 \\ \dot{x}_0 \\ \theta \\ \dot{\theta} \\ a_1 \\ a_2 \\ \dot{a}_1 \\ \dot{a}_2 \\ i_{control1} \\ i_{control2} \end{bmatrix}$$ and the new dynamic matrix

$$A_{total} = \begin{bmatrix} 0 & 1 & 0 & 0 & 0 & 0 & 0 & 0 & 0 & 0 \\ \frac{8750}{m} & 0 & 0 & 0 & \frac{-8750\times1.19029}{m} & 0 & 0 & 0 & \frac{3.5}{m} & \frac{3.5}{m} \\ 0 & 0 & 0 & 1 & 0 & 0 & 0 & 0 & 0 & 0 \\ 0 & 0 & \frac{1}{I_0}(\frac{L}{2}-l)^2\times8750 & 0 & 0 & \frac{1}{I_0}(\frac{L}{2}-l)\times8750\times0.608354 & 0 & 0 & -\frac{3.5}{I_0}(\frac{L}{2}-l) & \frac{3.5}{I_0}(\frac{L}{2}-l) \\ 0 & 0 & 0 & 0 & 0 & 0 & 1 & 0 & 0 & 0 \\ 0 & 0 & 0 & 0 & 0 & 0 & 0 & 1 & 0 & 0 \\ \frac{-8750\times1.19029}{0.272146} & 0 & 0 & 0 & \frac{-6.05762e6+8750\times1.19029^2}{0.272146} & 0 & 0 & 0 & \frac{-3.5\times1.19029}{0.272146} & \frac{-3.5\times1.19029}{0.272146} \\ 0 & 0 & \frac{(\frac{L}{2}-l)\times8750\times0.608354}{0.262297} & 0 & 0 & \frac{-4.4363e7+8750\times0.608354^2}{0.262297} & 0 & 0 & \frac{-3.5\times0.608354}{0.262297} & \frac{3.5\times0.608354}{0.262297} \\ 0 & 0 & 0 & 0 & 0 & 0 & 0 & 0 & \frac{-1}{2.2e-4} & 0 \\ 0 & 0 & 0 & 0 & 0 & 0 & 0 & 0 & 0 & \frac{-1}{2.2e-4} \end{bmatrix} \quad \text{. 3.61}$$

The total body model state space description becomes:

$$\dot{x}_{total} = A_{total}x_{total} + \begin{bmatrix} 0 & 0 \\ 0 & 0 \\ 0 & 0 \\ 0 & 0 \\ 0 & 0 \\ 0 & 0 \\ 0 & 0 \\ 0 & 0 \\ \frac{0.25}{2.2e-4} & 0 \\ 0 & \frac{0.25}{2.2e-4} \end{bmatrix} \begin{bmatrix} V_{control1} \\ V_{control2} \end{bmatrix} \quad \text{..... 3.62}$$

with

$$\begin{bmatrix} V_{sense1} \\ V_{sense2} \end{bmatrix} = 5000 \begin{bmatrix} 1 & 0 & -(\frac{L}{2} - l_2) & 0 & -1.93745 & -1.83546 & 0 & 0 & 0 & 0 \\ 1 & 0 & (\frac{L}{2} - l_2) & 0 & -1.93745 & 1.83546 & 0 & 0 & 0 & 0 \end{bmatrix} x_{total} \quad \text{.... 3.63}$$

The eigenvalues of the state matrix of the model obtained above correspond to both the rigid body, the bending mode and the current amplifier dynamics. These eigenvalues are the poles of the system. Table 3.4 gives the mode of the eigenvalues and their corresponding pole locations on the s-plane.

Mode/Dynamic	**Eigenvalues**
Rigid body rotor	182.4
Rigid body rotor	-182.4
Rigid body rotor	259.4
Rigid body rotor	-259.4
Current amplifier	-4545.5
Current amplifier	-4545.5
Bending body rotor	0+j13477.934
Bending body rotor	0-j13477.934
Bending body rotor	0+j5071.6159
Bending body rotor	0-j5071.6159

Table 3.4 Eigenvalues of bending mode model

Using the MATLAB commands below, the total system model can be obtained and it will be referred to as the "total system model" hereafter:

```
num=[1.25e-03 1.41];
den=[7.26e-09 3.52e-04 1];
[acont,bcont,ccont,dcont]=tf2ss(num,den);
cont=pck(acont,bcont,-ccont,dcont);
sysb=pck(ab,bb,cb,db);
sysbarb=starp(sysb,cont);
[abarb,bbarb,cbarb,dbarb]=unpck(sysbarb);
freq=lospace(1,5,200);
bode(abarb,bbarb,cbarb,dbarb,1,freq);
```

$$a_b = \begin{bmatrix} 0 & 1 & 0 & 0 & 0 & 0 & 0 & 0 & 0 & 0 \\ \frac{8750}{m} & 0 & 0 & 0 & \frac{-8750\times 1.19029}{m} & 0 & 0 & 0 & \frac{3.5}{m} & \frac{3.5}{m} \\ 0 & 0 & 0 & 1 & 0 & 0 & 0 & 0 & 0 & 0 \\ 0 & 0 & \frac{1}{I_0}(\frac{L}{2}-l)^2\times 8750 & 0 & 0 & \frac{1}{I_0}(\frac{L}{2}-l)\times 8750\times 0.608354 & 0 & 0 & -\frac{3.5}{I_0}(\frac{L}{2}-l) & \frac{3.5}{I_0}(\frac{L}{2}-l) \\ 0 & 0 & 0 & 0 & 0 & 0 & 1 & 0 & 0 & 0 \\ 0 & 0 & 0 & 0 & 0 & 0 & 0 & 1 & 0 & 0 \\ \frac{-8750\times 1.19029}{0.272146} & 0 & 0 & 0 & \frac{-6.05762e6+8750\times 1.19029^2}{0.272146} & 0 & 0 & 0 & \frac{-3.5\times 1.19029}{0.272146} & \frac{-3.5\times 1.19029}{0.272146} \\ 0 & 0 & \frac{(\frac{L}{2}-l)\times 8750\times 0.608354}{0.262297} & 0 & 0 & \frac{-4.4363e7+8750\times 0.608354^2}{0.262297} & 0 & 0 & \frac{-3.5\times 0.608354}{0.262297} & \frac{3.5\times 0.608354}{0.262297} \\ 0 & 0 & 0 & 0 & 0 & 0 & 0 & 0 & \frac{-1}{2.2e-4} & 0 \\ 0 & 0 & 0 & 0 & 0 & 0 & 0 & 0 & 0 & \frac{-1}{2.2e-4} \end{bmatrix}$$

$$b_b = \begin{bmatrix} 0 & 0 \\ 0 & 0 \\ 0 & 0 \\ 0 & 0 \\ 0 & 0 \\ 0 & 0 \\ 0 & 0 \\ 0 & 0 \\ \frac{0.25}{2.2e-4} & 0 \\ 0 & \frac{0.25}{2.2e-4} \end{bmatrix}; \quad c_b = \begin{bmatrix} 1 & 0 & -(\frac{L}{2}-l_2) & 0 & -1.93745 & -1.83546 & 0 & 0 & 0 & 0 \\ 1 & 0 & (\frac{L}{2}-l_2) & 0 & -1.93745 & 1.83546 & 0 & 0 & 0 & 0 \end{bmatrix}; \quad \text{and}$$

$$d_b = \begin{bmatrix} 0 & 0 \\ 0 & 0 \end{bmatrix}$$

All the values of the variables can be found in Table 3.2.

The Bode diagram of the combined rigid body and bending mode analytical model in open loop is shown in Figure 3.12. Figure 3.13 shows the significant poles and zeros of the open loop combined rigid body and bending mode analytical model.

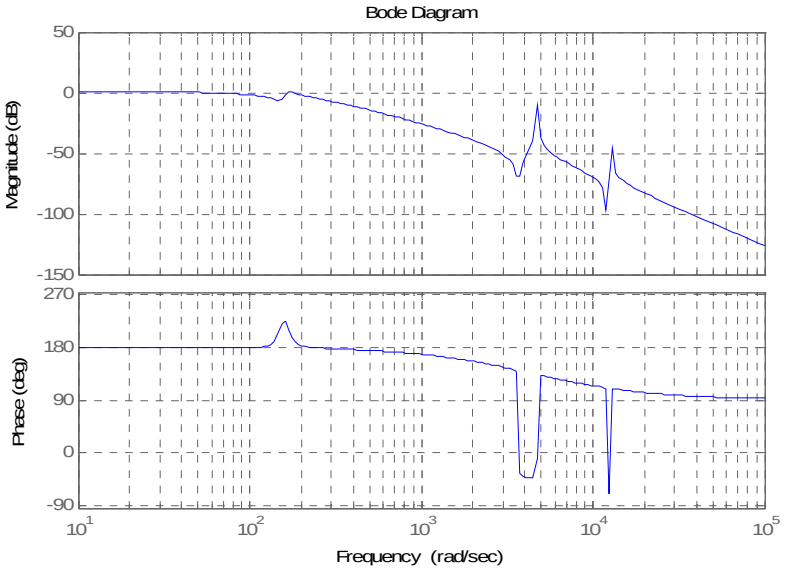

Figure 3.12 Bode diagram of the open loop combined rigid body and bending mode analytical model

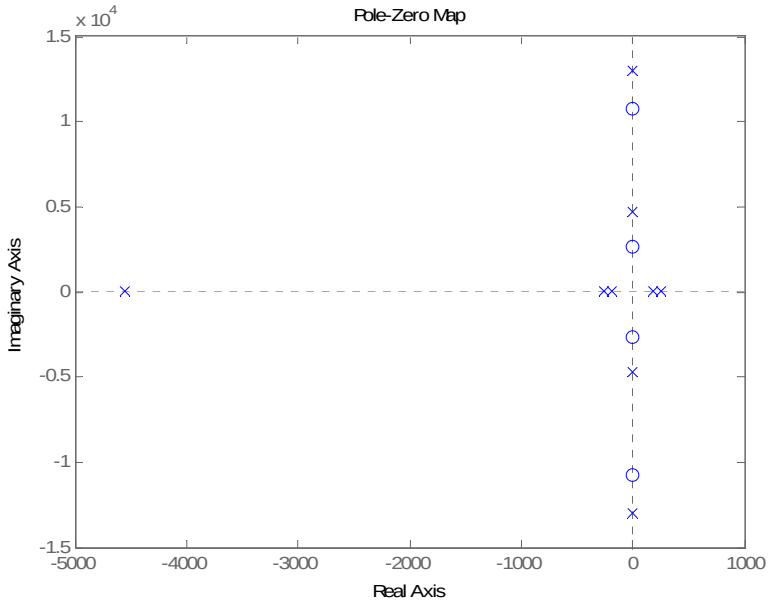

Figure 3.13 Significant poles and zeros of the open loop combined rigid body and bending mode analytical model

3.4 Magnetic Bearing System Identification

Experimental Set-up

Experimental determination of a system model is an important part of the modeling process in control engineering. This phase of modeling is referred to as system identification. The chosen approach to obtain the transfer function of the MBC 500 AMB system was to measure the frequency response of the closed-loop system. As previously mentioned, an AMB is inherently unstable; this is the reason behind performing a closed-loop experiment. Figure 3.14 is a block diagram of the setup used to collect the data.

The output from the function generator is sinusoidal signal with a frequency range of 10 Hz to 3.05 KHz and a peak magnitude of 500mV. A 4 KHz *Low Pass Filter (LPF)* is used in order to limit the high frequency noise and a ±10V *Voltage Limiter* is required to ensure high voltages do not reach the DSP card. The DSP consists of input-output channels with analog-to-digital converters (ADC) and digital-to-analog converters (DAC). The ADC transforms the sinusoidal signal input into discrete form, while the DAC transforms the discrete form into the sinusoidal signal. The output from the card is stored in a data file, which contains three data columns, namely, frequency, magnitude and phase.

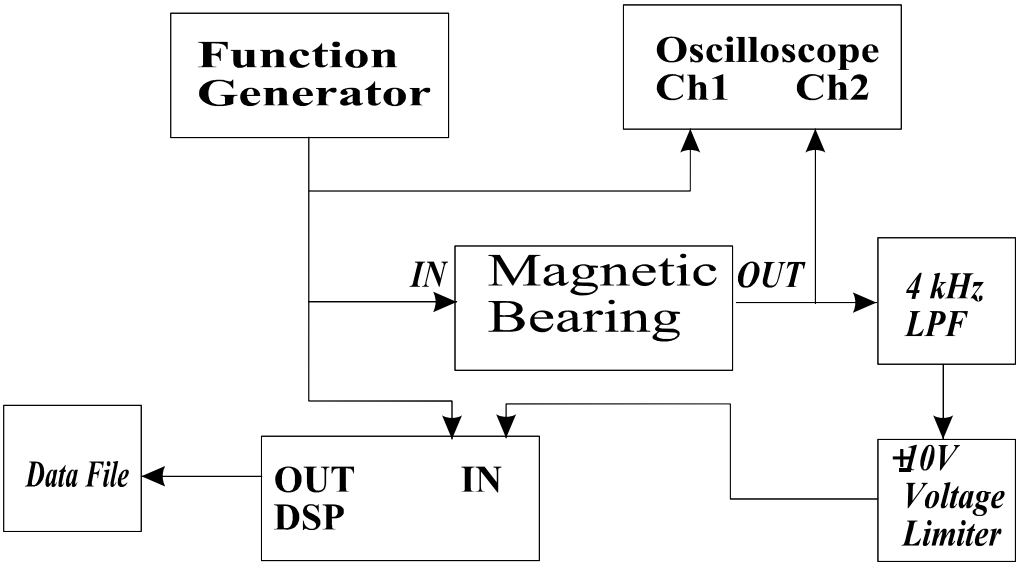

Figure 3.14 Block diagram of a system identification setup

Setting-Up the Magnetic Bearing for testing

The magnetic bearing system configuration is as shown on the magnetic bearing front panel block diagram in Figure 3.15. The bearing system contains four-on-board controllers. The on-board controllers levitate the bearing (Morse, Smith et al. 1996).

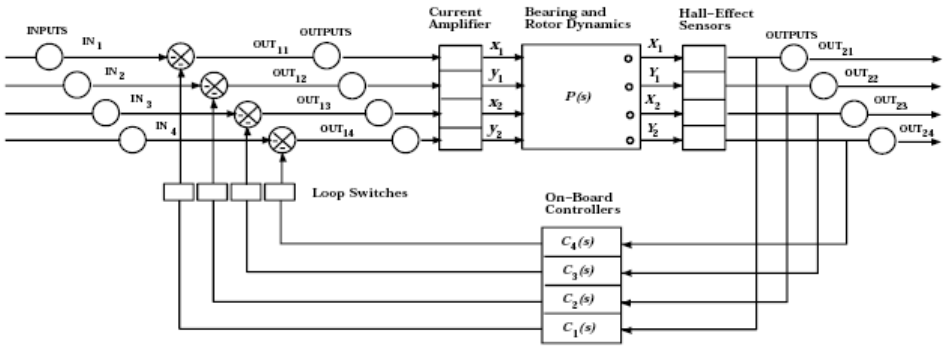

Figure 3.15 Magnetic bearing block diagram
Source: (Morse, Smith et al. 1996)

The magnetic bearing is an unstable system. If any on-board controllers are disconnected, then the rotor will hit the touch-down bushings in the bearing housings which form a physical limit for the rotor. Because of this instability, any data from the

bearing which will be used for determining the transfer function must be taken while the bearing is controlled. In short, the magnetic bearing experiment must be performed in closed-loop system identification rather than in more direct open-loop system identification techniques (Morse, Smith et al. 1996).

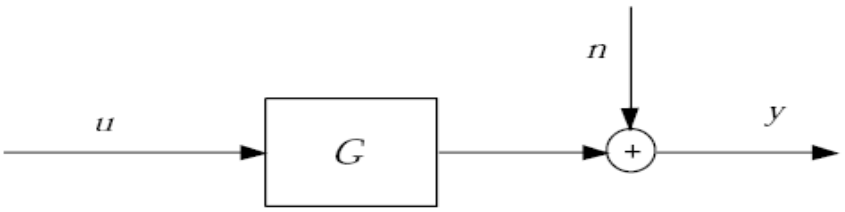

Figure 3.16 Magnetic bearing block diagram – open loop
Source: (Morse, Smith et al. 1996)

One of the major problems of system identification is to estimate the transfer function in the presence of noise. Suppose the system *G* in Figure 3.16 is to be identified. If *G* is stable, then the system will be performed in open-loop system identification. If an input u is applied and the response y is recorded, and the relationship becomes:

$$y = Gu + n \quad \text{..... 3.64}$$

Dividing y by *u* gives

$$\frac{y}{u} = G + \frac{n}{u} \quad \text{..... 3.65}$$

which can be used to estimate *G*. Typically, the output data y is collected over an extended period of time and the response *y/u* is averaged to determine an approximate transfer function for the bearing system. This process is valid for the open-loop system where u is uncorrelated with *n*. Since for most systems *n* has zero mean, the term *n/u* will average to zero and its effect on the average *y/u* will be minimal leading to the desired transfer function approximation (Morse, Smith et al. 1996):

$$G \cong \frac{y}{u} \quad \text{..... 3.66}$$

If, *u* were correlated with *n*, then the term *n/u* would not average to zero and would add to and corrupt the estimate of *G*.

For the closed-loop system configuration shown in Figure 3.17, the *y/u* = *G* + *n/u* again holds; however, the input *u* can be expressed as follows (Morse, Smith et al. 1996):

$$u = \frac{1}{1+GC} r - \frac{C}{1+GC} n \quad \text{..... 3.67}$$

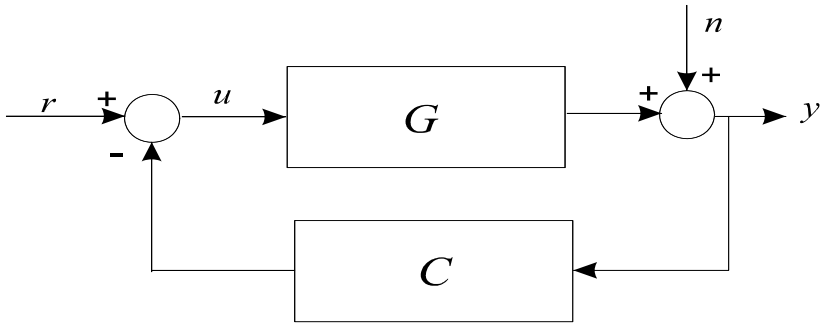

Figure 3.17 Magnetic bearing block diagram – closed loop
Source: (Dorf and Bishop 1995)

From the above equation, it is clearly showed that *u* and *n* are correlated, and therefore the term *n/u* will not average to zero as *y/u* is averaged. Since the effect of the noise on the system response cannot be neglected, its effect on the system estimate has to be found. Furthermore, *y/u* can be expressed in the following way (Morse, Smith et al. 1996):

$$\frac{y}{u} = \frac{n+Gr}{r-Cn} \quad \text{..... 3.68}$$

Notice that as *n* becomes small compared to *r*, *G* can be obtained using *y/u*:

$$\frac{y}{u} \cong G \quad \text{3.69}$$

However, if *n* is large compared to *r*, then *y/u* will yield:

$$\frac{y}{u} \cong -\frac{1}{C} \quad \text{3.70}$$

The actual system data *y/u* will be somewhere in between *G* and *-1/C*. However, without the exact knowledge of the noise *n*, *G* cannot be found. Consequently, the accuracy of the transfer function approximation depends on the relative size of *r* and *n* (Morse, Smith et al. 1996).

The following two-step, closed-loop system identification procedure avoids the noise problems of the process describe above. The system response can be expressed as follows (Morse, Smith et al. 1996):

$$y = \frac{G}{1+GC} r + \frac{1}{1+GC} n \quad \text{3.71}$$

Because the signal *r* and *n* are uncorrelated and the signal *n* has zero mean, the system response can be averaged as follows:

$$T_{yr} \overset{\Delta}{=} \frac{G}{1+GC} \cong \frac{y}{r} \quad \text{3.72}$$

This approximation becomes equal if the averaging is performed over an infinite time interval. Similarly:

$$u = \frac{1}{1+GC} r - \frac{C}{1+GC} n \quad \text{3.73}$$

And averaging gives:

$$T_{ur} \overset{\Delta}{=} \frac{1}{1+GC} \cong \frac{u}{r} \quad \text{..... 3.74}$$

Clearly, both T_{yr} and T_{ur} can be estimated without a noise bias. By simply dividing T_{yr} by T_{ur} , an unbiased estimate of the system response can be estimated as follows:

$$G = \frac{T_{yr}}{T_{ur}} \cong \frac{y/r}{u/r} \quad \text{..... 3.75}$$

Obtaining Frequency Response Data

Figure 3.18 shows the set up for obtaining the frequency response data in order to determine the transfer function T_{yr}. In this bearing configuration, the "Source" signal is the system input and OUT_{21} is the system output, yielding the transfer function $T_{yr}=y/r$. The range of frequency is from 0 Hz to 4000 Hz. As the data is taken, the amplitude can be adjusted during the experiment. This adjusted amplitude process is necessary in order to avoid certain resonances within the system. The rotor resonances are around 800 Hz and 2000 Hz (Morse, Smith et al. 1996).

A point to note is that, if the bearing hits one of its physical limits and makes a loud noise, it is an indication that the system is unstable at certain frequencies. However, this is not dangerous. Despite the fact that there is no danger, the process will corrupt the data so the experiment process must be stopped for a while before it can be turned on again (Morse, Smith et al. 1996).

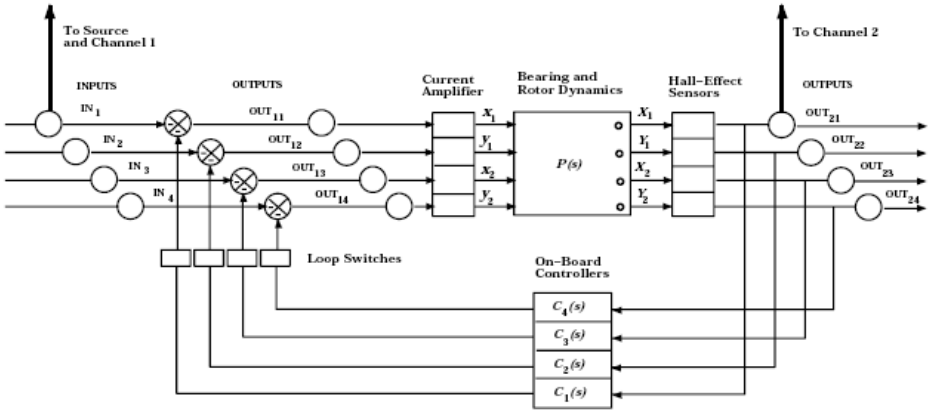

Figure 3.18 Bearing connections for estimation of T_{yr}
Source: (Morse, Smith et al. 1996)

The second step of the identification process is to estimate the transfer function $T_{ur} \cong u/r$. Figure 3.19 shows the bearing connections described above. Repeat the same process as for T_{yr} to get the frequency response data for determining T_{ur}.

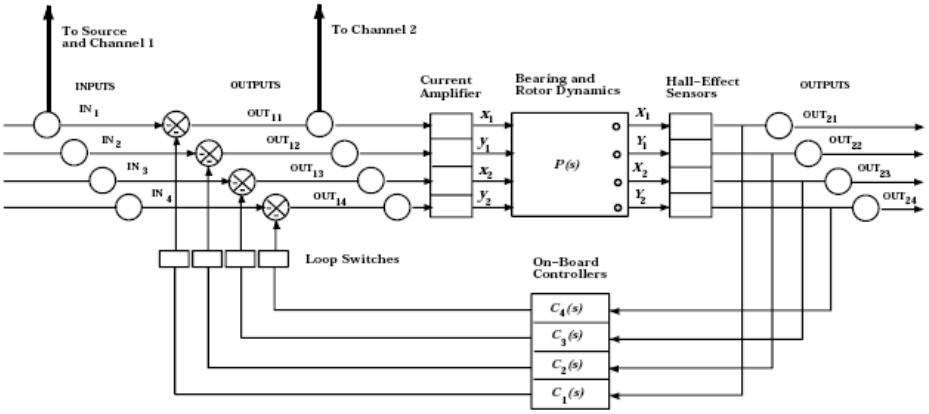

Figure 3.19 Bearing connections for estimation of T_{ur}
Source: (Morse, Smith et al. 1996)

Data Obtained

There are two sets of experimental results obtained. The first set is *yr* which is the response from input *r* to output *y*. The second is *ur* which is the response from input *r* to output *u*. A few simple MATLAB commands can be used to manipulate the data and plot the resulting Bode diagram. For a list of the MATLAB commands and the experimental data see Appendix A and B, respectively. Figure 3.20 and 3.21 show Bode diagram of each separate data collection.

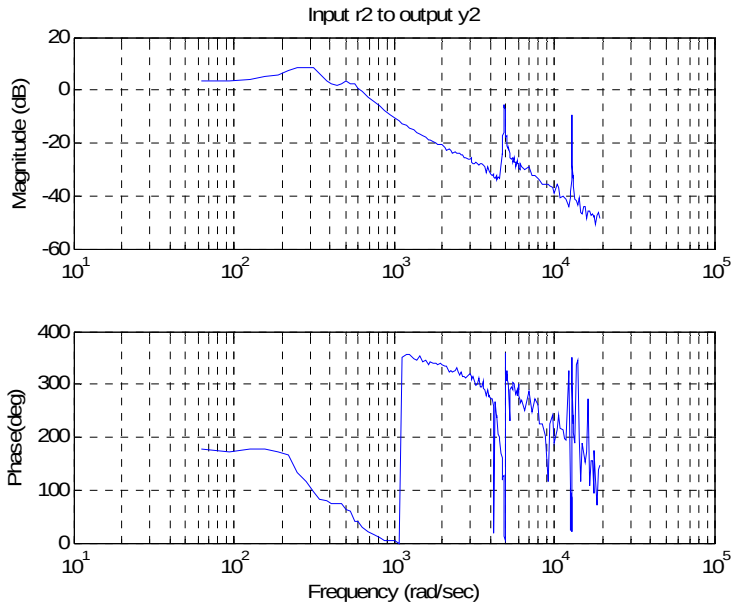

Figure 3.20 Input *r* to output *y*

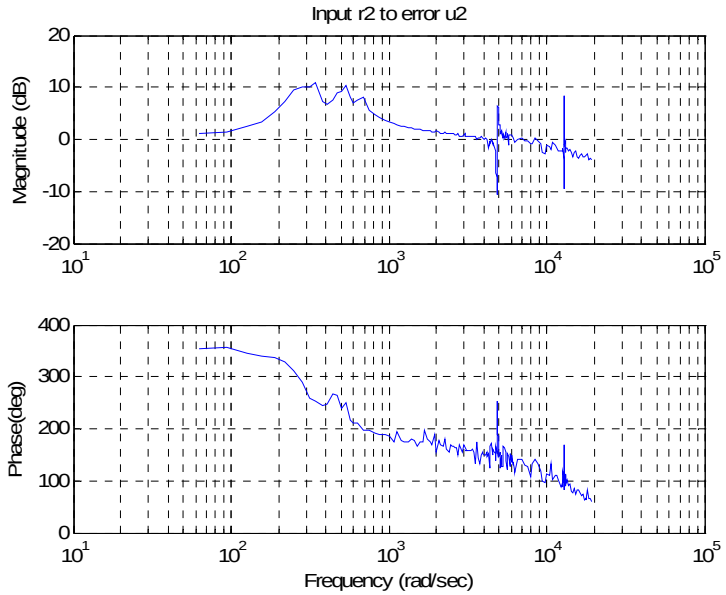

Figure 3.21 Input *r* to error *u*

Use of MATLAB System Identification Toolbox to obtain the model

MATLAB can be utilized to obtain a model for the data collected. The 'System Identification' toolbox in MATLAB is essential in this process, in that it requires specific functions to manipulate the data to achieve a system model. These commands can be put into a MATLAB m-file 'channel2.m', which can be viewed in the Appendix A. This m file fits a model to the data collected and calculates a transfer function according to the fit. Figure 3.22 shows the Bode plot of the transfer function between $V_{control1}$ and V_{sense1}. Figure 3.23 is a pole-zero map of the fitted model. Table 3.5 shows the zeros and poles of the identified model.

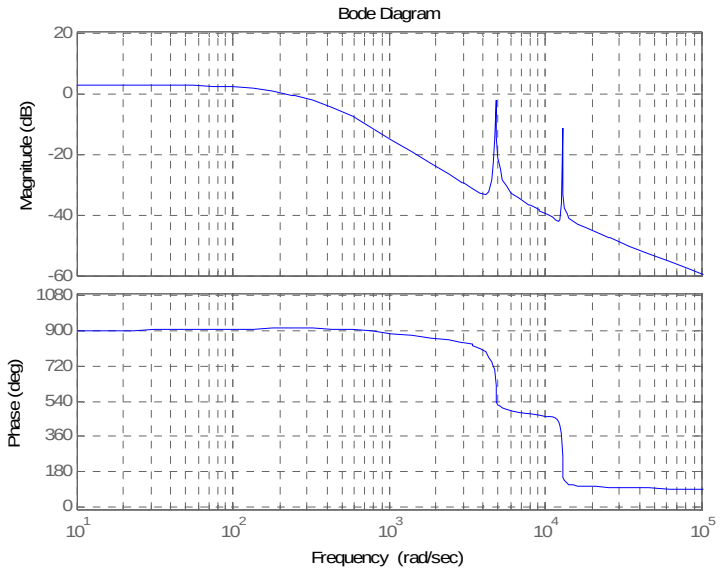

Figure 3.22 Bode plot of fitted model for transfer function between $V_{control1}$ and V_{sense1}

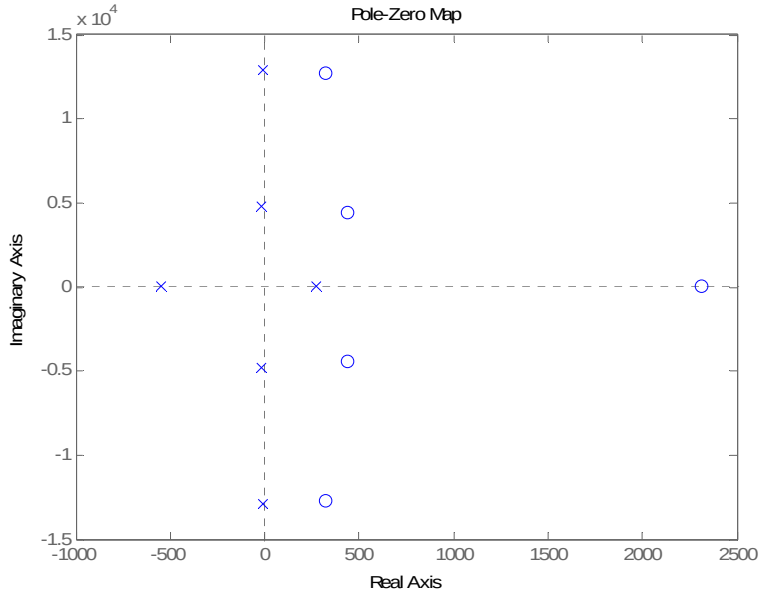

Figure 3.23 Pole-zero map of fitted model

Zeros	**Poles**
$323 + j12729$	$-12 + j12909$
$323 - j12729$	$-12 - j12909$
$441 + j4466$	$-17 + j4842$
$441 - j4466$	$-17 - j4842$
2311	-549
	270

Table 3.5 Poles and zeros of the identified model

3.5 Summary

This chapter has given brief information on the MBC500 magnetic bearing system parameters. The analytical model of the MBC500 magnetic bearing system has arrived at by drawing on physics principle. Both the rigid body model and bending body model have been described above. Finally, system identification, which includes data acquisition and parameter estimation, has also been presented.

4 Notch Filter and Conventional Controller Design and Implemetation for the MBC 500 Magnetic Bearing System

4.1 Overview

In this chapter the investigation of the conventional controller design process is reported. This chapter firstly describes the design of notch filters based on the resonant frequencies identified in the previous chapter. It then considers the design of the lead compensator to stabilise a single loop of the MBC 500 magnetic bearing system. Finally, the implementation of the designed conventional controller and notch filters for the MBC 500 magnetic bearing system in real time is reported.

4.2 Notch Filter Design

Notch Filtering of Resonant Modes

As can be seen from the previous chapter, both the analytical and experimental models consist of two resonant modes. The two resonant modes show a large increase in magnitude and a large fluctuation in phase on the frequency response Bode plot around the resonant frequencies. These resonant frequency points are located at approximately 749 Hz and 2069 Hz in the model, shown in the previous chapter. Resonant modes threaten the stability of the closed loop system. As a consequence, notch filters must be designed to filter out these two unwanted resonant frequencies. This is the first phase of the controller design, so as to get rid of unwanted characteristics.

The resonances constrain the choice of the controller *C(s)*. If the resonances were not in the system there would be more flexibility in the design of the controller *C(s)*.

Therefore, it is necessary to 'notch out' the two resonant modes in order to cancel the effect of the resonant frequencies. Hence, they will not have a significant effect on the stability. However, the filters must cancel out the resonant effect at almost exact position otherwise they threaten the stability of the system.

The magnetic bearing closed-loop system can be described by the block diagram shown in Figure 4.1. Figure 4.2 shows the controller $C_1(s)$ that was designed to stabilise the system.

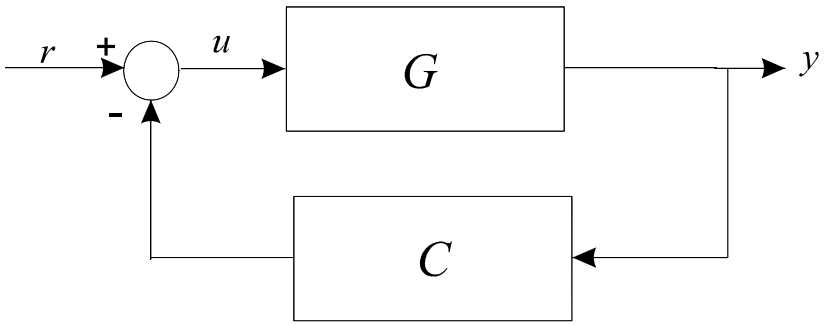

Figure 4.1 Magnetic bearing closed-loop configuration
Source: (Morse, Smith et al. 1996)

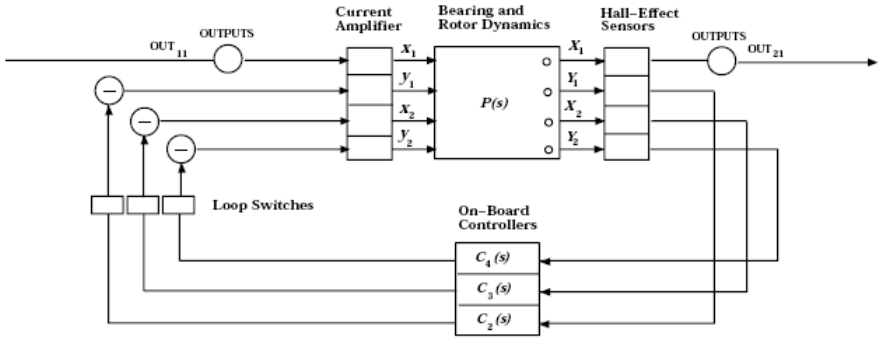

Figure 4.2 Magnetic bearing system
Source: (Morse, Smith et al. 1996)

Moreover, the notch filter's characteristic is shown in Figure 4.3 and has a transfer function defined by:

$$N(s) = a_2 \frac{s^2 + \omega_0^{\ 2}}{s^2 + s\frac{\omega_0}{Q} + \omega_0^{\ 2}} \quad \text{.....4.1}$$

where DC gain=high frequency gain=a_2

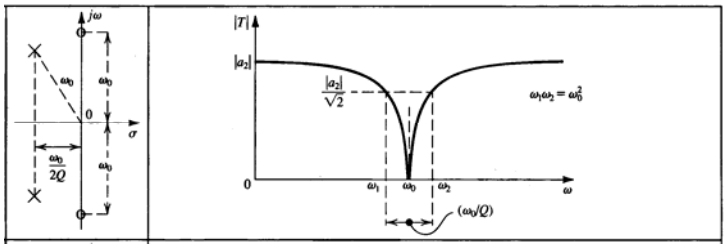

Figure 4.3 Notch filter characteristics

Source: (Morse, Smith et al. 1996; Revell 2000; Sedra and Smith 2004)

The above Figure shows an example of a resonance response curve. This method was used to determine the notch filters required to notch out the resonances.

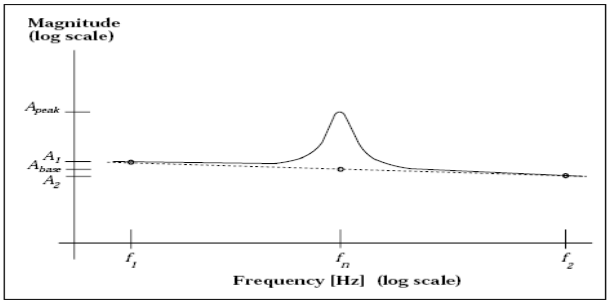

Figure 4.4 Approximation resonance Q from frequency data

Source: (Sedra and Smith 2004)

The resonance occurs at frequency f_n Hz with a corresponding magnitude A_{peak}. Two points need to be selected f_1 and f_2 either sides of the peak and on a section of the curve that is not affected by the resonance (Morse, Smith et al. 1996; Revell 2000) such that:

$$\frac{f_1}{f_n} = \frac{f_n}{f_2} \quad \text{.....4.2}$$

Alternatively,

$$f_2 = \frac{f_n^{\,2}}{f_1} \quad \text{.....4.3}$$

These places f_1 and f_2 are equidistant from f_n on a log scale. The magnitude of these points has a corresponding magnitude of A_1 and A_2, which form an average (Morse, Smith et al. 1996; Revell 2000):

$$A_{base} = \frac{A_1 + A_2}{2} \quad \text{.....4.4}$$

With the above information, the damping of the resonance mode Q can be estimated. The transfer function for a general resonance pole-pair, assuming unity gain at DC, can be written in the following form (Morse, Smith et al. 1996; Revell 2000):

$$G_{RES}(s) = \frac{\omega_0^{\,2}}{s^2 + s\frac{\omega_0}{Q} + \omega_0^{\,2}} \quad \text{.....4.5}$$

where ω_0 is the resonant frequency in radians per second. Drawing on (Morse, Smith et al. 1996; Revell 2000), if the resonance transfer function is evaluated at the resonant frequency ω_0, $G_{RES}(s)$ becomes

$$G_{RES}(j\omega_0) = \frac{\omega_0^{\,2}}{j\frac{\omega_0^{\,2}}{Q}} \quad \text{.....4.6}$$

and

$$\left|G_{RES}(j\omega_0)\right| = Q \quad \text{.....4.7}$$

The total bearing system can be expressed as a product of the resonance transfer function and the rest of the system (Morse, Smith et al. 1996; Revell 2000):

$$\left|G_{RES}(j\omega_0)\right| = \left|G_{SYS}(j\omega_0)G_{RES}(j\omega_0)\right| = \left|G_{SYS}(j\omega_0)\right|Q \quad \text{.....4.8}$$

The peak at the resonance frequency f_n is known (Morse, Smith et al. 1996; Revell 2000):

$$\left|G(j\omega_0)\right| = A_{peak} \quad \text{.....4.9}$$

and the system magnitude (Morse, Smith et al. 1996; Revell 2000):

$$\left|G_{SYS}(j\omega_0)\right| \cong A_{base} \quad \text{.....4.10}$$

Therefore, Q and ω_0 can be approximated by (Morse, Smith et al. 1996; Revell 2000):

$$Q \cong \frac{A_{peak}}{A_{base}} \quad \text{.....4.11}$$

$$\omega_0 = 2\pi f_n \quad \text{.....4.12}$$

Having equations relating the system plots for Q and ω_0, both the transfer functions for the general resonance and the notch filters can be determined for both resonant frequencies.

Design of Notch Filters based on the Analytical Model

With all the theory from the previous section, both notch filters were designed based on the analytical model. Tables 4.1 and 4.2 give the frequency points of interest and the calculated variables.

	Resonance 1		**Resonance 2**	
	Freq (Hz)	**Peak (log)**	**Freq (Hz)**	**Peak (log)**
f_n	749.62	0.32359	2069.01	0.00549
f_1	595.24	0.00038	1893.94	1.348e-5
f_2	945.38	0.00263	2260	0.00033388

Table 4.1 Frequency points of interest

	Resonance 1	**Resonance 2**
A_{base}	0.001505229	0.000176167
Q	214.9797291	31.19433318
ω_o	4710	13000
ω_o^2	2.21841E+07	1.69000E+08

Table 4.2 Calculated variables

From these calculations, the analytical notch filters are:

$$N_1(s) = \frac{s^2 + 2.218e7}{s^2 + 21.909s + 2.218e7} \quad \text{.....} \quad 4.13$$

$$N_2(s) = \frac{s^2 + 1.69e8}{s^2 + 416.74s + 1.69e8} \quad \text{.....} \quad 4.14$$

The two notch filters can be plotted on the same Bode diagram as the bending system model.

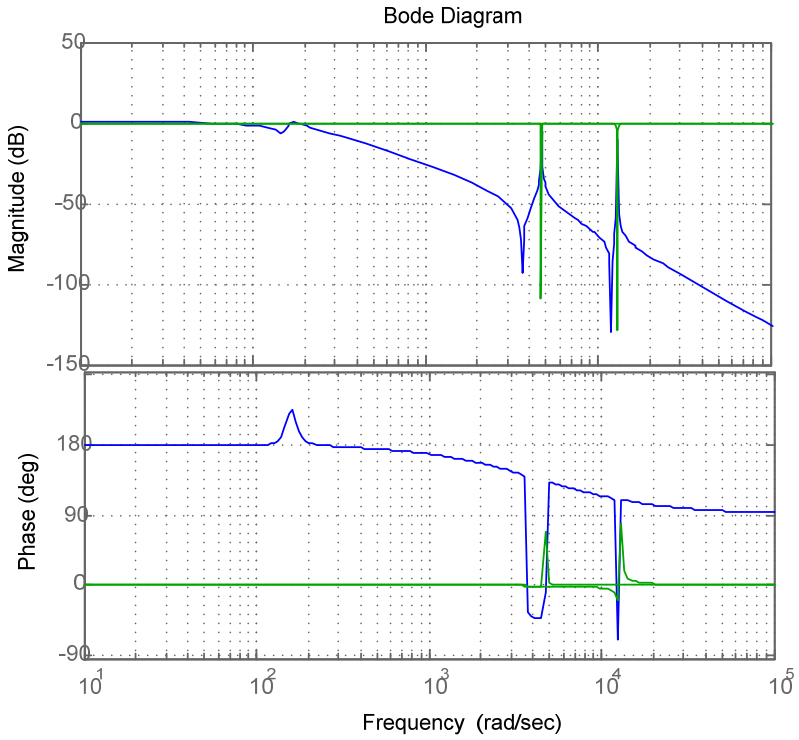

Figure 4.5 Bode plot of bending model and notch filters

Figure 4.5 above shows that the notches occur exactly at the resonant frequencies, as desired. This will cancel out the effect that the resonance modes bring into the system. However, the resonant modes of the model obtained via system identification must also be taken into account because the resonant frequencies were measured in the real system. Therefore, the resonant frequencies of the experimental model must be obtained. These can be determined from the model bode plot.

Design of Notch Filter based on the Identified Experimental Model

In this section, the notch filters were designed based on the experimental model. Tables 4.3 and 4.4 give the frequency points of interest and the calculated variables.

	Resonance 1		**Resonance 2**	
	Freq (Hz)	**Peak (log)**	**Freq (Hz)**	**Peak (log)**
f_n	770.31	0.777141319	2053.1	0.266072506
f_1	671.63	0.021877616	1893.94	0.008128305
f_2	884.90	0.031622777	2212.25	0.009549926

Table 4.3 Frequency points of interest

	Resonance 1	**Resonance 2**
A_{base}	0.026750196	0.008839116
Q	29.051799	30.10171161
ω_o	4840	12900
ω_o^2	2.34e7	1.664e8

Table 4.4 Calculated variables

Based on the frequency information and the calculated values shown in the above Tables, the transfer functions of the designed notch filters can be shown as follows:

$$N_1(s) = \frac{s^2 + 2.34e7}{s^2 + 166.59s + 2.34e7} \quad \text{.....} \quad 4.15$$

$$N_2(s) = \frac{s^2 + 1.664e8}{s^2 + 428.54s + 1.664e8} \quad \text{.....} \quad 4.16$$

The two notch filters can be plotted on the same Bode diagram as the bending system model.

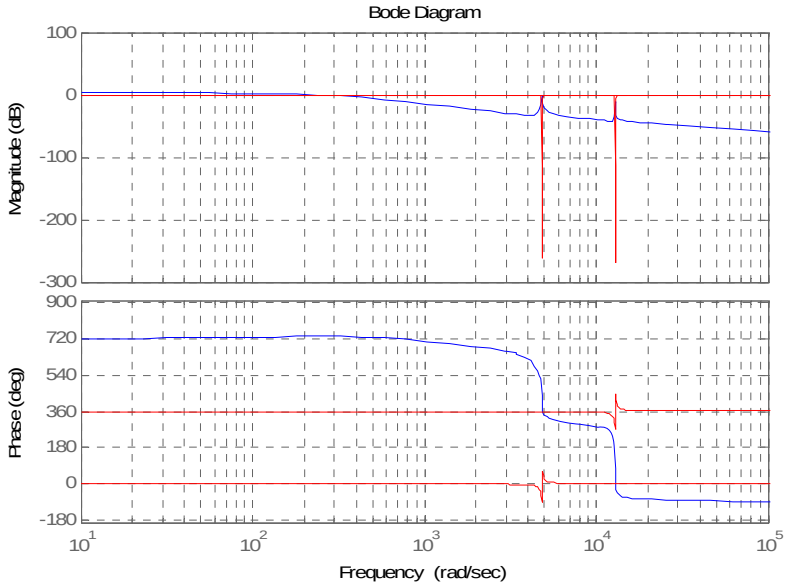

Figure 4.6 Bode plot of the identified model and notch filters

Figure 4.6 shown above shows that the notches occur at the resonant frequencies; this was the desired outcome. These notches will cancel out the effect that the resonance modes bring into the system.

4.3 Lead Compensator Design

Lead Compensator Theory

The MBC 500 magnetic bearing system has four internal lead compensators for stabilisation. A lead compensator will also be designed and implemented using the DSP card in order to stabilise the magnetic bearing system. The first design stage is based on the analytical rigid body model where the shaft is a point mass with no angle variable θ.

The bode plot for a typical lead compensator is given in Figure 4.7.

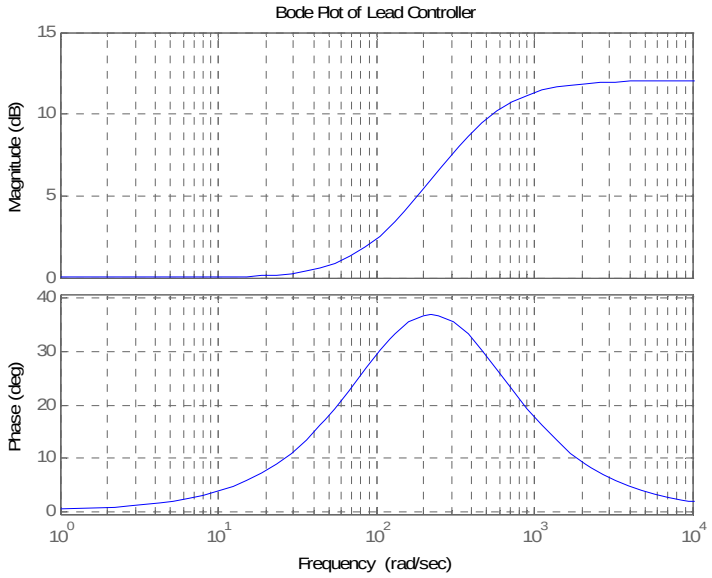

Figure 4.7 Lead compensator bode plot

A general transfer function of a lead compensator is as follows:

$$C(s) = \frac{k(s+\frac{1}{\alpha\tau})}{(s+\frac{1}{\tau})} \quad \text{with } \alpha > 1 \qquad \text{4.17}$$

The transfer function of low pass filter is given below:

$$LPF = \frac{2\pi f_L}{s + 2\pi f_L} \qquad \text{4.18}$$

The combined transfer function of lead compensator and low pass filter are:

$$C(s) = \frac{k(s+\frac{1}{\alpha\tau})}{(s+\frac{1}{\tau})} \frac{2\pi f_l}{s + 2\pi f_l} \qquad \text{4.19}$$

A lead compensator provides a positive (lead) phase angle $\phi_{\max}$ where:

$$\phi_{\max} = \sin^{-1}\left(\frac{\alpha - 1}{\alpha + 1}\right) \qquad \text{4.20}$$

Occurring at

$$\omega_{\max} = \frac{1}{\sqrt{\alpha\tau}} \quad \text{.....} \quad 4.21$$

For a system to be stable, it must have a positive phase margin. The lead compensator adds positive phase to the system in a given frequency range. The positive phase margin specification implies that at the gain crossover frequency, the phase plot must be less than 180 degrees, to ensure stability. An important aspect to note about lead compensators is that they are high pass filters. This feature is not always desired. Therefore, a low pass filter shown in equation 4.18 must be added to the lead compensator to get rid of the high frequency noises which can affect the stability of the magnetic bearing system.

Design of Lead Compensator

Rigid Body Point Mass Design

The first step of the lead compensator design is to stabilise the rigid body system using the rigid body model shown in equations 3.13 and 3.14 in Chapter 3. The model can be simplified by keeping the unstable pole pair and ignoring the dynamics of other poles and zeros but keeping the same DC gain. This model can be further simplified using the rigid body point mass system. However, the physical meaning of a point mass system must be known. Looking at the rotor in the rigid body case, it can still move up and down and sometimes one end will move higher than the other. This diagonal movement provides an angle θ (see Figure 4.8).

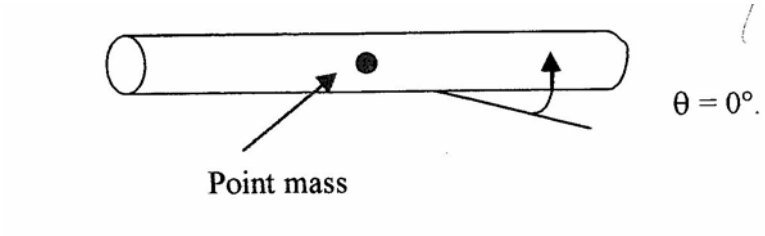

Figure 4.8 Point mass diagram

The angle is defined in the state-space representation system vector. From the results obtained in Chapter 3 for output matrix C_r with respect to output V_{sense} it was found that:

$$\begin{bmatrix} V_{sense_1} \\ V_{sense_2} \end{bmatrix} = \begin{bmatrix} 5000 & 0 & -658.5 & 0 & 0 & 0 \\ 5000 & 0 & 685.5 & 0 & 0 & 0 \end{bmatrix} \begin{bmatrix} x_0 \\ x_0 \\ \theta \\ \theta \\ i_{c_1} \\ i_{c_2} \end{bmatrix}$$

Noting that there is a value in matrix C_r for the angle θ of -685.5 and 685.5 for the outputs V_{sense1} and V_{sense2} respectively. However, these values should be set to 0; therefore there is no diagonal movement of the rotor. The simplified transfer function for the system becomes:

$$G_{point\,mass}(s) = \frac{75642e7}{(s+182.4)(s-182.4)(s+4546)} \quad \text{..... 4.22}$$

The transfer function defined as $G_{pointmass}(s)$ comes from the rigid body model derivation. However there are only three system poles instead of six for simplicity. The other two pole pairs, due to the rigid body at $s = \pm 259.4$, have been excluded because the focus is on one channel. The current amplifier pole at $s = -4545.5$ has also been ignored.

Using the rltool function in MATLAB, the lead compensator pole and zero can be placed at the optimum positions. Figure 4.9 shows the rltool design window. Moreover, Figure 4.10 is a zoomed out plot of the root locus diagram of the new rigid body point mass system with the compensator $C_{lead1}(s)$ incorporated. As can be seen, the red points are the closed loop poles, and it can be shown that the system is stable because the red points are on the left half of the s-plane.

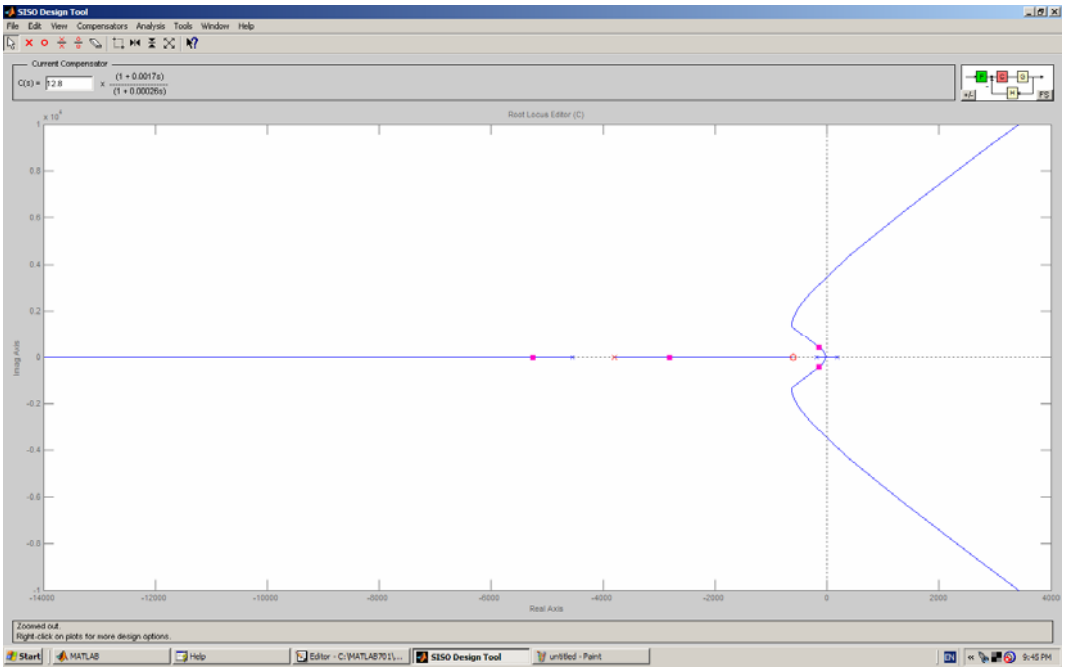

Figure 4.9 Rltool function window in MATLAB with $C_{lead1}(s)$

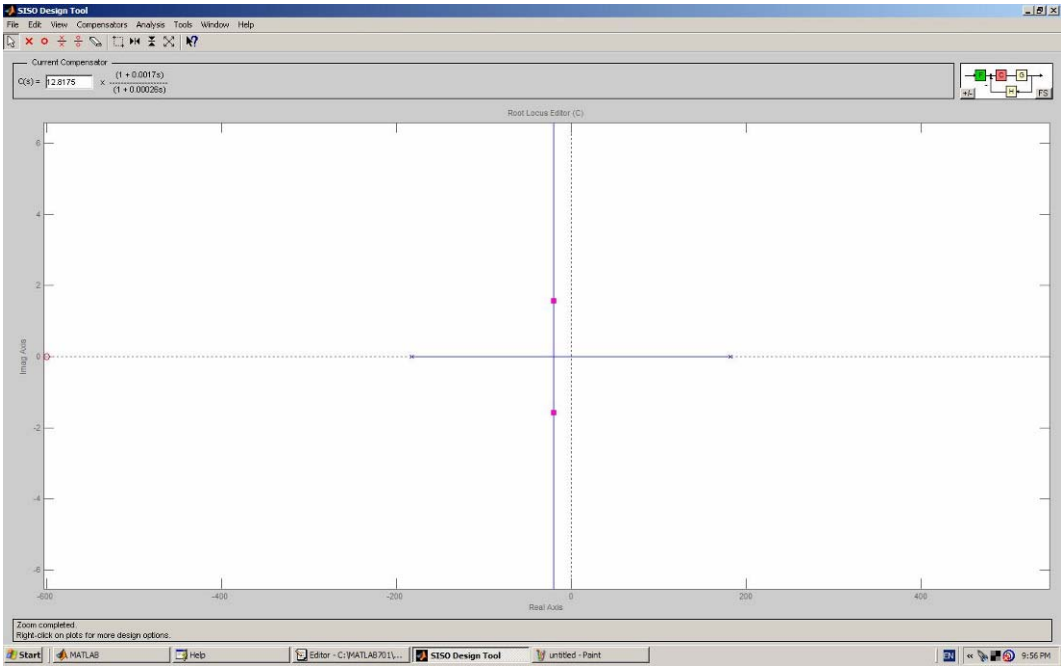

Figure 4.10 Zoomed root locus of $G_{pointmass}(s)$ with lead compensator

The transfer function of the lead compensator is thus obtained as:

$$C_{lead_1}(s) = \frac{12.8175(s+600)}{(s+3800)} \quad \text{.....} \quad 4.23$$

This can be compared to the on-board controller in the system parameter reported in Chapter 3:

$$C(s) = \frac{1.41(1+8.9e-4s)}{(1+3.3e-4s)(1+2.2e-5s)}$$

$$C(s) = \frac{3.78(s+1128)}{(s+3030)} \frac{45454.5}{(s+45454.5)} \quad \text{.....} \quad 4.24$$

The given controller is broken into two functions, one is the lead compensator and the other one is a low pass filter. The low pass filter will cut off unknowns about the system 45454.5 rad/sec (7234 Hz). This low pass filter has no effect on the low frequency system dynamics as the filter is more than ten times the bandwidth.

This compensator designed should work but unfortunately when it was implemented on the real MBC 500 magnetic bearing system, it was unsuccessful. The reason behind this unsuccessfull implementation was the value of α . It was observed that in order to have the stability for the magnetic bearing system, one should not be too ambitious to provide a large phase margin. Otherwise, it can lead to system instability. Therefore a redesign was required.

Obtaining an Optimum α value

To overcome the above problem, the best α value needs to be determined which will provide the optimum system stability. From the general lead compensator transfer function equation and $C_{lead1}(s)$ equation shown in equations 4.17 and 4.23, the value of α can be obtained as follows:

$$\frac{1}{\tau} = 3800; \qquad \frac{1}{\alpha\tau} = 600; \qquad \alpha = \frac{1}{\tau * 600} = \frac{3800}{600} = 6.33$$

Meanwhile, the combination of the general transfer function and the given compensator equation is shown in equations 4.17 and 4.24 . Out of these, the value of α becomes the following:

$$\frac{1}{\tau} = 3030; \qquad \frac{1}{\alpha\tau} = 1128; \qquad \alpha = \frac{1}{\tau * 1128} = \frac{3030}{1128} = 2.686$$

Because of the big differences between the above two α values, the optimal value of α needs to be determined. There must be a certain range for α that will stabilise the system. Observing the two compensators' bode plots shown in Figure 4.11, it is obvious that the alpha value of $C_{lead1}(s)$ provides a much larger phase angle. Another point is

that ω_{max} (the frequency at which the phase angle is at its maximum) occurs at a lower frequency.

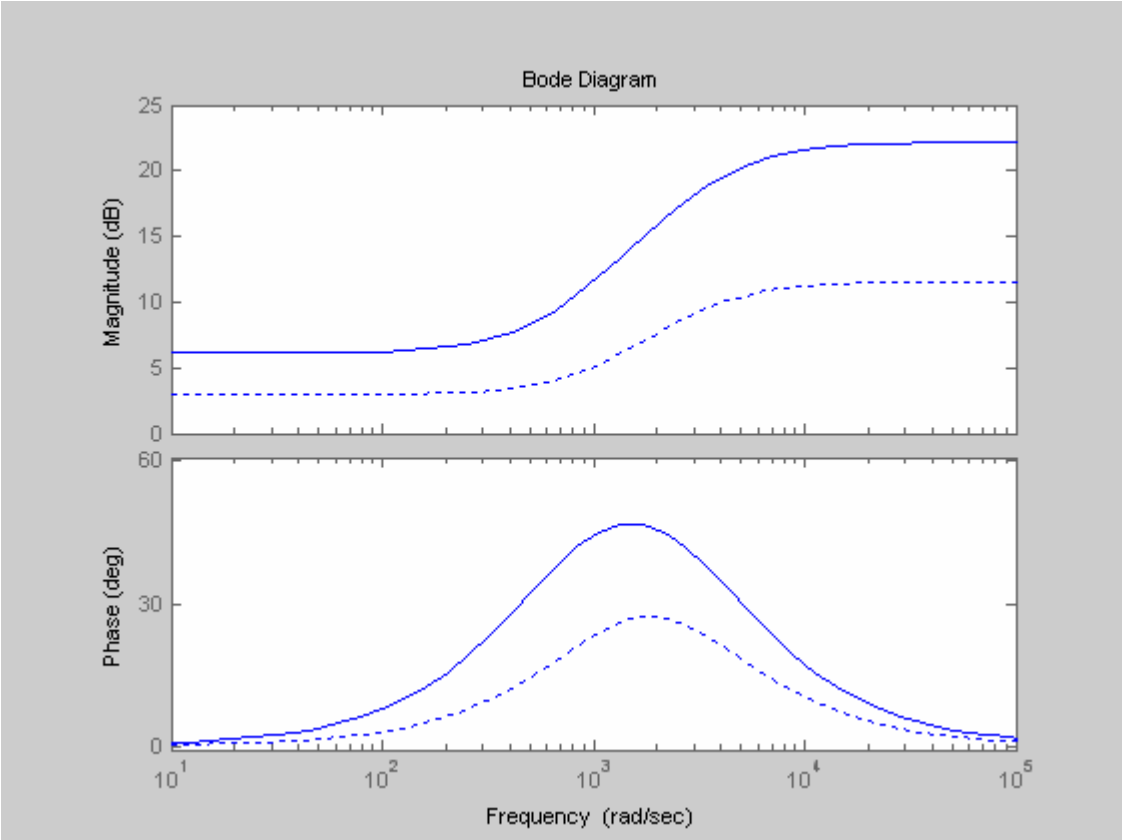

Figure 4.11 $C_{lead1}(s)$ (solid line) and $C(s)$ (dotted line) bode plots

Using the equations for α, a range of lead compensators were determined that corresponded to a range of α values. For each of the compensators, there are related variables. These related variables are the DC gain and ω_{max} with DC gain = 1.41 (same as DC gain for given compensator) and $\omega_{max} = 1848.7$ rad/sec.

After calculations and lead compensator implementation on channel 1, the following stability range for α was determined.

$$1 \langle \alpha \langle 5$$

Therefore, for the redesign of the lead compensator for channel 2, the algebraic mean of the range obtained for α used was $\Rightarrow \alpha = 3$.

Redesign of the Lead Compensator

As determined in the previous section, $\alpha = 3$ and $\omega_{\max} = 1848.7$ rad/sec. Therefore, the compensator's zero, pole and gain values can be calculated as follows:

$$\frac{1}{T} = \omega_{\max}\sqrt{\alpha} = 3202 \qquad \frac{1}{\alpha T} = \frac{3202}{3} = 1067.3 \qquad k = 1.41x\frac{pole}{zero} = 4.23$$

Therefore, the lead compensator is given by:

$$C_{lead_2}(s) = \frac{4.23(s+1067.3)}{(s+3202)} \quad \text{..... 4.25}$$

Moreover, the lead compensator with the low pass filter having a cut off frequency of 7 KHz incorporated is given by:

$$C_{lead_2}(s) = \frac{4.23(s+1067.3)}{(s+3202)}\frac{43982}{(s+43982)} \quad \text{..... 4.26}$$

This lead compensator has a DC gain of 1.41 and it also provides a phase angle of 30°. Observing the two compensators' bode plots in Figure 4.12, it can be seen that both of the compensators have the peak phase at the same frequency $\omega_{\max} = 1849$ rad/sec. Moreover, the phase angle of $C_{lead2}(s)$ is lower compared to the phase angle of $C_{lead1}(s)$ as can be seen in Figure 4.13. Finally, a comparison of the frequency response of $C_{lead1}(s)$, $C_{lead2}(s)$ and $C(s)$ can be seen in Figure 4.14.

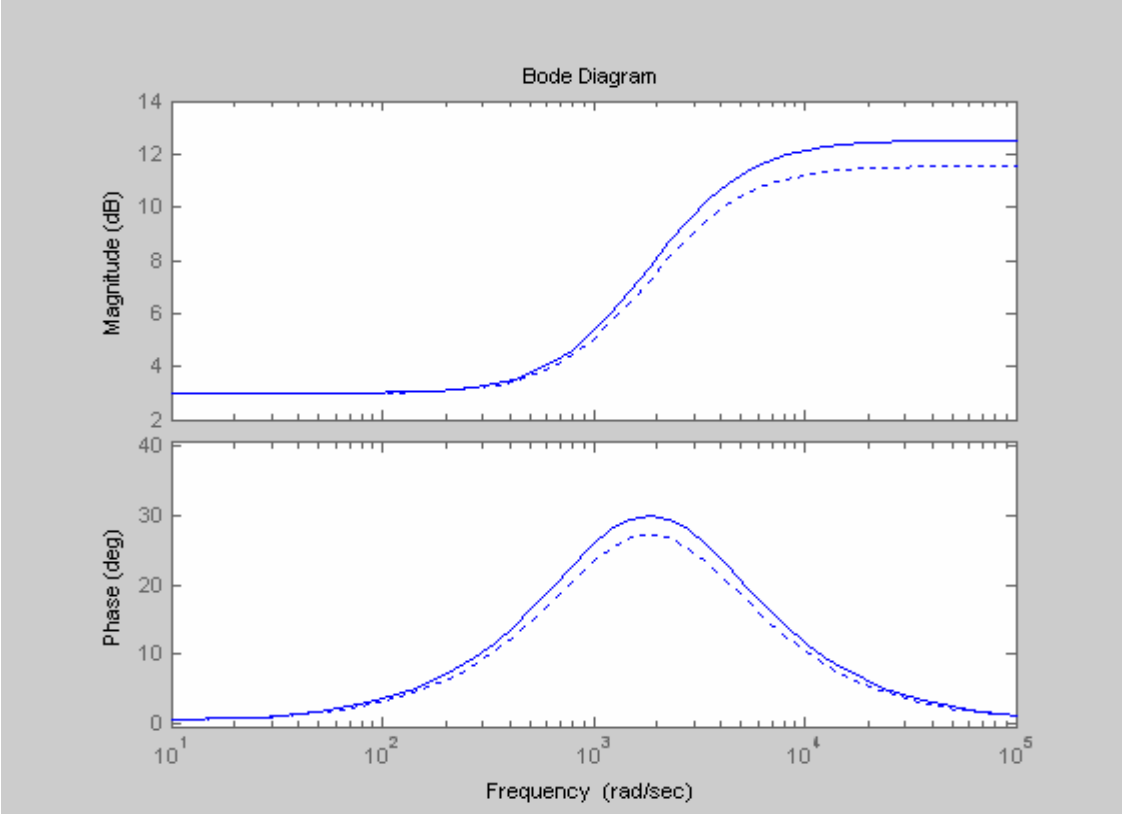

Figure 4.12 $C_{lead2}(s)$ (solid line) and $C(s)$ (dotted line) bode plots

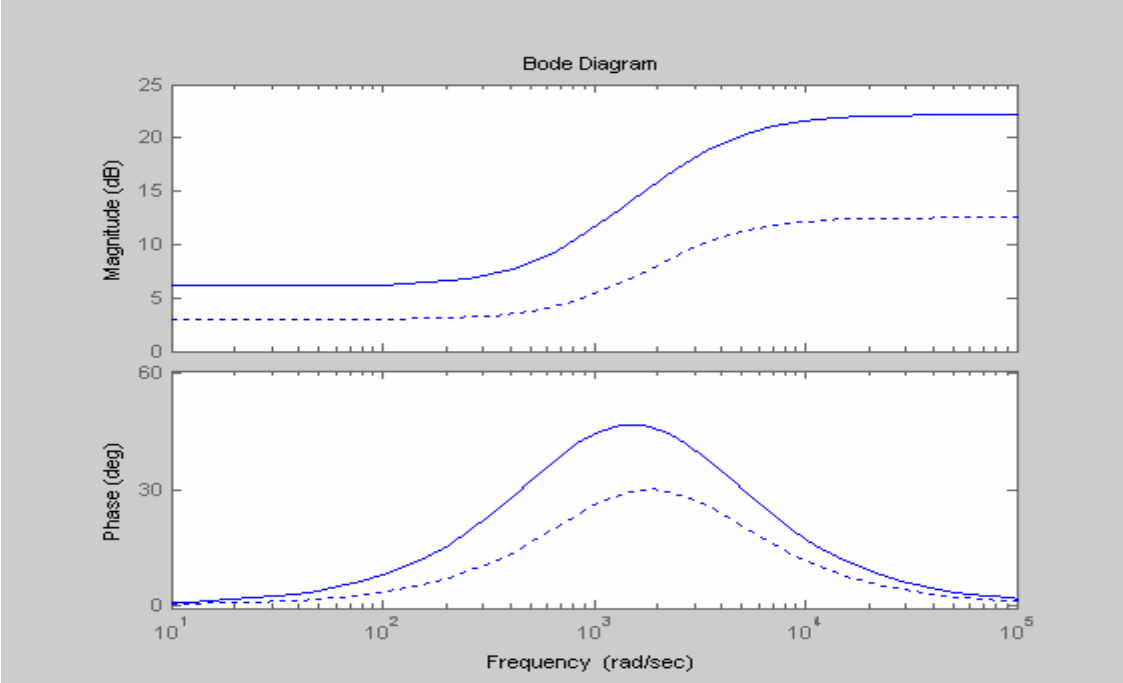

Figure 4.13 $C_{lead1}(s)$ (solid line) and $C_{lead2}(s)$ (dotted line) bode plots

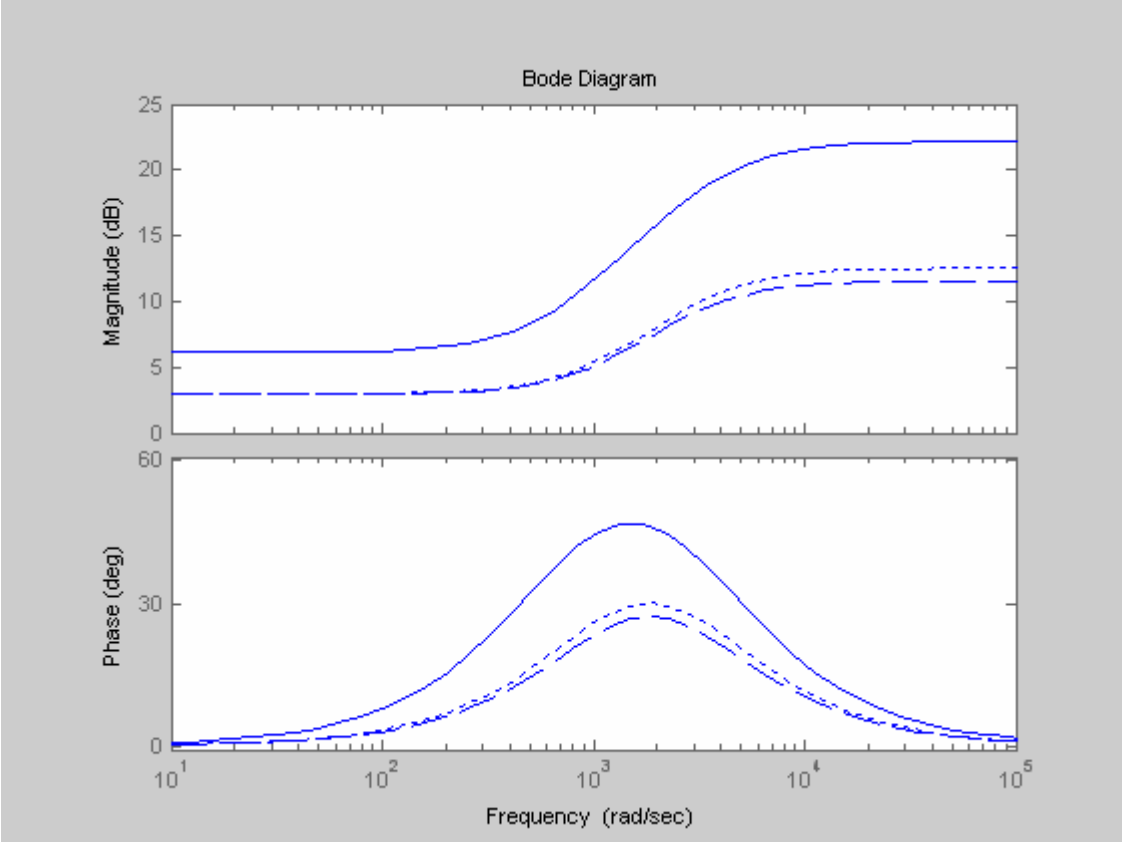

Figure 4.14 $C_{lead1}(s)$ (solid line), $C_{lead2}(s)$ (dotted line) and $C(s)$ (dashed line) bode plots

Digital Controller Design

Since the notch filter and lead compensator have to be implemented using DSP, it must be transformed into digital form. The transformation from continuous time to discrete time enables the system to be controlled through the computer with the use of MATLAB, SIMULINK and dSPACE DSP card. A few MATLAB commands can transform the transfer function of the continuous time controller into discrete form. The sampling period used is 4×10^{-5} seconds. As a result, the sampling frequency is about ten times the highest resonant frequency. Appendix C describes the 'c2dm' function, which converts continuous linear time-invariant systems to discrete time.

4.4 Simulation Using SIMULINK

Controller Simulation using Analytical Model

Now that the lead compensator $C_{lead2}(s)$ and notch filters $N_1(s)$ and $N_2(s)$ have been designed, the whole system can be simulated using SIMULINK. The bending state-space model will be used to represent the bearing system dynamics. The rigid body model will not be used in the simulation as the real system does have distinct resonant modes. Figure 4.15 shows the MATLAB SIMULINK simulation window with all the required blocks. Note that only the *x* direction is taken into account, hence channel 1 and channel 2 only are included in the simulation. For channel 1, $C(s)$ is used and $C_{lead2}(s)$ for channel 2. The two outputs V_{sense1} and V_{sense2} can be plotted for a step input.

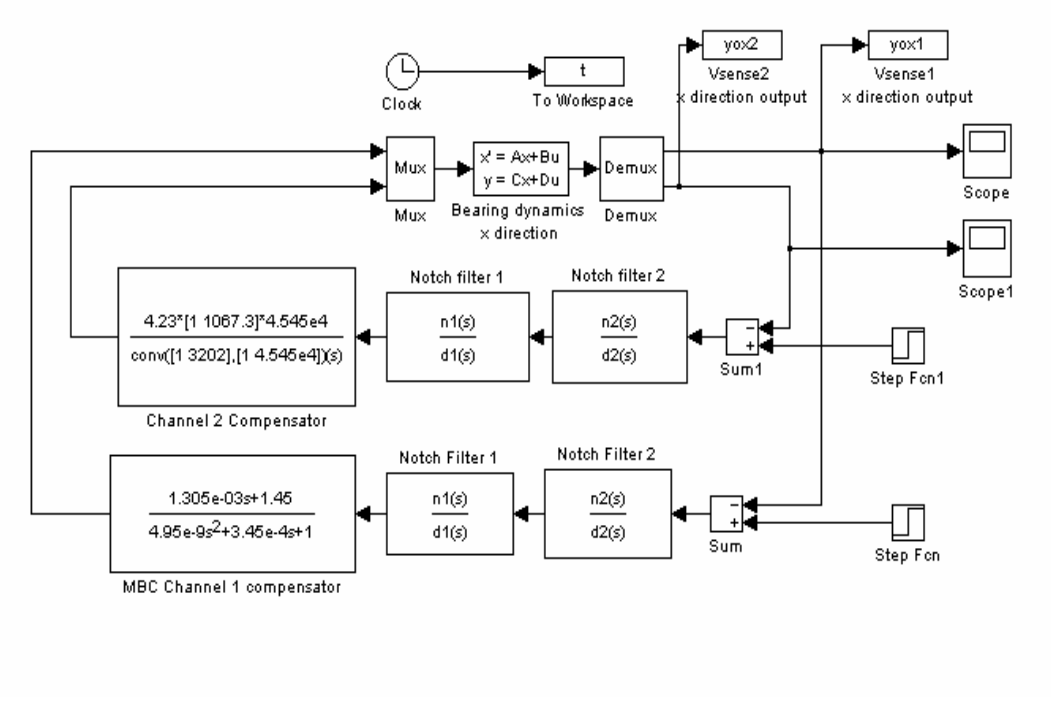

Figure 4.15 SIMULINK description of bending body model with controller

For a step input of magnitude 0.001 applied to channel 1 at time *t=0*, the conventional controller and the two notch filters failed to stabilise the magnetic bearing system initially. Investigation has revealed that the two notch filters designed based on the analytical model did not notch out the resonant at the two exact resonant frequencies. As a result, the two notch filters have to be redesigned to cover a wide frequency range around the two resonant frequencies. The magnetic bearing output response is given in Figure 4.16 after the redesign of the two notch filters. Note that the system is stable with a large overshoot to begin with.

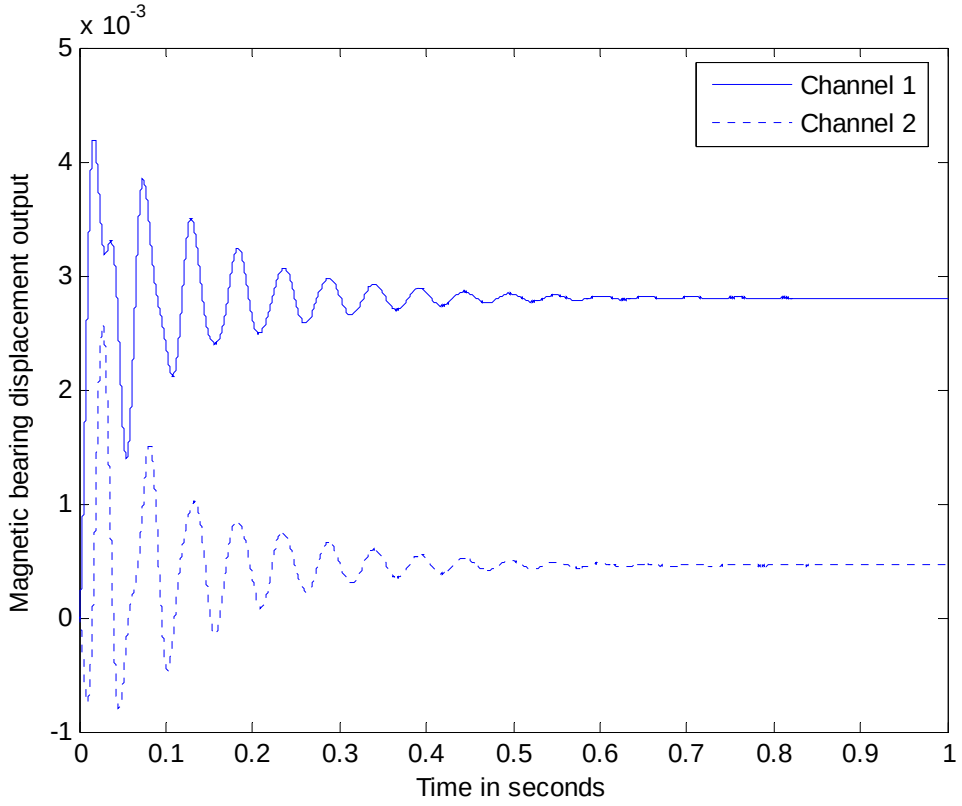

Figure 4.16 Step response of the magnetic bearing system-channel 1 (solid) and channel 2 (dotted)

For input into channel 2, the result is the same, however the magnitudes are reversed. This was the expected result as the designed conventional controllers and notch filters stabilised both channels successfully.

Controller Simulation using the Identified Experimental Model

After the controller had been tested with the analytical model, the controller was also tested with the identified experimental model. The experimental model that was used in the simulation was the reduced order model $G_{red(s)}$. The assumption was that if a reasonable response was achieved, then the experimental implementation would be successful. Figure 4.17 shows the SIMULINK block diagram containing the simplified model obtained via system identification, the designed lead compensator and notch filters.

A step input of magnitude 0.001 occuring at t=0 was applied for 1 second and the response that was obtained is plotted in Figure 4.18. The horizontal scale is not in seconds, the plot shown occurred over 0.1 seconds. Notice that the system showed stability, and therefore it can be concluded that the designed controller should theoretically work on the real system. The reason behind this claim is that the identified experimental model is the closest estimate to the real system.

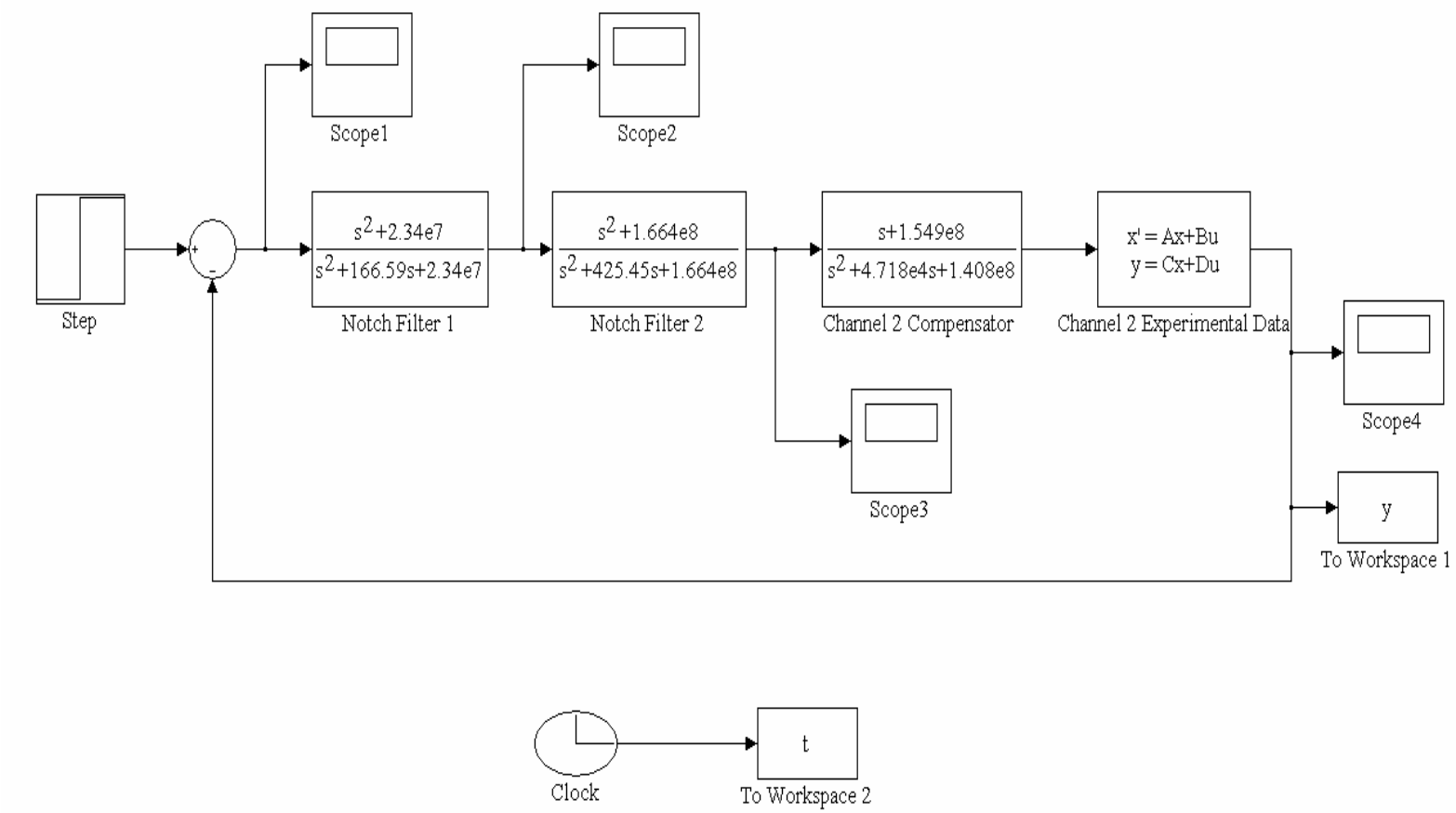

Figure 4.17 SIMULINK description of the simplified model obtained via system identification with the designed compensator and notch filters

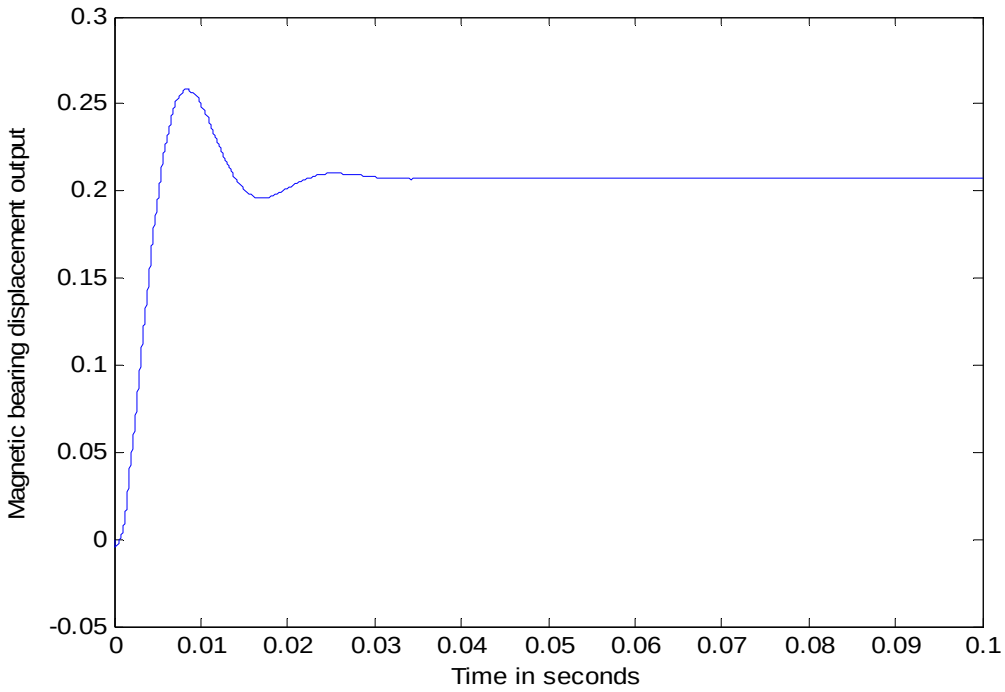

Figure 4.18 Step response of the magnetic bearing system using the simplified model obtained via system identification

Controller Implementation

The designed lead compensator and notch filters were implemented to test the MBC 500 magnetic bearing system stability. For this part MATLAB, SIMULINK and dSPACE Control Desk were required to access the DS1102 DSP board. The controller was drawn in a SIMULINK file, which was connected to the ADC (Analogue to Digital Converter) and the DAC (Digital to Analogue Converter). The DSP card could then access the designed controller through real time processing. Figure 4.19 shows the SIMULINK block diagram that was used including the lead compensator with notch filters. The controller variables were defined in the m-file.

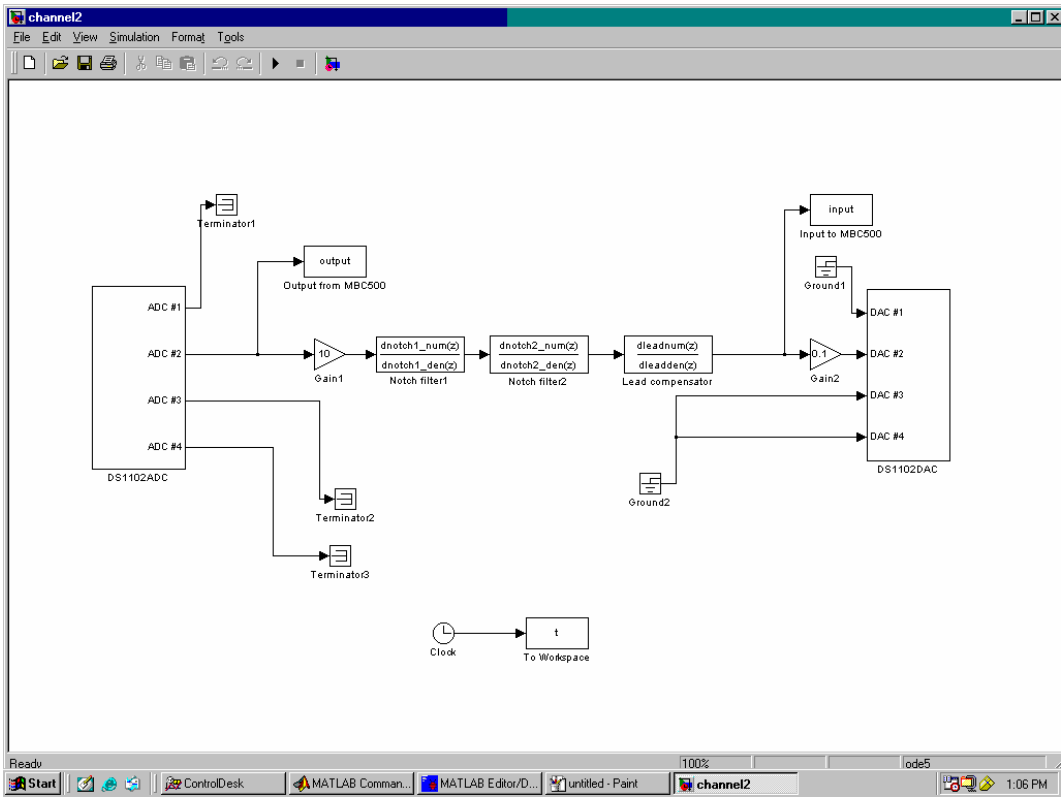

Figure 4.19 SIMULINK block diagram including digital controller for real time implementation

The controller designed worked for all four channels. Figure 4.20 shows the experimental setup of the whole system in full operation. The designed digital controllers and notch filters have been implemented using the DSP card installed in the computer to ensure the stability of the MBC 500 magnetic bearing system. The on screen software is MATLAB utilising the SIMULINK toolbox. The computer was powered by a $\pm 15V$ DC power supply that was connected to it.

Figure 4.20 Experimental setup of the digital control system for the MBC 500 magnetic bearing

Figure 4.21 is an image of the MBC 500 magnetic bearing system taken while the designed controller was stabilising channel 2. It is shown that the BNC cables were connected to the input and output connectors of channel 2. The loop switch for channel 2 was turned off in order to disable the internal controller and all four lights indicated the system was stable. At this stage the rotor shaft was levitating as desired.

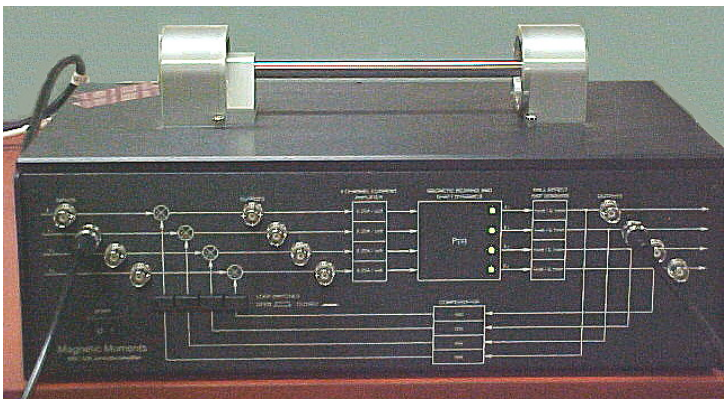

Figure 4.21 MBC 500 magnetic bearing levitated using the designed digital controller on channel 2

Another test that was deemed suitable to be applied to the system was the robustness test. The test involved injecting a disturbance signal in the path after the controller in the SIMULINK block, but before the DAC block. Figure 4.22 shows the SIMULINK block diagram of the robustness test implemented with a step disturbance added to the system.

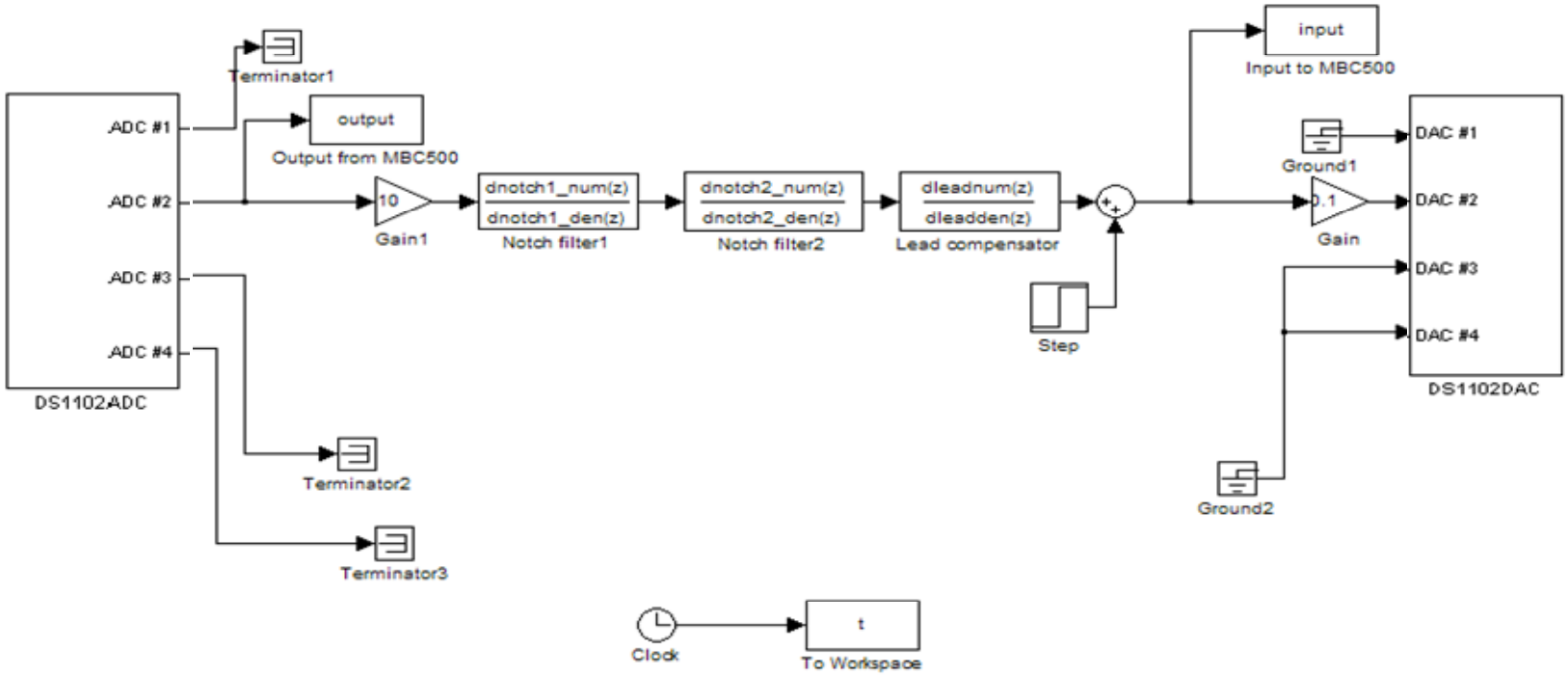

Figure 4.22 SIMULINK block diagram for robustness test with step disturbance applied to the system

The designed lead compensator and notch filters maintained system stability even with a disturbance step value of 0.1 applied to the system. The system response subjected to a step disturbance of 0.1 applied to channel 2 is given in Figure 4.23. All four channels were tested for robustness and each test was successful.

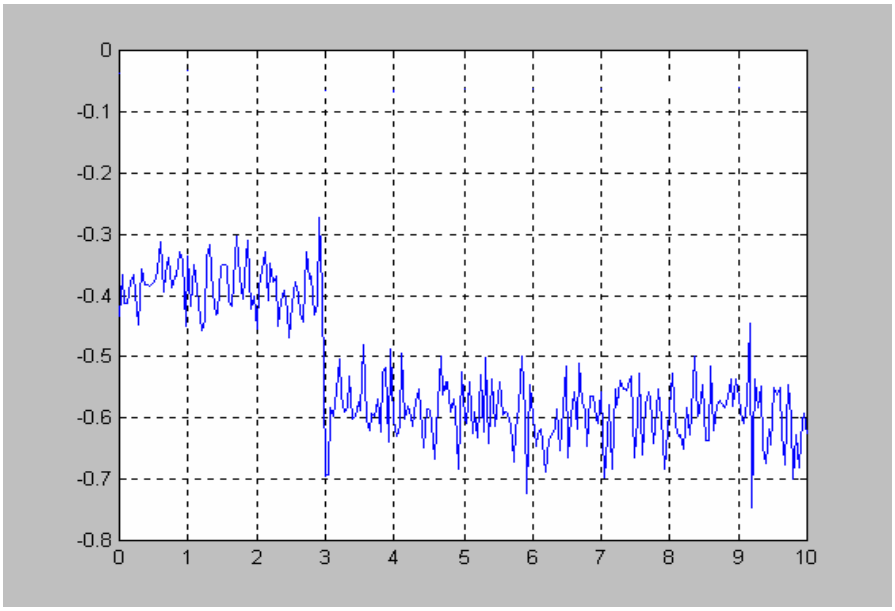

Figure 4.23 System response subjected to a step disturbance of 0.2 applied to channel 2

The final test was to input a step signal to the input of the MBC 500 magnetic bearing system. When the step was enforced, the movement of the rotor was observed. Figure 4.24 is the SIMULINK block diagram with the step input. The step response plot is given in Figure 4.25.

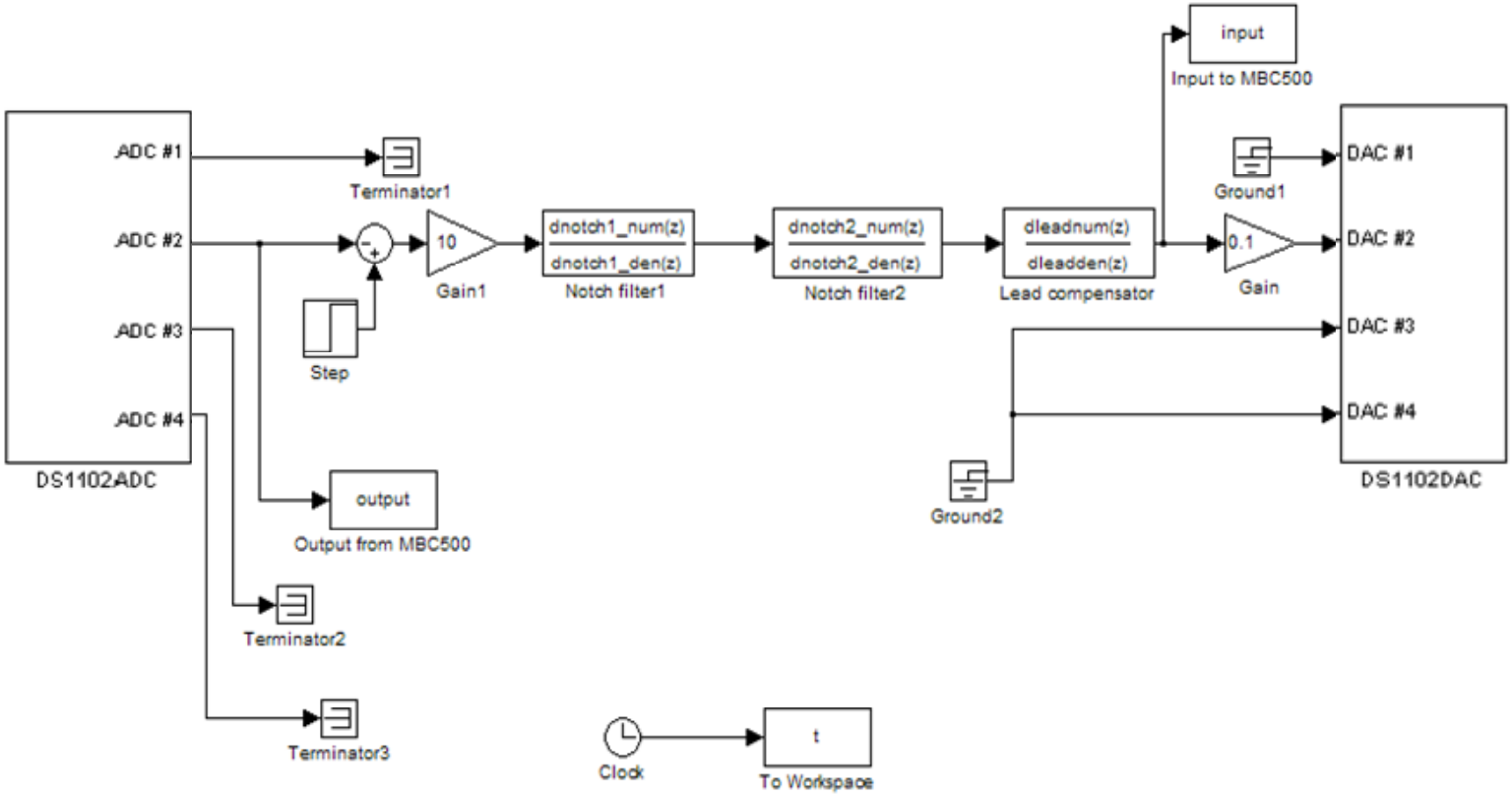

Figure 4.24 SIMULINK block diagram with step input

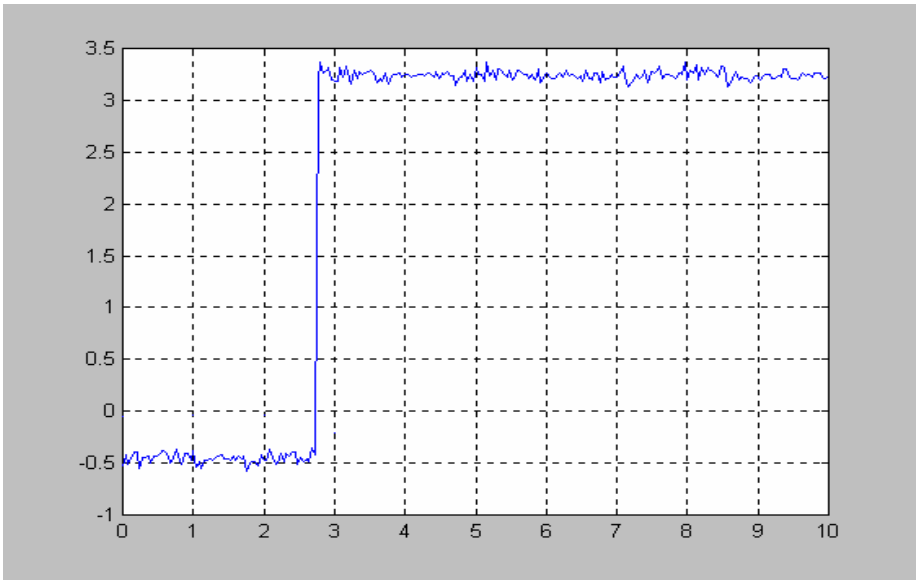

Figure 4.25 Step input response on channel 2

4.5 Summary

This chapter has described the design of notch filters based on the resonant frequencies identified in Chapter 3. A conventional lead compensator has been designed for the stabilisation of the magnetic bearing system. The performance of the designed notch filters and lead compensator have been evaluated via simulation using both the analytical model and the model obtained via system identification. The simulation results have shown that the designed notch filters and lead compensator have stabilised the magnetic bearing system successfully. Finally, the designed notch filters and lead compensator have been implemented for the MBC 500 magnetic bearing system in real time. Both the step response and robustness tests have demonstrated the effectiveness of the conventional controller and notch filters designed.

5 Fuzzy Logic Controller (FLC) Design for the MBC 500 Magnetic Bearing System

5.1 Overview

In this chapter, the structure of Fuzzy Logic Controller (FLC) is first described. Two different fuzzy inference methods, Mamdani and Sugeno methods are then reviewed. FLC is then designed to stabilise the MBC 500 magnetic bearing system. The performance of the designed FLC will be evaluated via computer simulation. Comparison studies of the FLC performance with different inference methods and different number of rules will be investigated. Finally, this chapter presents comparative studies of the conventional controller and the advanced PD-like Fuzzy Logic Controller (FLC) designed that were carried out in this research.

5.2 Fuzzy Logic Controller

A block diagram of a fuzzy control system is shown in Figure 5.1. The fuzzy logic controller is composed of four elements (Passino and Yurkovich 1998):

- *A rule-base*, which contains a set of *If-Then* rules with fuzzy logic quantification of the expert's description, linguistically, of how to achieve good control.
- *An inference mechanism* (an inference engine or fuzzy inference module) that emulates how the expert makes the decision in interpreting and applying knowledge about the best way to control the plant.

- *A fuzzification* interface, which converts controller inputs into information that the inference mechanism can use easily to activate and apply rules.
- *A defuzzification* interface converts the inference mechanism's conclusions into actual inputs for the process.

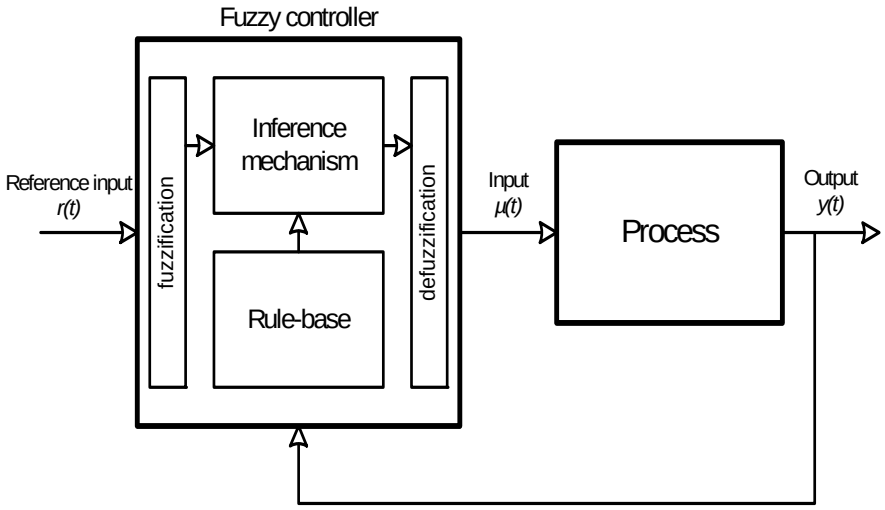

Figure 5.1 Block diagram of a fuzzy controller
Sources: (A Zadeh 1995; Passino and Yurkovich 1998)

In Chapter 4 it has been stated that a classical lead compensator and two notch filters have been designed for the MBC500 magnetic bearing system. The control algorithm of a lead compensator is equivalent to a PD controller. As a result a PD-like fuzzy controller was designed for stabilising the MBC 500 magnetic bearing system. A block diagram of a PD-like fuzzy control system is shown in Figure 5.2. As can be seen in Figure 5.2, the fuzzy controller inputs are *error* and *change-of-error*. The details of the fuzzy controller design will be shown in the following section.

Figure 5.2 Block-diagram of a PD-like fuzzy control system
Sources: (Reznik 1997; Passino and Yurkovich 1998)

5.3 FLC Design for AMB stabilisation

This section is focused on the design of a FLC for magnetic bearing system stabilisation. Figure 5.3 below shows a fuzzy logic control system for one of the four channels of the magnetic bearing system. V_{sense} is the sensor output of the magnetic bearing system representing the displacement in either x or y direction. The block of *Magnetic Bearing* in Figure 5.3 is composed of a power amplifier, sensor and rotor. The FLC is designed below. The performance of the fuzzy logic control system was investigated via simulation. The models identified in Chapter 3 were used in the simulation.

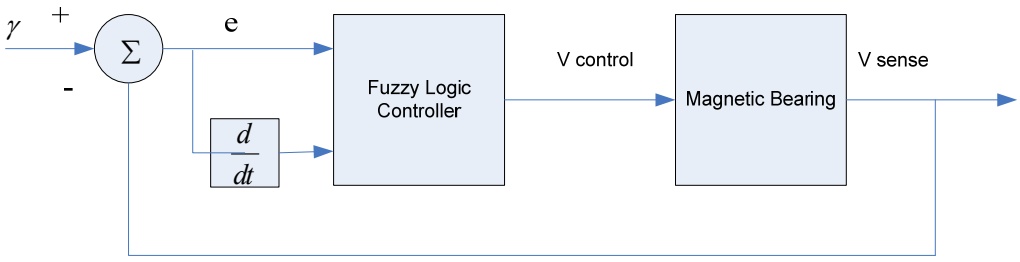

Figure 5.3 FLC for MBC500 magnetic bearing system

Fuzzy Logic Controller (FLC) Design

FLC Inputs and Output Selection

The inputs for the PD-like FLC are *error* and *change-of-error*. The output of the FLC is $V_{controli}$ that regulates the current into the bearing which in turn will regulate the magnetic bearing force. The value of i is from 1 to 4 representing 4 channels of the magnetic bearing. Four PD-like FLCs need to be designed for controlling the four channels of the MBC500 magnetic system. The design of the FLC for channel x_2 is described in detail in this section. The design of the rest of the FLCs for channels x_1, y_1 and y_2 follow the same procedure.

Figure 5.4 illustrates the MBC500 magnetic bearing shaft with the corresponding centre reference line, and its output and input at the right hand side for channel x_2.

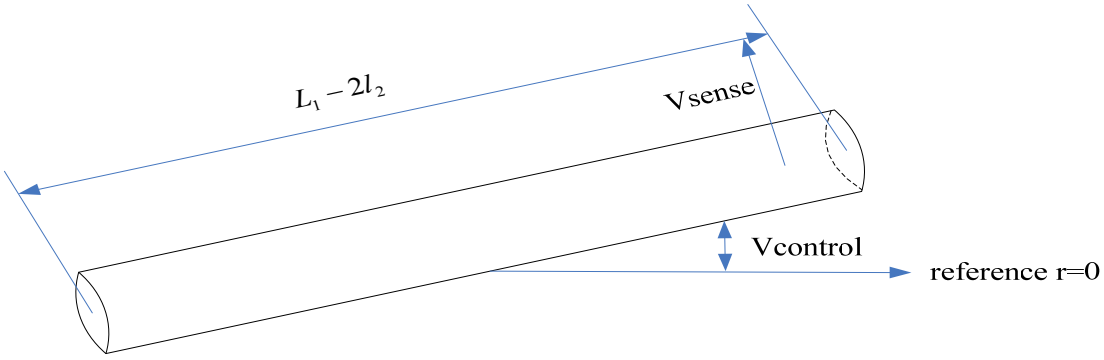

Figure 5.4 MBC 500 magnetic bearing control at right hand side for channel x_2

The displacement output x_2 is sensed by the Hall-effect sensor with the output voltage V_{sense2}. Hence the error signal is defined for channel x_2 as:

$$e(t) = r(t) - V_{sense2}(t)$$

For the magnetic bearing stabilisation problem, the reference input $r(t) = 0$. As a result,

$$e(t) = -V_{sense2}(t)$$

and $\frac{d}{dt}e(t) = -\frac{d}{dt}V_{sense2}(t)$

The linguistic variables which describe the FLC inputs and outputs are:

"error" describes e(t)

"change-in-error" describes $\frac{d}{dt}e(t)$

"force" describes $V_{control2}$

The above linguistic variables "error," "change-in-error," and "force" will take on the following linguistic values:

"NB" = Negative Big

"NM" = Negative Medium

"NS" = Negative Small

"ZO" = Zero

"PS" = Positive Small

"PM" = Positive Medium

"PB" = Positive Big

The following statements quantify different configurations of the magnetic bearing.

- The statement "error is PB" represents the situation where the magnetic bearing shaft is significantly below the reference line.
- The statement "error is NS" represents the situation where the magnetic bearing shaft is just slightly above the reference line. However, it is neither too close to the position to quantify it as "ZO" nor is it too far away to quantify it as "NM".
- The statement "error is ZO" represents the situation where the magnetic bearing shaft is very close to the centre reference position. As a linguistic quantification is not precise, any value of the error around *e(t) = 0* will be accepted as "ZO"

since this can be considered as a better quantification than "PS" or "NS".

- The statement "error is PB **and** change-in-error is PS" represents the situation where the magnetic bearing shaft is below the reference line and, since $\frac{d}{dt}V_{sense2} < 0$, the magnetic bearing shaft is moving away from the centre position.
- The statement "error is NS **and** change-in-error is PS" represents the situation where the magnetic bearing shaft is slightly above the centre reference line and, since $\frac{d}{dt}V_{sense2} < 0$, the magnetic bearing shaft is moving toward the centre position.

Rule-Base Formulation

The above linguistic quantification would be used to specify a set of rules or a rule-base. The following three situations will demonstrate how the rule-base is developed.

1. **If** error is NB **and** change-in-error is NB **Then** force is NB.

   Figure 5.5 below shows that the magnetic bearing shaft at the right end has a large displacement and is moving up away from the centre reference line. Therefore, it is clear that a strong negative force should be applied so that the shaft will move to the centre reference position.

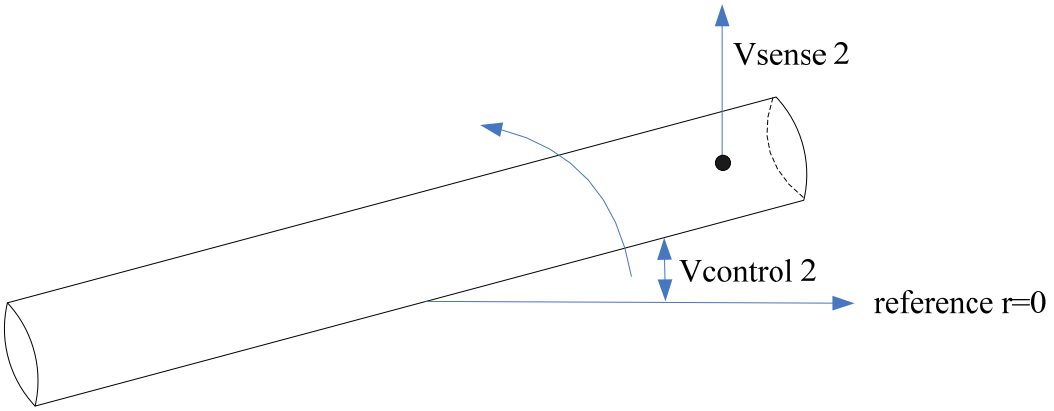

Figure 5.5 Magnetic bearing shaft at the right end with a positive displacement

2. **If** error is ZO **and** change-in-error is PS **Then** force is PS.

   Figure 5.6 below shows that the bearing shaft at the right end has nearly a zero displacement with the centre reference position (a linguistic quantification of zero does not imply that *e(t)=0* exactly) and is moving away from the centre reference line. Therefore, a small positive force should be applied to counteract the movement so that it moves toward 1the centre reference position. If a negative force is applied to the magnetic bearing then it could result in overshooting the desired position.

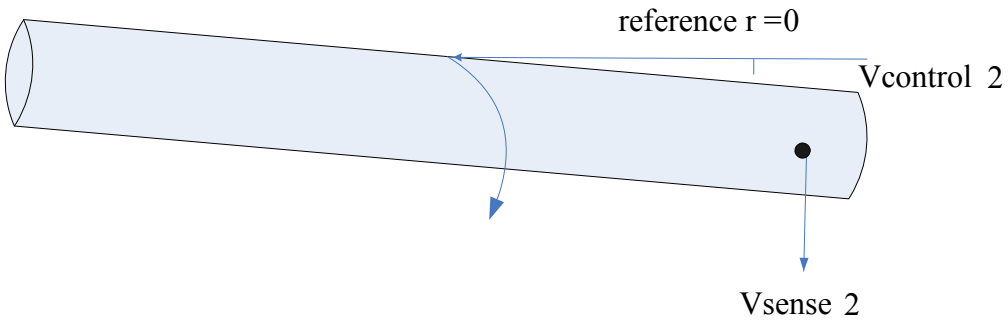

Figure 5.6 Magnetic bearing shaft at the right end with zero displacement

3. **If** error is PB **and** change-in-error is NS **Then** force is PS.

   Figure 5.7 below shows that the bearing shaft at the right end is far below the centre reference line and is moving towards the centre reference position. Therefore, a small positive force should be applied to assist the movement. However, it should not be a big force since the bearing shaft at the right end is already moving in the proper direction.

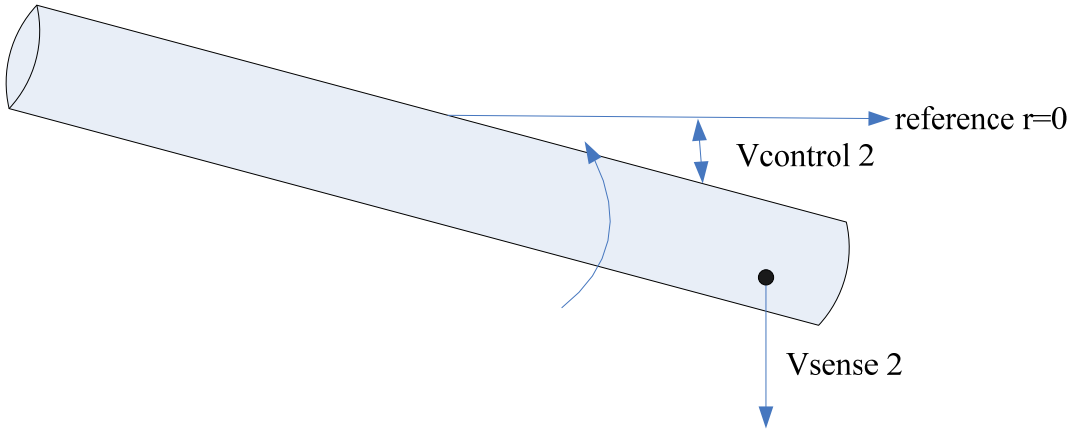

Figure 5.7 Magnetic bearing shaft at the right end with a negative displacement

Following a similar analysis, the rules of the FLC for controlling the magnetic bearing shaft can be developed. For the FLC with two inputs and five linguistic values for each input, there are $5^5 = 25$ possible rules with all combination for the inputs. Similarly, for the FLC with two inputs and seven linguistic values for each input, there are $7^2 = 49$ possible rules with all combination for the inputs. A set of possible linguistic values for two inputs and one output with 25 rules are NB, NS, ZO, PS and PB. Furthermore, A set of possible linguistic values for two inputs and one output with 49 rules are NB, NM, NS, ZO, PS, PM and PB. One way to list all possible rules where inputs are less than or equal to two or three is by using a tabular representation. The tabular representations of the FLC rule base (25 rules and 49 rules) of the magnetic bearing

fuzzy control system are shown in Tables 5.1 and 5.2 respectively.

"force" V		"change-in-error" $\dot{e}$				
		NB	NS	ZO	PS	PB
"error" e	NB	NB	NB	NB	NS	ZO
	NS	NB	NB	NS	ZO	PS
	ZO	NB	NS	ZO	PS	PM
	PS	NS	ZO	PS	PB	PB
	PB	ZO	PS	PB	PB	PB

Table 5.1 Rule table with 25 rules

"force" V		"change-in-error" ė						
		NB	NM	NS	ZO	PS	PM	PB
"error" e	NB	NB	NB	NB	NB	NM	NS	ZO
	NM	NB	NB	NB	NM	NS	ZO	PS
	NS	NB	NB	NM	NS	ZO	PS	PM
	ZO	NB	NM	NS	ZO	PS	PM	PB
	PS	NM	NS	ZO	PS	PM	PB	PB
	PM	NS	ZO	PS	PM	PB	PB	PB
	PB	ZO	PS	PM	PB	PB	PB	PB

Table 5.2 Rule table with 49 rules

The body of the FLC rule tables shown above lists the linguistic-numeric consequents. The left column and top row of the table contain the linguistic-numeric terms of the inputs. Tables 5.1 and 5.2 present abstract knowledge that the expert has about how to control the magnetic bearing shaft's given error and its derivative as inputs. All those rules have been determined to be complete, consistent and continuous.

Fuzziffication (Fuzzy Quantification of Knowledge)

Up to now, linguistic values have been used to describe the inputs and output of the FLC to specify a set of rules (a rule-base) about how to control the plant. The meaning of these linguistic values is quantified using membership functions. Figure 5.8 shows the FLC constructed using MATLAB's fuzzy logic toolbox with inputs "error" and "change-of-error" and the output "force". The input "change-of-error" has been quantified using the triangular memberships as shown in the figure. The membership functions for "error" and the output "force" have been defined using similar membership functions in a normalised universe of discourse [-1,1].

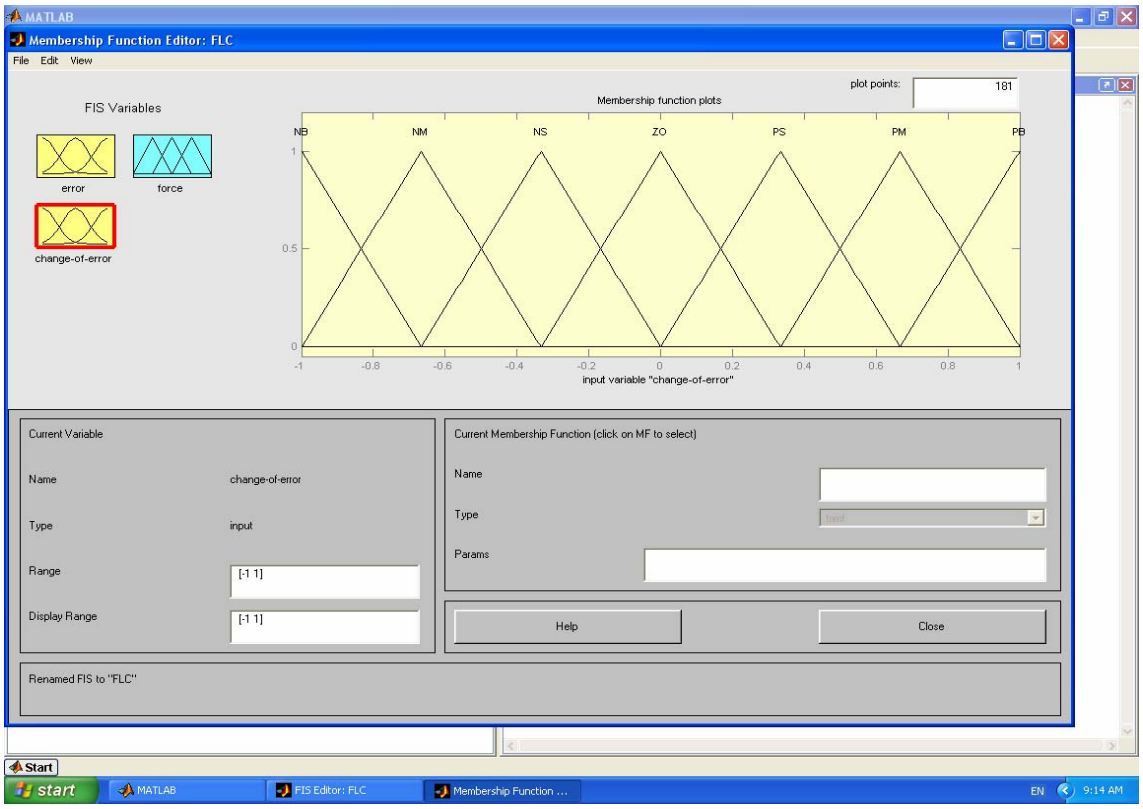

Figure 5.8 Membership functions for the input "change-of-error" in a normalised universe of discourse

Different types of membership functions have been chosen, different methods for fuzzy intersection (t-norm) and union (s-norm), different numbers of rules (25 rules and 49 rules), and different fuzzy inference methods have been investigated to explore the effectiveness of the designed FLC.

Simulation Results

The transfer function of the magnetic bearing model obtained via system identification, shown previously in Chapter 3, was used here in the simulation and the transfer function is repeated below:

$$G(s) = \frac{-105.2\,s^5 + 4.038e005\,s^4 - 1.961e010\,s^3 + 6.086e013\,s^2 - 3.814e017\,s + 7.938e020}{s^6 + 334.6\,s^5 + 1.899e008\,s^4 + 5.897e010\,s^3 + 3.881e015\,s^2 + 1.086e018\,s - 5.8e020}$$

Figure 5.9 shows the SIMULINK block diagram of the magnetic bearing system with the designed FLC. In contrast to the conventional control approach which has two notch filters taking care of the two resonant modes, the two notch filters are not present in the fuzzy control approach. Using notch filters designed as reported in Chapter 4, a sampling frequency of $f_s=25\ kHz$ was used when implementing the conventional controller and notch filters. As a result a delay time of $4\times10^{-5}\ seconds$ was chosen for the unit delay which was used to calculate the change-of-error signal.

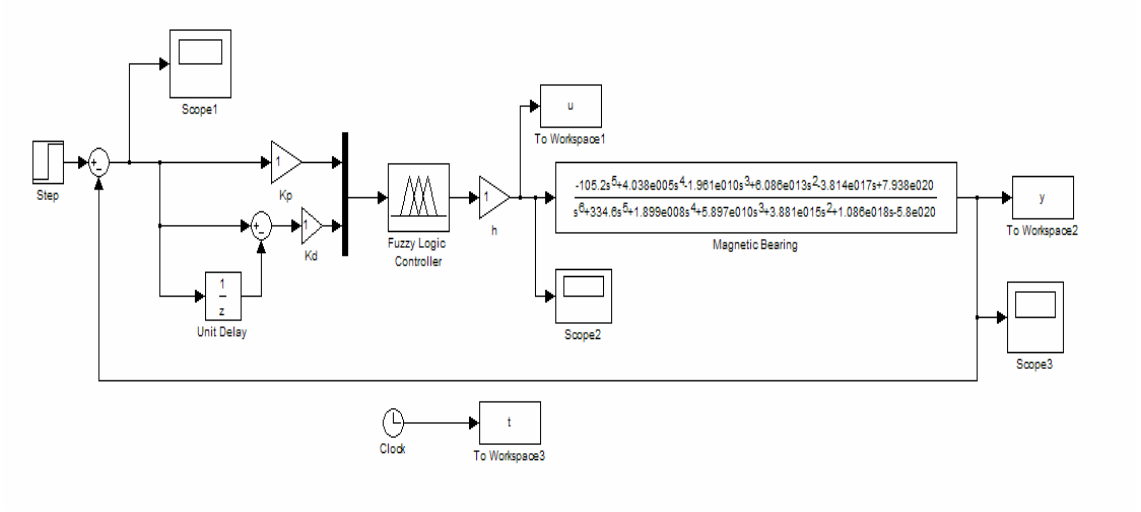

Figure 5.9 SIMULINK block diagram of the magnetic bearing system with the designed FLC

Different membership functions, such as the triangular and Gaussian membership functions, have been used for the FLC. The effect of using different methods for fuzzy intersections (***t***-norm) and unions (***s***-norm) have been investigated. Both Mamdani and Sugeno inference methods have been studied. Thus, four typical methods have been investigated with four cases in each method.

Some of the concepts used in MATLAB's Fuzzy Logic Toolbox are repeated here to avoid any confusion. *Aggregation* refers to the methods of determining the combination of the consequents of each rule in a Mamdani fuzzy inference system in preparation for defuzzification. *Implication* refers to the process of shaping the fuzzy set in the consequent based on the results of the antecedent in a Mamdani-type fuzzy inference system. In the MATLAB fuzzy logic toolbox, two built in ***t***-norm (AND) operations are supported: ***MIN*** (minimum) and ***PROD*** (product). Two built in ***s***-norm (OR) operations are supported: ***MAX*** (maximum) and probabilistic OR method ***PROBOR***. The probabilistic OR method is calculated according to the following equation:

PROBOR (a,b) = a + b –ab

Method 1: FLC with 25 Rules Using Mamdani Inference Method

Case 1

In the first case, the designed FLC uses triangular membership functions for the inputs and output. The FLC uses ***MIN*** for ***t***-norm operation, ***MAX*** for ***s***-norm operation, ***MAX*** for aggregation, ***MIN*** for implication, and ***CENTROID*** for defuzzification.

Case 2

In the second case, the designed FLC uses triangular membership functions for the inputs and output. The FLC uses ***PROD*** for ***t***-norm operation, ***PROBOR*** for ***s***-norm operation, ***MAX*** for aggregation, ***PROD*** for implication, and ***CENTROID*** for defuzzification.

Case 3

In the third case, the designed FLC uses Gaussian membership functions for both inputs and output. The FLC also uses **MIN** for **t**-norm operation, **MAX** for **s**-norm operation, **MAX** for aggregation, **MIN** for implication, and **CENTROID** for defuzzification. However, the FLC failed to stabilise the magnetic bearing system in this case.

Case 4

In the last case, the designed FLC uses Gaussian membership functions for both inputs and output. The FLC also uses **PROD** for **t**-norm operation, **PROBOR** for **s**-norm operation, **MAX** for aggregation, **PROD** for implication, and **CENTROID** for defuzzification.

Figure 5.10 shows the step responses of the magnetic bearing system with the designed FLCs for the four cases described above. It can be seen that the system is stable with the FLCs in cases 1, 2 and 4. The FLC in case 3 failed to stabilise the magnetic bearing system. The step responses with the FLCs in cases 2 and 4 have less damping and longer settling time than case 1. From the step responses shown in this figure, it can be seen that the FLC in case 1 provides the best result. However, all results exhibit a large steady-state error as the reference step size is 0.1.

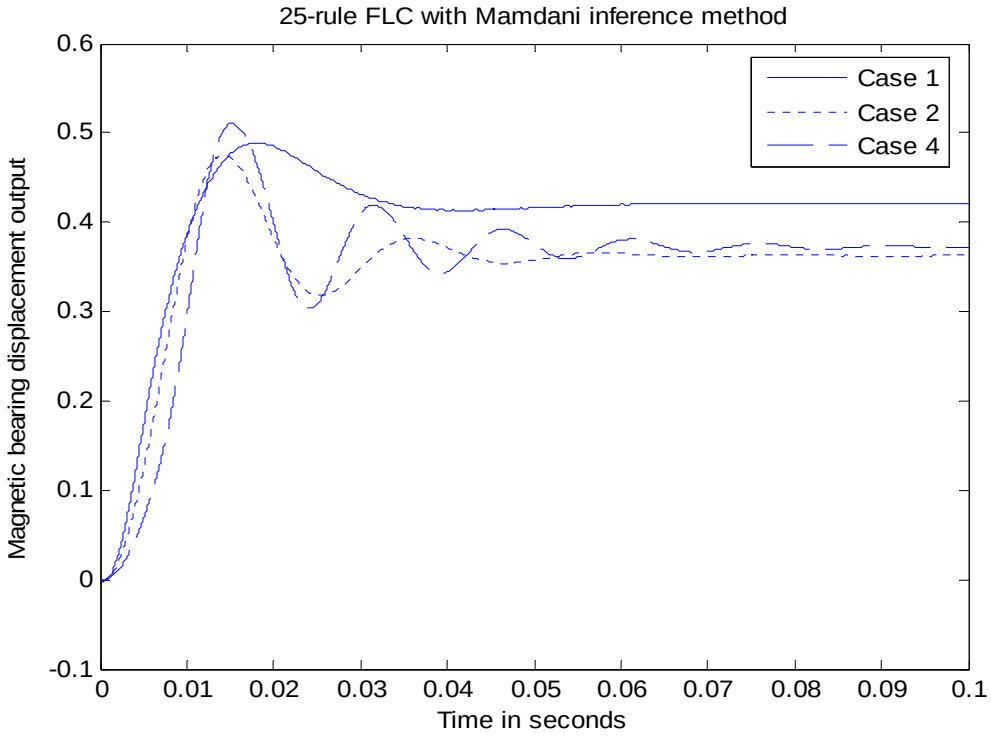

Figure 5.10 Step response of the magnetic bearing system with the designed FLC (25 rules, Mamdani inference method)

Method 2: FLC with 49 Rules Using Mamdani Inference Method

Figure 5.11 shows the step responses of the magnetic bearing system with the designed 49-rule FLC for the same four cases described in method 1. Comparing the simulation results in these figures, it can be seen that the FLC used in case 1 provides the step

response with the smallest overshoot. The FLC in case 2 provides the step response with the smallest steady-state error. The FLC in case 1 provides the best step response in terms of overall performance. Again, all results exhibit a large steady-state error as the reference step size is 0.1.

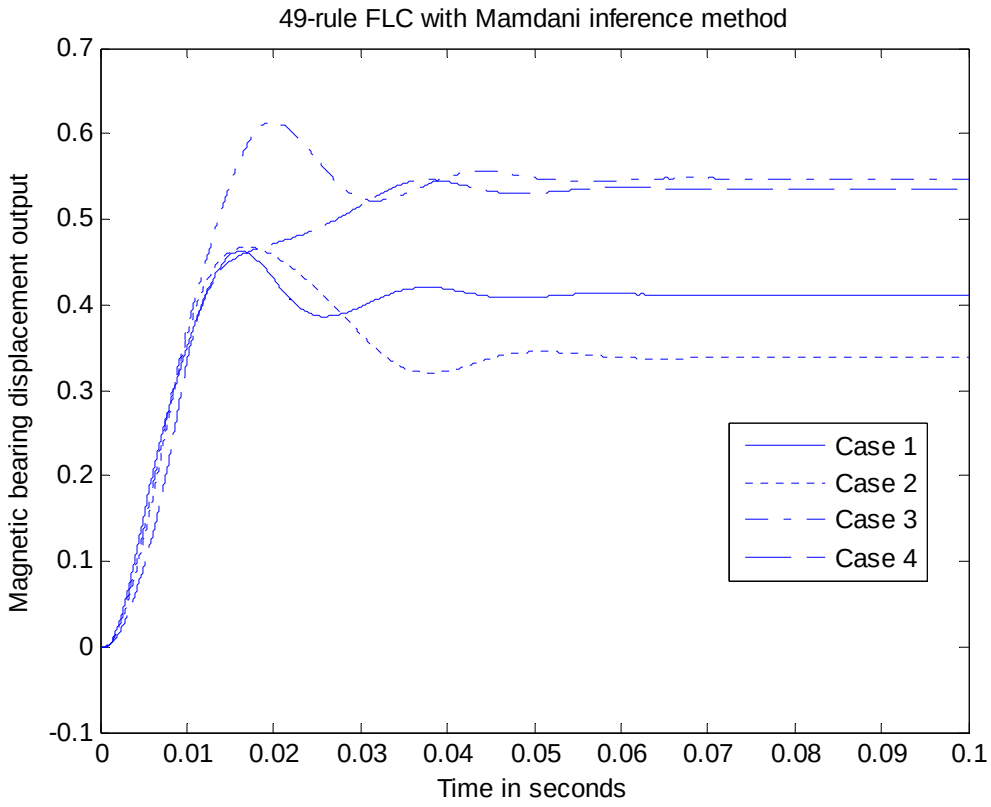

Figure 5.11 Step response of the magnetic baring system with the designed FLC (49 rules, Mamdani inference method)

Method 3: 25-rule FLC with Sugeno Fuzzy Inference Method

Case 1

In the first case, the designed FLC uses triangular membership functions for the inputs and output. The FLC also uses ***MIN*** for ***t***-norm operation, ***MAX*** for ***s***-norm operation, and the ***WTAVER*** (weighted average) is the defuzzification method used.

Case 2

In the second case, the designed FLC uses triangular membership functions for the inputs and output. The FLC uses ***PROD*** for ***t***-norm operation, ***MAX*** for ***s***-norm operation, and ***WTAVER*** for defuzzification.

Case 3

In the third case, the designed FLC uses Gaussian membership functions for both inputs and output. The FLC also uses **MIN** for **t**-norm operation, **MAX** for **s**-norm operation, and **WTAVER** for defuzzification.

Case 4

In the last case, the designed FLC uses Gaussian membership functions for both inputs and output. The FLC also uses **PROD** for **t**-norm operation, **MAX** for **s**-norm operation, and **WTAVER** for defuzzification.

Figure 5.12 shows the step responses of the magnetic bearing system with the designed FLCs for the four cases described above. It can be seen that the system is stable and there is not much of difference in terms of steady-state error. The step response with the FLC in case 1 provides the best result as it has more damping and faster settling time. However, all results exhibit a large steady-state error as the reference step size is 0.1.

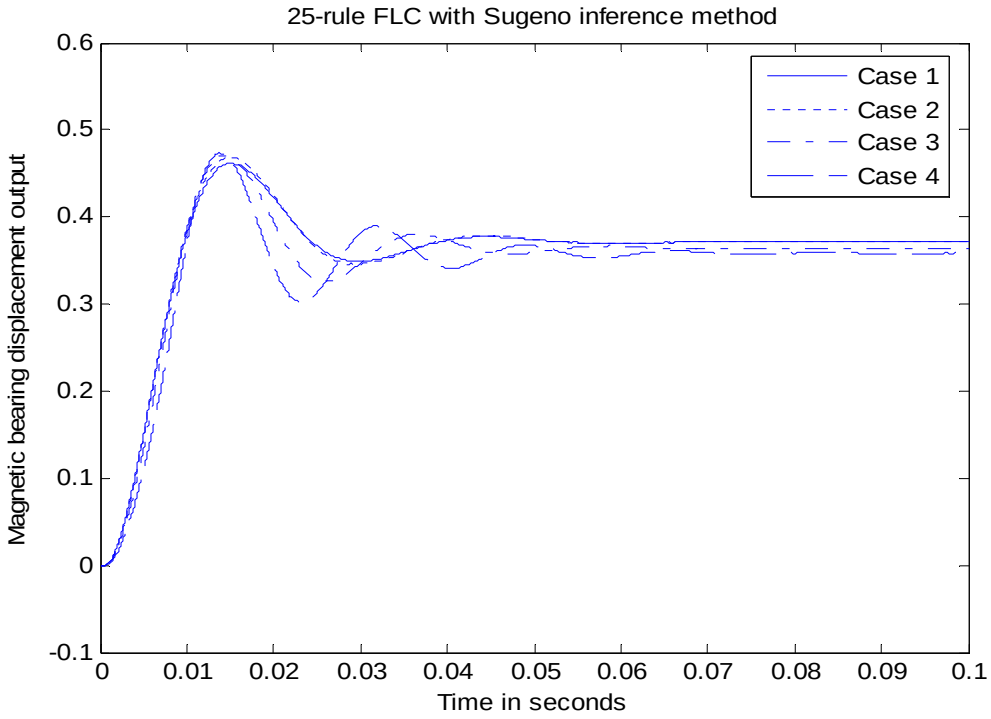

Figure 5.12 Step response of the magnetic bearing system with the designed FLC (25 rules, Sugeno inference method)

Method 4: 49-rule FLC with Sugeno Fuzzy Inference Method

Figure 5.13 shows the step responses of the magnetic bearing system with the designed FLCs for the the same four cases described in method 3. Comparing the simulation results in this figure, it can be seen that the FLC in case 1 provides the result with the most damping and faster settling time. Again, all results exhibit a large steady-state error as the reference step size is 0.1.

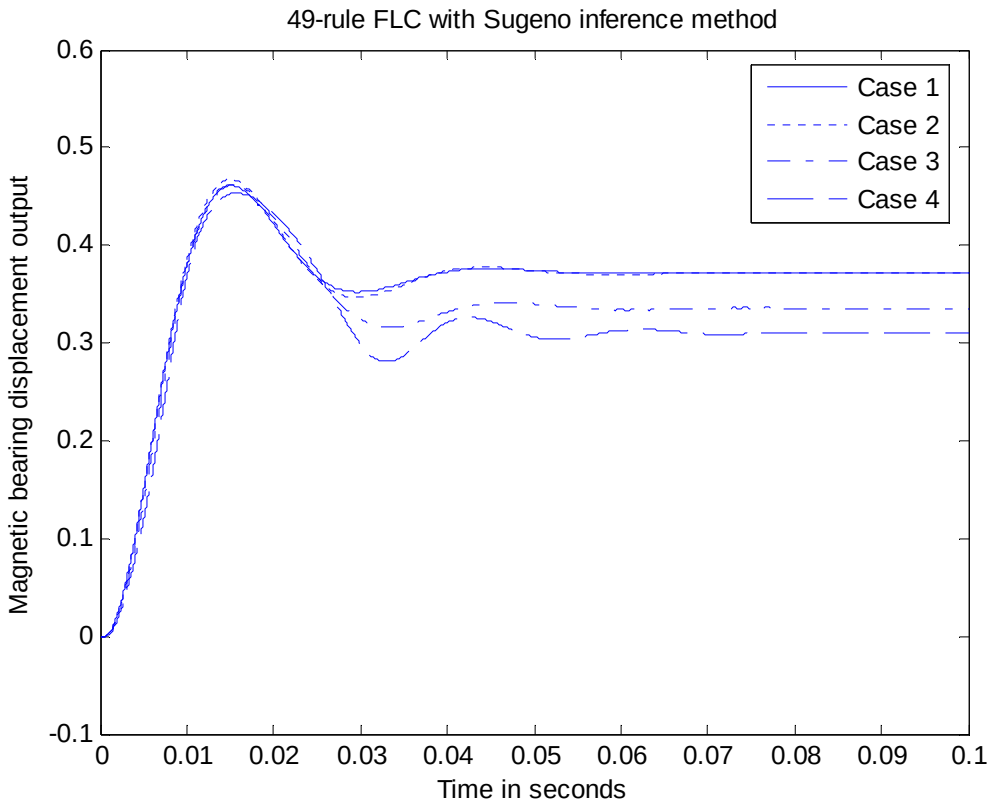

Figure 5.13 Step response of the magnetic bearing system with the designed FLC (49 rules, Sugeno inference method)

5.4 Comparison of the performances of the designed FLCs

The performances of the designed FLCs using the four methods described in the previous section can be compared by studying the dynamic responses of the magnetic bearing output and the FLC output. This can be achieved by observing Figures 5.10, 5.11, 5.12 and 5.13 respectively. Table 5.3 shows the comparison results by evaluating the rise time T_r, the maximum percentage overshoot, settling time T_s, steady-state error (SSE) and the range of control signals shown in Figure 5.10 for the FLC with method 1 (except case 3 as the FLC with Gaussian membership function failed to stabilise the magnetic bearing system).

	T_r	Overshoot	T_s	SSE	Control signal range
Case 1	0.011	16.4%	0.056	-0.32	-0.368 to 0.138
Case 2	0.01	30.9%	0.05	-0.263	-0.392 to 0.09
Case 3	N/A	N/A	N/A	N/A	N/A
Case 4	0.01	36.7%	0.056	-0.273	-0.439 to 0.057

Table 5.3 Performance comparison of the designed FLC with method 1

It can be seen that the designed FLC in case 1 uses the triangular membership functions for the inputs and output, ***MIN*** for ***t***-norm operation, ***MAX*** for ***s***-norm operation, ***MIN*** for implication, and **CENTROID** for defuzzification gave the best result among others.

Table 5.4 shows the comparison results by evaluating the rise time T_r, the maximum percentage overshoot, settling time T_s, steady-state error (SSE) and the range of control signals shown in Figure 5.11 for the FLC with method 2.

	T_r	Overshoot	T_s	SSE	Control signal range
Case 1	0.012	12.4%	0.03	-0.312	-0.37 to 0.24
Case 2	0.01	38.05%	0.046	-0.24	-0.35 to 0.15
Case 3	0.015	12.23%	0.04	-0.45	-0.47 to 0.2
Case 4	0.022	2.1%	0.03	-0.435	-0.4 to 0.1

Table 5.4 Performance comparison of the designed FLC with method 2

It can be seen from Table 5.4 that the FLC uses triangular membership functions for the inputs and outputs, ***MIN*** for ***t***-norm operation, ***MAX*** for ***s***-norm operation, ***MAX*** for aggregation, ***MIN*** for implication, and ***CENTROID*** for defuzzification (case 1) provides the best result in terms of overshoot, settling time and steady state error.

Table 5.5 shows the comparison results by evaluating the rise time T_r, the maximum percentage overshoot, settling time T_s, steady-state error (SSE) and the range of control signals shown in Figure 5.12 for the FLC with method 3.

	T_r	*Overshoot*	T_s	*SSE*	*Control signal range*
Case 1	0.01	24.40%	0.036	-0.2713	-0.3619 to 0.2856
Case 2	0.01	26.39%	0.036	-0.2714	-0.3694 to 0.2
Case 3	0.01	29.12%	0.03	-0.264	-0.3793 to 0.2
Case 4	0.01	32.12%	0.058	-0.2583	-0.4054 to 0.1397

Table 5.5 Performance comparison of the designed FLC with method 3

It can be seen from Table 5.5 that the FLC in case 1 uses triangular membership functions for the inputs and output, ***MIN*** for ***t***-norm operation, ***MAX*** for ***s***-norm operation, and **WTAVER** for defuzzification (case 1) provides the best result among others.

Table 5.6 shows the comparison results by evaluating the rise time T_r, the maximum percentage overshoot, settling time T_s, steady-state error (SSE) and the range of control signals shown in Figure 5.13 for the FLC with method 4.

	T_r	*Overshoot*	T_s	*SSE*	*Control signal range*
Case 1	0.01	24.11%	0.035	-0.2721	-0.3613 to 0.2501
Case 2	0.01	26.05%	0.036	-0.2716	-0.3666 to 0.2
Case 3	0.009	37.50%	0.04	-0.2355	-0.3581 to 0.2078
Case 4	0.009	46.13%	0.053	-0.2104	-0.3444 to 0.1585

Table 5.6 Performance comparison of the designed FLC with method 4

Comparing the performance of the FLC in Table 5.6, it can be seen that the 49-rule FLC used in case 1 uses triangular membership functions for the inputs and output, **PROD**

for **t**-norm operation, **MAX** for **s**-norm operation, and **WTAVER** for defuzzification provides the best result.

Figure 5.14 shows the four best step responses of the magnetic bearing system under fuzzy logic control using the four methods, respectively. The solid line shows the best response of the magnetic bearing system using the 25-rule FLC with Mamdani inference method. The dotted line illustrates the best response of the magnetic bearing system using the 25-rule FLC with the Sugeno inference method. The dash-dotted line is the best response of the magnetic bearing system using the 49-rule FLC with the Mamdani inference method and the dashed line provides the best response of the magnetic bearing system using the 49-rule FLC with the Sugeno inference method.

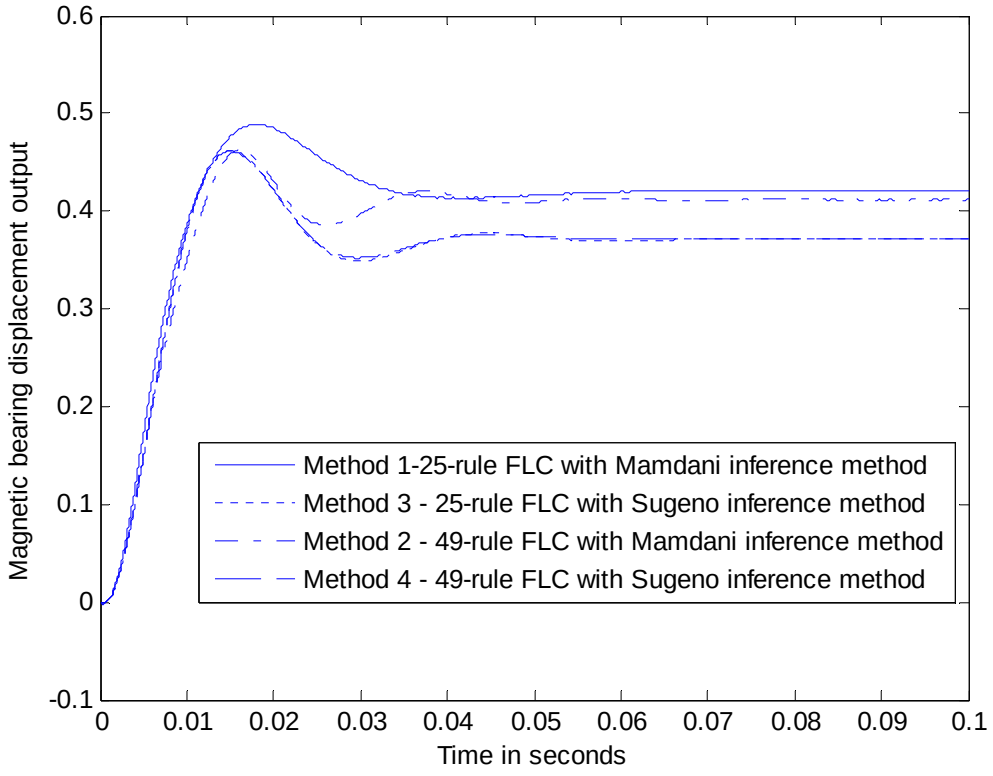

Figure 5.14 Comparison of the best step responses of the magnetic bearing control system with the FLC designed using the four methods

From Figure 5.14 it can be seen that method 2 provides the best result as it leads to a quicker and well damped response.

Investigation of Different Deffuzification Methods

Further studies have been carried out by investigating the effect of different defuzzification methods. The following methods are provided in the MATLAB fuzzy logic toolbox: the centroid of area method (centre of gravity), the bisector of area method, the mean of maximum method, the smallest of maximum method, and the largest of maximum method. All methods have been investigated and it is found that the centroid of area method provides the best simulation result.

Tuning via Scaling the Input and Output Universes of Discourses

The simulation results shown previously all have a large steady-state error. This error cannot be completely eliminated as the controller designed is a PD-like FLC which doesn't have integration property. However, the output response can be improved by adjusting the scaling factors K_p, K_d and h shown in Figure 5.9. This in turn will adjust the universe of discourses for the input and output membership functions. Figure 5.15 shows a comparison result with different scaling factors. It can be seen that the steady-state error has been reduced dramatically with $K_p=1$, $K_d=1$ and $h=2$. However, the damping on the step response has been reduced. The response with $K_p=1$, $K_d=1$ and $h=1.4$ provides the result with a small steady-error and faster settling time.

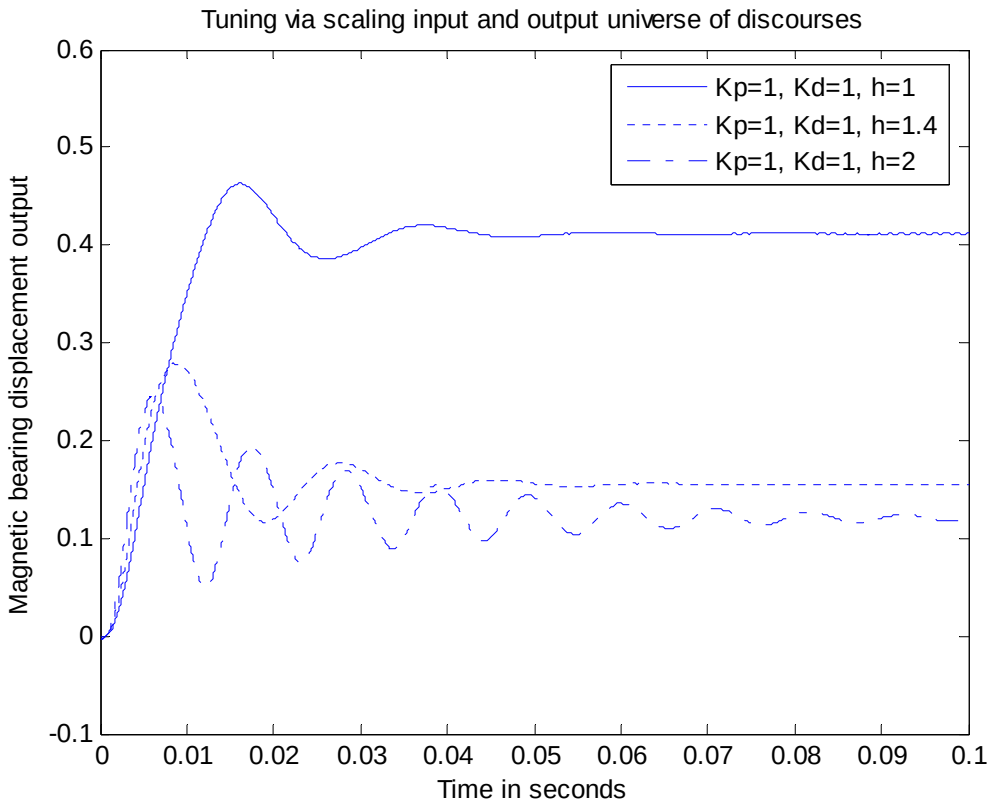

Figure 5.15 Step responses of the magnetic bearing system with the FLC design using different scaling factors

Simulation of the Magnetic Bearing System with the Designed FLC Using the Analytical Model

The block diagram of the magnetic bearing system under the control of the designed FLCs based on the analytical model (both rigid and bending modes) is shown in Figure 5.16. Figure 5.17 shows the step response of the displacement corresponding to a step change with the designed PD-like FLCs. The solid line shows the step response of channel 1 and the dotted line shows the response of channel 2. It can be seen that the designed FLCs stabilise the system without introducing the notch filters if the system model is represented in the combined rigid body and bending modes.

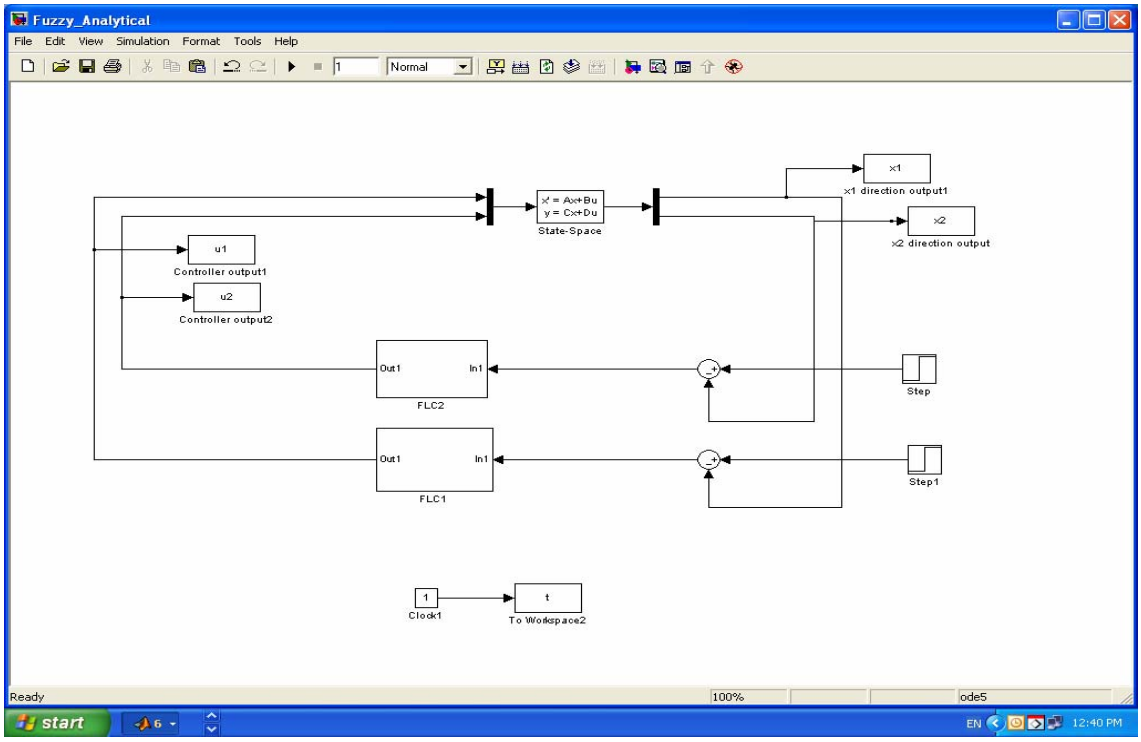

Figure 5.16 Block diagram of the fuzzy control approach with the analytical model

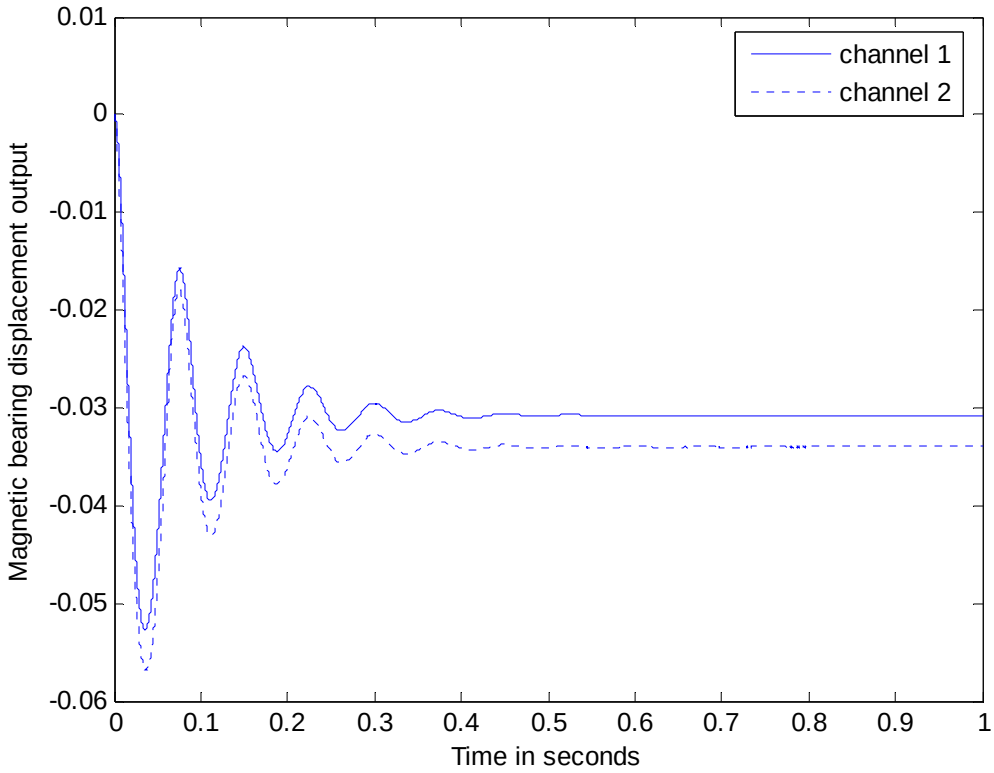

Figure 5.17 Step response with the designed FLC using the analytical model

Implementation of the FLC Designed for the MBC 500 Magnetic Bearing System

The FLC was programmed in C language. The sampling period used in the implementation is 4×10^{-5} seconds. However, it was found that the DSP was unable to execute all the code in the specified sample period. One solution to this problem is to program the FLC using Assembler language. The other alternative is to purchase a much faster DSP card. However, due to time and financial constraints, these alternatives could not be explored in this research; these have been left as further work to be carried out at a later stage.

5.5 Comparison between the Conventional Controller and the Advanced Fuzzy Logic Controller (FLC) for Magnetic Bearing Stabilisation

Conventional Controller

It was demonstrated previously in Chapter 4 that there were two resonant modes which threaten the stability of the closed loop magnetic bearing system. The conventional lead compensator cannot handle the two dominant resonant modes of the magnetic bearing system. This necessitates the design of two notch filters to filter out the unwanted characteristics at the resonant frequencies. From the analytical and experimental models of the MBC500 magnetic bearing system, it was found that the two resonant modes are located at approximately 749 Hz and 2069 Hz. After two notch filters were designed to handle the two resonant modes, a lead compensator was designed to stabilise the magnetic bearing system. The lead compensator added a positive phase to the system in a given frequency range. The compensator design was based on the analytical rigid body model where the shaft was a point mass with no angle variable θ.

The performances of the conventional lead compensator and the two notch filters designed have been evaluated via simulation using both the analytical model and the model obtained via system identification. The designed lead compensator and notch filters were also implemented in real time for the MBC 500 magnetic bearing system. The controller designed worked for all four channels of the MBC 500 magnetic bearing system. Tests were performed to test the dynamic response and robustness of the conventional controller and the notch filter designed and each test was successful.

Advanced Fuzzy Logic Controller (FLC)

A PD-like FLC was designed for stabilising the magnetic bearing system. Two different numbers of rule sets (25-rule and 49-rule) were formulated for the PD-like FLC. Two different fuzzy inference methods, the Mamdani and Sugeno methods, have been used. The performance of the designed FLC has been evaluated via simulation. Comparison studies of the FLC performances with two different sets of rules, two different inference methods, different membership functions, different *t*-norm and *s*-norm operations, and different defuzzification methods have been investigated. Simulation results show that the FLC designed leads to a good system performance. To further improve system performance, scaling factors have been tuned. Simulation has also been carried out based on the analytical model derived that represented both the rigid body and bending modes. Again, simulations have shown highly promising results.

The simulation performance showed that the FLC designed can handle the resonant modes very well without the presence of the two notch filters.

Based on all the simulation results reported above, it was concluded that the designed 49-rule FLC uses triangular membership functions for the inputs and output, ***MIN*** for ***t***-

norm operation, ***MAX*** for ***s***-norm operation, ***MAX*** for aggregation, ***MIN*** for implication, and ***CENTROID*** for defuzzification provides the best result.

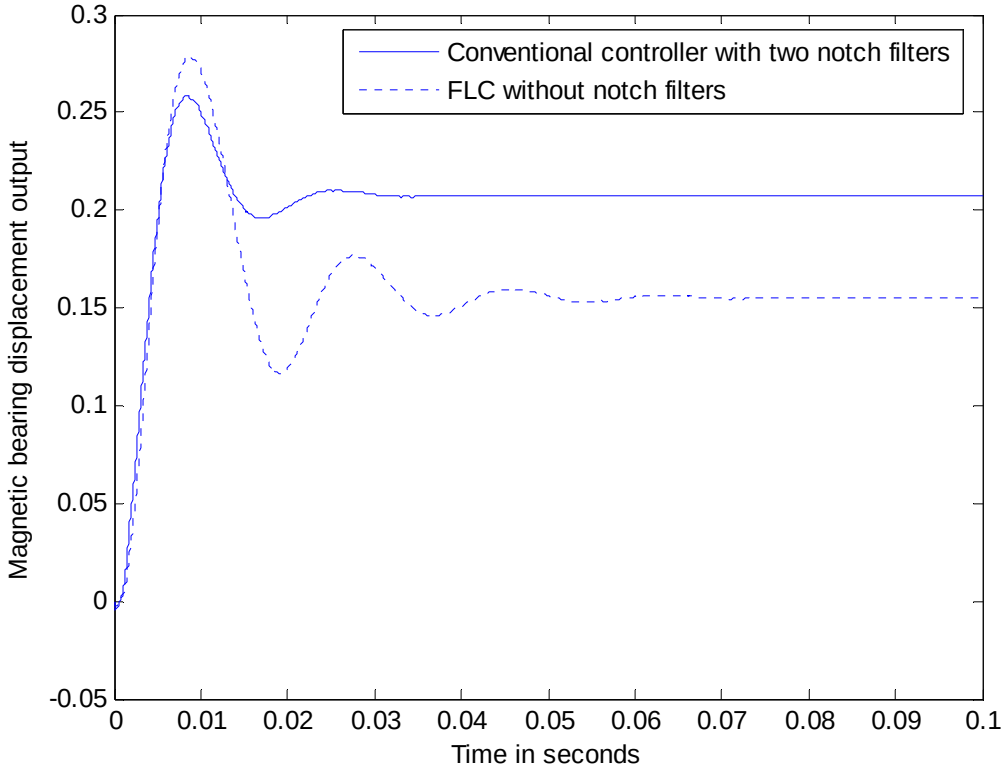

Figure 5.18 Comparison results of the step response of the magnetic bearing system with the designed conventional controller and the designed FLC

Figure 5.18 shows the step response of the magnetic bearing system with the designed conventional controller and the designed FLC based on the identified model of the MBC 500 magnetic bearing system. Comparing the simulation results of the conventional controller and the advanced PD-like FLC, it can be seen that the response with the designed conventional controller has less settling time. The step response with the designed advanced PD-like FLC has longer setting time but less steady-state error. Moreover, the advanced PD-FLC can handle the two resonant modes without the need of using the two notch filters.

5.6 Summary

This chapter started with the structure of a basic FLC. Two different fuzzy inference methods, the Mamdani and Sugeno methods, have been reviewed. The process of developing and designing the FLC for the stabilisation of the magnetic bearing system has been described. The performance of the designed FLC has been evaluated via simulation. The simulation result shows that the FLC designed leads to a good system performance. Comparison studies of the FLC performances with two different sets of rules, two different inference methods, different membership functions, different *t*-norm and *s*-norm operations, and different defuzzification methods have been investigated. To further improve system performance, scaling factors have been tuned. Again, simulations have shown highly promising results.

Finally, this chapter has compared the controller simulation for both the conventional controller and advanced PD-like fuzzy logic controller via evaluating controller performance. The advantage of using the conventional controller lies in its simplicity for real-time implementation. The disadvantage of using the conventional controller is that it cannot handle the resonant modes and as a result additional notch filters are needed in this method. If the notch filters are not designed properly, they can lead to the instability of the system. In addition, four separate conventional controllers were designed, based on the four models of the four channels of the magnetic bearing system. The first advantage of the PD-like FLC is that it can handle the resonant modes well without using notch filters. As a result, this will not threaten the stability of the system. The second advantage of the PD-like FLC is that as the FLC is nonlinear, the PD-like FLC designed for one channel should work for all other three channels. However, the PD-like FLCs are more computationally intensive than the conventional controller. Due

to the speed limit of the DS1102 DSP card, the PD-like FLC cannot be implemented at this stage. The overall conclusion and direction for future development will be discussed in the next chapter.

6 Conclusion and Future Work

6.1 Overview

In this last chapter, all the preceding chapters will be brought together with the aim to examine the extent to which the objectives have been achieved. This chapter also will present some directions for future development and other related work.

6.2 General Conclusion

The study has investigated the techniques for identifying a system model and designing both the conventional and advanced controllers for Active Magnetic Bearing (AMB) system stabilisation.

In Chapter 3 it has been reported that an analytical model of the MBC 500 magnetic bearing system has been derived. This provided the basic knowledge of the AMB system's rigid body and bending body models. In the same Chapter 3 it has been reported that a model has been obtained via a two-step closed-loop system identification. This research concludes that the magnetic bearing system is complex to model both analytically and experimentally. Although complex, the analytical model has provided a realistic view of the real system. The model obtained via system identification has provided adequate information on the low frequency and the two resonant modes of the MBC 500 magnetic bearing system.

In Chapter 4 the design of notch filters based on the resonant frequencies as reported in Chapter 3 has been carried out. The two notch filters have been designed in order to control the magnitude and phase fluctuations at the resonant modes in the system. A conventional controller has been designed and implemented based on the model obtained as reported in Chapter 4. A significant conclusion has been drawn when designing the lead compensator. It has been found that a controller with too large a positive phase angle has a negative effect on the magnetic bearing system. This finding is very significant because it restricts the controller design specifications and yields an optimum lead angle for the compensator. The performance of the designed controller and the two notch filters have been evaluated via computer simulation using MATLAB and SIMULINK. This conventional controller and the two notch filters have also been implemented using the dSPACE DS1102 DSP card.

In Chapter 5 the Fuzzy Logic theory and Fuzzy Logic Controller (FLC) structures with two different fuzzy inference methods that this study has drawn upon have been reported. These inference methods are Mamdani and Sugeno-Type fuzzy inference methods. PD-like FLC has then been designed for the AMB system stabilisation. Two different numbers of rule sets (25-rule and 49-rule) were formulated for the PD-like FLC. Two different fuzzy inference methods, Mamdani and Sugeno methods, have been used. The performance of the designed FLC has been evaluated via simulation. Comparison studies of the FLC performances with two different sets of rules, two different inference methods, different membership functions, different *t*-norm and *s*-norm operations, and different defuzzification methods have been investigated. The simulation result showed that the FLC designed leads to a good system performance. To

further improve system performance, scaling factors have been tuned. Again, simulations based on both the identified model and the analytical models of the MBC500 magnetic bearing system have shown highly promising results. It must be pointed out that the simulation performance has shown that the FLC designed can handle the resonant modes very well without the presence of the two notch filters.

Comparison studies of the designed conventional and the advanced PD-like FLC for the AMB system stabilisation have been evaluated via controller performance simulation. This has been reported in chapter 5. The simulation results have shown that both the conventional and the advanced PD-like FLC stabilise the MBC 500 magnetic bearing system successfully. The advantage of using the conventional controller lies in its simplicity for real-time implementation. The disadvantage of using the conventional controller is that it cannot handle the resonant modes and as a result additional notch filters are needed in this method. If the notch filters are not designed properly, it can lead to the instability of the system. The first advantage of the PD-like FLC is that it can handle the resonant modes well without using notch filters. As a result, this will not threaten the stability of the system. The second advantage of the PD-like FLC is that as the FLC is nonlinear, the PD-like FLC designed for one channel should work for all other three channels. However, the PD-like FLC are more computationally intensive than the conventional controller. Due to the speed limit of the DS1102 DSP card, the PD-like FLC cannot be implemented at this stage.

6.3 Suggestions for Future Research

The extensions of this research lie primarily in the areas of implementation and applications of the FLC. It is highly recommended that a faster DSP be used for the implementation of the FLC.

The rotor in the MBC 500 magnetic bearing system has been suspended but is not rotating. In magnetic bearings the shafts (rotors) are often required to rotate at high speeds and unbalanced masses in these systems generate significant disturbance forces called synchronous forces. The synchronous forces cause vibration of the rotors and can often lead to severe problems in rotating machines. Another extension of the research is to investigate both conventional and advanced approaches for attenuating the effects of synchronous disturbances in the magnetic bearing systems.

Bibliography

Designing Lead and Lag Compensator. Control Tutorials for Matlab, The University of Michigan. **2005**.

A Zadeh, L. (1995). Fuzzy Logic Toolbox. Release Notes for Release 14 with Service Pack 1. Berkeley, CA.

Allaire, P. E., D. W. Lewis, et al. (1981). "Feedback Control of a Single Mass Rotor on Rigid Supports." J. Franklin Inst. **312**(1): pp.1-11.

Allaire, P. E., D. W. Lewis, et al. (1983). "Active Vibration Control of a Single Mass Rotor of Flexible Supports." J.Franklin Inst **315**(3): pp.211-222.

Balas, G. J., J. C. Doyle, et al. (1995). Matlab μ-Analysis and Synthesis Toolbox. Natick, MA, USA, The Mathworks.

Bleuler, H., C. Gahler, et al. (1994). "Application of Digital Signal Processors for Industrial Magnetic Bearings." IEEE Trans. Control System Technology **2**(4): pp.280-289.

Chen, M. and C. L. Knospe (2005). "Feedback Linearization of Active Magnetic Bearings: Current-Mode Implementation." IEEE/ASME Transaction On Mechatronics **10**(6): pp.632-639.

Dorf, R. C. and R. H. Bishop (1995). Modern Control Systems, Addison-Wesley Publishing Company.

Fujita, M., F. Matsumura, et al. (1990). Experiments on the H Disturbances Attenuation Control of A Magnetic Suspension System. Proc of the 29 th IEEE Conference Decision and Control.

Habib, M. M. and J. I. Hussain (2003). Control of Dual Acting Magnetic Bearing Actuator System Using Fuzzy Logic. IEEE International Symposium on Computational Intelligence in Robortics and Automation, Kobe, Japan, IEEE.

Hajjaji, A. E. and M. Ouladsine (2001). "Modeling and Nonlinear Control of Magnetic Levitation Systems." IEEE Transactions on Industrial Electronics **48**(4): pp.831-838.

Hartavi, A. E., O. Ustun, et al. (2003). "A Comparative Approach on PD and Fuzzy Control of AMB Using RCP." IEEE.

Hong, S.-K., R. Langari, et al. (1997). Fuzzy Modeling Control of a Nonlinear Magnetic Bearing System. Proc. of the 1997 IEEE International Conference On Control Applications.

Humphris, R. R., R. D. Kelm, et al. (1986). "Effect of Control Algorithms On Magnetic Journal Bearing Properties." Journal of Engineering For Gas, Turbine & Power **108**: pp.393-632.

Humphris, R. R., R. D. Kelm, et al. (1986). "Effect of Control Algorithms on Magnetic Journal Bearing Properties." J. Eng. Gas Turbines Power **108**: pp.624-632.

Hung, J. Y. (1991). Nonlinear Control of Electromagnetic Systems. Proc. 17th Annu. Conf. IEEE Ind. Electron Soc., Kobe, Japan.

Hung, J. Y. (1995). "Magnetic Bearing Control Using Fuzzy Logic." IEEE Transactions on Industry Applications **31**(6): pp.1492-1497.

Ishidori, A. (1987). Nonlinear Control Systems: An Introduction. New York, Springer-Verlag.

Keith, F., R. Williams, et al. (1988). Digital Control of Magnetic Bearings Supporting a Multimass Flexible Rotor. Mag. Suspension Technology Workshop, NASA Lang;ey Research Center, Hampton, VA.

Komori, M., M. Kumamoto, et al. (1998). "A Hybrid-Type Superconducting Magnetic Bearing System with Nonlinear Control." IEEE Transactions on Applied Superconductivity **8**(2): pp.79-83.
Krstic, M., I. Kanellakopoulos, et al. (1995). Nonlinear and Adaptive Control Design. New York, Wiley.
Lin, L. C. and T. B. Gau (1997). "Feedback Linearization and Fuzzy Control for Conical Magnetic Bearings." IEEE Trans. Control System Technology **5**(4): pp.417-426.
Lindlau, J. D. and C. R. Knospe (2002). "Feedback Linearization of An Active Magnetic Bearing With Voltage Control." IEEE Transaction On Control Systems Technology **10**(1): pp.21-31.
Liu, K. and F. L. Lewis (1993). Some Issues About Fuzzy Logic Control. The 32nd Conference on Decision and Control, San Antonio, Texas, IEEE.
Lun, K. Y., V. T. Coppola, et al. (1996). "Adaptive Auto Centering Control For An Active Magnetic Bearing Supporting A Rotor With Unknown Mass Imbalance." IEEE Transactions on Control System Technology **4**(5): pp.587-597.
Magnetic Moments, E. (1995). MBC 500 Magnetic Bearing System Operating Instructions. USA, Magnetic Moments. **1995**.
Matsumura, F., T. Namerikawa, et al. (1996). "Application of Gain Scheduled H Robust Controllers to a Magnetic Bearing." IEEE Transactions on Control System Technology **4**(5): pp.484-493.
McFarlane, D. and K. Glover (1992). "A Loop Shaping Design Procedure Using H Synthesis." IEEE Trans. on Automatic Control **37**(6): pp.759-769.
Mizuno, T. and M. Aizawa (2002). Repulsive Magnetic Bearing Using a Piezoelectric Actuator For Stabilization. 8th International Symposium On Magnetic Bearing, Mito, japan.
Mohamed, A. M. and I. Busch-Vishniac (1995). "Imbalance Compensation and Automation Balancing in Magnetic Bearing Systems Using the Q-Parameterization Theory." IEEE Transactions on Control System Technology **3**(2): pp.202-211.
Mohamed, A. M. and F. P. Emad (1992). "Conical Magnetic Bearings with Radial and Thrust Control." IEEE Trans. Automatic Control **37**(12): pp.1859-1868.
Morse, N., R. Smith, et al. (1995). Analytical Modelling of a Magnetic Bearing System. **2004**.
Morse, N., R. Smith, et al. (1996). Magnetic Bearing Lab#2: Magnetic Bearing System Identification. **2004**.
Morse, N., R. Smith, et al. (1996). Magnetic Bearing Lab#3: Notch Filtering of Resonant Modes. **2004**.
Motee, N. and M. S. D. Queiroz (2002). Control of Active Magnetic Bearing. Proc. of the 41st IEEE Conference on Decision and Control, Las Vegas, Nevada, USA, IEEE.
Mukaidono, M. (2001). Fuzzy Logic For Beginners. Singapore, World Scientific Publishing Co. Pte.Ltd.
Namerikawa, T., M. Fujita, et al. (1998). Wide Area Stabilization of A Magnetic Bearing Using Exact Linearization. Proc. 6th International Symposium on Magnetic Bearings, Cambridge, Massachusetts, USA.
Nonami, K. and T. Ito (1996). "μ Synthesis of Flexible Rotor-Magnetic Bearing Systems." IEEE Transactions on Control System Technology **4**(5): pp.503-512.

Passino, K. M. and S. Yurkovich (1998). Fuzzy Control, Addison-Wesley Longman, Inc.
Petrov, M., I. Ganchev, et al. (2002). Fuzzy PID Control of Nonlinear Plants. 2002 First International IEEE Symposium "Intelligent Systems", IEEE.
Polajzer, B., D. Dolinar, et al. (1999). "Modeling and Control of Horizontal-Shaft Magnetic Bearing System." IEEE: pp.1051-1055.
Revell, J. (2000). Digital Controller Design and Implementation for a Magnetic Bearing System. Melbourne, Australia**:** pp.1-92.
Reznik, L. (1997). Fuzzy Controllers, Newnes.
Rundell, A. E., S. V. Drakunov, et al. (1996). "A Sliding Mode Observer and Controller for Stabilization of Rotational Motion of a Vertical Shaft Magnetic Bearing." IEEE Transactions on Control System Technology **4**(5): pp.598-608.
Rutland, N. K., P. S. Keogh, et al. (1995). The Avoidance of Saturation Limits in Magnetic Bearing Systems during Transient Excitation. Proc. 3rd International Symposium on Magnetic Suspension Technology, Tallahasse, Florida.
Sedra, A. S. and K. C. Smith (2004). Microelectronic Circuits. Oxford, New York, Oxford University Press.
Shiau, T. N., G. J. Sheu, et al. (1997). "Vibration & Control of A Flexible Rotor in Magnetic Bearings Using Hybrid Method & H Control Theory." Journal of Engineering For Gas, Turbine & Power **119**: pp.179-195.
Shuliang, L. (2001). Synthesis and Fuzzy Logic Control Of Flexible Rotor Systems With Active Magnetic Suspensions. Mechanical Engineering. Texas, Texas A & M University**:** 235.
Smith, R. D. and W. F. Weldon (1995). "Nonlinear Control of a Rigid Rotor Magnetic Bearing System: Modeling and Simulation with Full State Feedback." IEEE Transaction On Magnetic **31**(2): pp.973-980.
Tokat, S., I. Eksin, et al. (2003). "A New PI+D Type Hierarchical Fuzzy Logic Controller." IEEE: pp.570-575.
Torres, M., H. S. Ramirez, et al. (1999). Sliding Mode Nonlinear Control of Magnetic Bearings. International Conference on Control Applications, Kohala Coast-Island of Hawai'i, IEEE.
Trumper, D. L., S. M. Olson, et al. (1997). "Linearizing Control of Magnetic Suspension Systems." IEEE Trans. on Control System Technology **5**(4): pp.427-437.
Zhang, H., Z. Lin, et al. (2002). A Convex Optimization Approach to Robust Controller Design for Active Magnetic Bearing Suspension Systems. 8th International Symposium on Magnetic Bearing, Mito, Japan.

APPENDICES

APPENDIX A

File : channel2
Description: Program for data

```
load c:\MATLAB701\work\channel2.mat %Data collected by Jared
%bode plot of magnetic bearing channel 2 from r2 to y2
figure(1)
subplot(211),semilogx(yr2(:,1)*2*pi,20*log10(yr2(:,2)));
title('Input r2 to output y2')
ylabel('Magnitude'), grid on
subplot(212),semilogx(yr2(:,1)*2*pi,yr2(:,3));
ylabel('Phase'), grid on
xlabel('radians')
%bode plot of magnetic bearing channel 2 from r2 to u2
figure(2)
subplot(211),semilogx(ur2(:,1)*2*pi,20*log10(ur2(:,2)));
title('Input r2 to error u2')
ylabel('Magnitude'), grid on
subplot(212),semilogx(ur2(:,1)*2*pi,ur2(:,3));
ylabel('Phase'), grid on
xlabel('radians')
%data Tyr/Tur
amp=yr2(:,2)./ur2(:,2); %Amplitude
pha=(yr2(:,3)-ur2(:,3));%Phase
rps=2*pi*yr2(:,1); %Frequency in rad/s
%Transform amplitude and phase to a complex valued response
i=sqrt(-1);
zfr=amp.*exp(i*pha*pi/180);
Ts=0; %sample time is 0 for continuous time system
gfr=idfrd(zfr,rps,Ts);
figure(3)
bode(gfr)
%Use frequency domain data for estimation to get a continuous time
model
%For a polynomial model with nb as numerator coefficient and nf as
%estimated denominator coefficient
nb=2;
nf=3;
modeloe=oe(gfr,[nb nf]);
%compute the prediction error estimate of a general
%liner model with default choice of order
```

```
modelpem=pem(gfr);
figure(4)
compare(gfr,modeloe,modelpem);
```

APPENDIX B

Frequency Response Data for Channel 2

This is the frequency response of the bearing system under closed loop stable operation.

Input r2 to Output u2

Freq(Hz)	Gain (V/V)	Phase (deg)
10	1.127	352.64
15	1.1746	355.46
20	1.3247	345.78
25	1.4927	339.98
30	1.8381	337.86
35	2.3276	330.06
40	2.9659	312.61
45	3.1892	288.22
50	3.2256	259.75
55	3.5073	251.86
60	2.3002	245.85
65	2.1902	248.63
70	2.354	267.43
75	2.8338	263.34
80	2.8693	237.82
85	3.296	249.67
90	2.5625	216.87
95	2.2629	212.49
100	2.3918	210.28
110	2.5179	198.2
120	1.8941	197.14
130	1.7446	192.44
140	1.6242	189.64
150	1.5384	187.58
160	1.4782	184.92
170	1.4151	175.49
180	1.3789	194.94
190	1.3487	178.57
200	1.3193	176.19
210	1.2969	175.96
220	1.2778	179.79
230	1.2576	176.73

Input r2 to Output y2

Freq(Hz)	Gain (V/V)	Phase (deg)
10	1.4905	177.78
15	1.5322	172.71
20	1.6388	177.82
25	1.7708	178.05
30	1.9853	172.1
35	2.3384	167.71
40	2.5987	132.32
45	2.7345	115.12
50	2.6902	96.733
55	2.0613	82.346
60	1.4488	79.698
65	1.3547	74.828
70	1.2551	74.898
75	1.2859	73.05
80	1.477	62.932
85	1.2818	60.806
90	1.3318	39.963
95	1.0511	39.415
100	0.961	28.27
110	0.7306	21.419
120	0.5934	15.429
130	0.4959	8.9109
140	0.4071	5.3251
150	0.3497	3.0341
160	0.2967	3.5176
170	0.2634	0
180	0.2354	351.63
190	0.2125	356.34
200	0.1905	356.58
210	0.1751	349.04
220	0.1602	344.93
230	0.1504	352.57

240	1.2564	165.05	240	0.1355	343.77
250	1.233	173.73	250	0.1318	344.69
260	1.2108	173.59	260	0.1151	338.08
270	1.2162	196.15	270	0.1104	343.28
280	1.1999	180.8	280	0.1051	339.97
290	1.2004	174.08	290	0.1027	340.8
300	1.1796	169.19	300	0.0962	336.13
310	1.1726	189.27	310	0.0912	339.26
320	1.1956	156.55	320	0.0913	338.07
330	1.1786	177.74	330	0.0832	332.89
340	1.1529	168.54	340	0.0741	332.92
350	1.1479	166.1	350	0.0755	323.51
360	1.1687	181.43	360	0.0716	325.98
370	1.1497	161.38	370	0.0651	322.58
380	1.1558	156.03	380	0.0686	325.29
390	1.1268	168.38	390	0.0649	331.33
400	1.1237	165.79	400	0.0635	323.31
410	1.1223	167.42	410	0.0627	317.33
420	1.1148	163.23	420	0.0588	323.81
430	1.1093	164.64	430	0.0604	314.92
440	1.1355	148.7	440	0.0529	314.43
450	1.0767	169.57	450	0.0512	311.2
460	1.0792	155.42	460	0.0478	316.68
470	1.1163	168.82	470	0.0505	320.62
480	1.1204	155.27	480	0.0509	316.02
490	1.0767	159.3	490	0.0427	309.69
500	1.0781	157.48	500	0.0403	315.5
510	1.0801	158.84	510	0.041	305.56
520	1.0798	157.02	520	0.0444	298.74
530	1.0737	158.63	530	0.0418	300.37
540	1.0661	159.8	540	0.0389	311.28
550	1.0644	154.71	550	0.0396	294.91
560	1.0776	132.1	560	0.0415	295.88
570	1.008	173.94	570	0.0401	307.32
580	0.9983	175.11	580	0.0375	293.08
590	1.0345	144.2	590	0.0346	288.29
600	1.0476	134.18	600	0.0272	277.9

610	1.054	149.98	610	0.0357	288.61
620	1.0362	154.81	620	0.0296	274.94
630	1.0206	153.82	630	0.029	279.01
640	1.0066	149.02	640	0.0265	271.38
650	1.0303	149.96	650	0.0242	273.47
660	0.9977	154.29	660	0.0256	260.13
670	0.9892	147.92	670	0.0222	18.397
680	0.8211	152.25	680	0.0216	266.18
690	0.966	124.83	690	0.0239	237.13
700	0.9051	165.79	700	0.0203	241.8
710	1.0123	171.53	710	0.0226	204.81
720	0.9111	149.38	720	0.0233	201.08
730	0.9369	160.49	730	0.0214	195.4
740	0.8445	155	740	0.0375	168.55
750	0.7801	153.97	750	0.0656	161.32
751	0.7789	153.33	751	0.061	137.52
752	0.7387	146.97	752	0.069	149.48
753	0.7321	153.01	753	0.069	145.67
754	0.7381	151.73	754	0.0762	154.61
755	0.7379	140.28	755	0.0797	150.42
756	0.666	139.46	756	0.0819	156
757	0.6657	145	757	0.0865	139.03
758	0.6944	161.14	758	0.085	136.47
759	0.661	160.83	759	0.0898	125.66
760	0.6333	156.55	760	0.1045	127.56
761	0.5858	146.69	761	0.1046	119.24
762	0.5627	153.08	762	0.1139	133.31
763	0.5435	143.09	763	0.1245	129.26
764	0.4849	149.67	764	0.1299	125.44
765	0.4838	165.05	765	0.1374	125.07
766	0.4269	152.44	766	0.1613	126.66
767	0.3904	156.5	767	0.162	118.68
768	0.351	173.73	768	0.1822	121.89
769	0.3063	176.91	769	0.1984	118.1
770	0.2944	191.51	770	0.2237	96.118
771	0.3089	213.96	771	0.2421	96
772	0.3783	224.93	772	0.2735	104.24

773	0.5211	228.99	773	0.3073	101.14
774	0.7585	253.42	774	0.3531	94.286
775	0.9015	248.22	775	0.4982	74.885
776	1.1528	237.53	776	0.4351	68.79
777	1.4089	231.84	777	0.4356	52.342
778	1.7302	222.2	778	0.5145	55.02
779	1.9159	205.63	779	0.5273	31.104
780	2.0716	202.54	780	0.4959	26.678
781	2.0973	190.08	781	0.4799	12.038
782	2.0998	187.2	782	0.4513	4.3254
783	2.0288	181.15	783	0.3963	358.18
784	1.9576	171.95	784	0.3393	350
785	1.8732	168.8	785	0.3042	343.48
786	1.7989	162.69	786	0.2837	342.52
787	1.7382	167.88	787	0.2775	338.51
788	1.6935	166.15	788	0.2372	333.03
789	1.6517	159.49	789	0.2306	337.3
790	1.5953	164.9	790	0.2174	324.24
791	1.5443	153.04	791	0.2091	330.13
792	1.5487	158.26	792	0.1931	327.09
793	1.5032	155.28	793	0.1793	329.8
794	1.4881	153.04	794	0.1622	323.56
795	1.4283	153.79	795	0.1615	317.46
796	1.4351	152.04	796	0.1469	322.95
797	1.4047	147.51	797	0.1562	315.96
798	1.3879	147.86	798	0.1302	325.18
799	1.3664	152.78	799	0.1321	318.36
800	1.215	125.09	800	0.1361	327.17
801	1.3429	148.24	801	0.1208	308.37
802	1.3318	152.44	802	0.1277	319.8
803	1.3199	153.87	803	0.1091	321.81
804	1.3212	148.48	804	0.1212	313.94
805	1.3188	150.25	805	0.1155	320.81
806	1.2877	148.48	806	0.1008	306.69
807	1.2754	149.46	807	0.1105	320.63
808	1.2633	145.07	808	0.0899	313.65
809	1.2462	147.92	809	0.1046	322.93

810	1.1362	123.22	810	0.0855	312.51
820	1.2036	148.34	820	0.0772	299.81
830	1.1342	126.12	830	0.0803	297.18
840	1.0266	127.39	840	0.0622	230.05
850	1.1438	165.36	850	0.0526	289.13
860	1.0434	162.42	860	0.0504	295.27
870	1.1827	154	870	0.0527	289.5
880	1.0436	138.05	880	0.044	303.77
890	1.0711	121.78	890	0.0537	301.59
900	1.1477	153.65	900	0.042	296.74
910	0.8928	147.1	910	0.042	282.1
920	1.0945	147.27	920	0.0365	279.93
930	1.1106	128.38	930	0.0453	289.57
940	1.1189	151.93	940	0.0403	279.39
950	1.0994	135.73	950	0.0416	299.66
960	1.0924	149.14	960	0.0345	276.99
970	1.0264	130.48	970	0.0311	269.86
980	1.0214	136.04	980	0.0419	265.05
990	0.9255	119.29	990	0.0349	270.73
1000	0.947	116.71	1000	0.035	269.41
1050	0.9964	139.9	1050	0.032	250.83
1100	1.0317	141.11	1100	0.0367	286.12
1150	0.9821	129.3	1150	0.0243	248.44
1200	0.964	127.88	1200	0.0242	272.07
1250	0.895	108.81	1250	0.0209	260.31
1300	0.903	132.05	1300	0.02	225.86
1350	1.039	141.1	1350	0.0169	224.8
1400	0.966	132.2	1400	0.0161	202.09
1450	0.9037	119.81	1450	0.0164	114.95
1500	0.7552	98.33	1500	0.015	225
1550	0.7323	97.644	1550	0.0142	241.64
1600	0.8835	113.59	1600	0.011	188.31
1650	0.8644	111.78	1650	0.0165	214.99
1700	0.7894	131.57	1700	0.0148	242.35
1750	0.9437	102.47	1750	0.009	218.09
1800	0.8657	109.15	1800	0.01	212.75
1850	0.8238	109.88	1850	0.0094	198.27

1900	0.7782	103.37	1900	0.0085	193.91
1950	0.7617	88.129	1950	0.0061	324.9
2000	0.7738	97.278	2000	0.0092	108.78
2010	0.7829	88.918	2010	0.0091	24.597
2020	0.7647	99.085	2020	0.0093	108.02
2030	0.8231	118.7	2030	0.0123	96.515
2040	0.6362	105.55	2040	0.0199	85.714
2041	0.7133	102.01	2041	0.0238	89.918
2042	0.7417	111.56	2042	0.0198	90.041
2043	0.6434	118.7	2043	0.0222	90.768
2044	0.676	96.825	2044	0.0229	92.701
2045	0.6955	110.54	2045	0.0268	85.913
2046	0.658	96.759	2046	0.0322	71.837
2047	0.6426	96.475	2047	0.0303	73.072
2048	0.6129	100.95	2048	0.0377	70.588
2049	0.6057	116.73	2049	0.0425	70.109
2050	0.5441	93.496	2050	0.057	69.136
2051	0.5111	85.246	2051	0.0567	80.109
2052	0.3745	112.29	2052	0.0802	74.188
2053	0.3305	156.31	2053	0.098	63.76
2054	0.9922	130.97	2054	0.1672	65.041
2055	0.7007	135.51	2055	0.3299	20.683
2056	2.6229	169.81	2056	0.1627	348.74
2057	2.0399	95.473	2057	0.2933	350.43
2058	1.2033	87.686	2058	0.2563	283.76
2059	1.1479	92.461	2059	0.1549	268.12
2060	1.2029	114.1	2060	0.092	265.92
2061	1.0229	85.014	2061	0.086	276.96
2062	1.1166	89.796	2062	0.0859	268.32
2063	0.9589	110.88	2063	0.0552	240.7
2064	0.8515	100.69	2064	0.0454	257.56
2065	1.0106	87.243	2065	0.0453	258.39
2066	0.931	95.872	2066	0.037	251.94
2067	0.9314	96.326	2067	0.0434	242.45
2068	1.0094	84.182	2068	0.0444	238.34
2069	0.8058	83.039	2069	0.0357	256.72
2070	0.9516	85.714	2070	0.0336	234.07

2071	0.8919	94.526	2071	0.0259	235.98
2072	0.9999	112.12	2072	0.0267	224.18
2073	0.8492	97.386	2073	0.0234	243.29
2074	0.8873	100.14	2074	0.0224	224.48
2075	0.8708	95.872	2075	0.0381	304.11
2076	0.9663	109.52	2076	0.0213	226.04
2077	0.9755	113.09	2077	0.0241	235.03
2078	0.9667	113.42	2078	0.0225	238.19
2079	0.9613	91.803	2079	0.0203	239.34
2080	0.7441	97.79	2080	0.0174	240.65
2090	0.7486	100.27	2090	0.0202	241.5
2100	0.8299	93.724	2100	0.0151	209.42
2150	0.8343	102.26	2150	0.0089	188.03
2200	0.7706	92.176	2200	0.008	336.93
2250	0.7918	93.527	2250	0.0065	346.34
2300	0.7447	79.42	2300	0.0093	197.65
2350	0.6889	76.034	2350	0.0047	114.87
2400	0.7394	85.493	2400	0.0045	187.51
2450	0.7819	74.755	2450	0.0062	167.86
2500	0.6842	81.84	2500	0.0061	151.55
2550	0.6511	82.4	2550	0.0037	171.99
2600	0.709	75.85	2600	0.0052	271.41
2650	0.7345	72.12	2650	0.0052	108.18
2700	0.69	75.271	2700	0.0043	154.06
2750	0.6752	63.905	2750	0.0044	156.3
2800	0.6798	66.661	2800	0.0039	93.705
2850	0.6923	63.586	2850	0.0043	174.15
2900	0.7299	81.134	2900	0.0029	120.64
2950	0.6325	66.948	2950	0.0043	72.623
3000	0.6551	64.392	3000	0.0048	137.68
3050	0.6454	60.508	3050	0.0038	147.53

APPENDIX C

C2DM Conversion of continuous LTI systems to discrete-time

C2DM Conversion of continuous LTI systems to discrete-time.

[Ad,Bd,Cd,Dd] = C2DM(A,B,C,D,Ts,'method') converts the continuous-time state-space system (A,B,C,D) to discrete time using 'method':

'zoh' Convert to discrete time assuming a zero order hold on the inputs.

'foh' Convert to discrete time assuming a first order hold on the inputs.

'tustin' Convert to discrete time using the bilinear (Tustin) approximation to the derivative.

'prewarp' Convert to discrete time using the bilinear (Tustin) approximation with frequency prewarping. Specify the critical frequency with an additional argument, i.e. C2DM(A,B,C,D,Ts,'prewarp',Wc)

'matched' Convert the SISO system to discrete time using the matched pole-zero method.

[NUMd,DENd] = C2DM(NUM,DEN,Ts,'method') converts the continuous-time polynomial transfer function G(s) = NUM(s)/DEN(s) to discrete time, G(z) = NUMd(z)/DENd(z), using 'method'.

APPENDIX D

Equation Derivation

1. Equation 3.16

$$\sum M = I_0 \ddot{\theta} = F_2(\tfrac{L}{2} - l)\cos\theta - F_1(\tfrac{L}{2} - l)\cos\theta$$

is derived from equation 3.7 ; 3.8 and 3.15 :

$$x_1 = x_0 - (\tfrac{L}{2} - l)\sin\theta$$

Equation 3.7

$$x_2 = x_0 + (\tfrac{L}{2} - l)\sin\theta$$

Equation 3.8

$$\sum F = m\ddot{x}_0 = F_1 + F_2$$

Equation 3.15

2. Equation 3.20

$$\ddot{\chi}_0 = \frac{F_1}{m} + \frac{F_2}{m}$$

is derived from equation 3.15

$$\sum F = m\ddot{x}_0 = F_1 + F_2$$

3. Equation 3.21

$$\ddot{\theta} = \frac{F_2(\frac{L}{2} - l)}{I_0} - \frac{F_1(\frac{L}{2} - l)}{I_0} = -\frac{1}{I_0}(\frac{L}{2} - l)F_1 + \frac{1}{I_0}(\frac{L}{2} - l)F_2$$

is derived from equation 3.16

$$\sum M = I_0 \ddot{\theta} = F_2(\tfrac{L}{2} - l)\cos\theta - F_1(\tfrac{L}{2} - l)\cos\theta$$

4. Equation 3.22

$$X_1 = x_0 - (\tfrac{L}{2} - l_2)\theta$$

is derived from equation 3.9

$$X_1 = x_0 - (\tfrac{L}{2} - l_2)\sin\theta$$

5. Equation 3.23

$$X_2 = x_0 + (\tfrac{L}{2} - l_2)\theta$$

is derived from equation 3.10

$$X_2 = x_0 + (\tfrac{L}{2} - l_2)\sin\theta$$

6. Equation 3.24

$$\begin{bmatrix} \dot{x}_0 \\ \ddot{x}_0 \\ \dot{\theta} \\ \ddot{\theta} \end{bmatrix} = \begin{bmatrix} 0 & 1 & 0 & 0 \\ 0 & 0 & 0 & 0 \\ 0 & 0 & 0 & 1 \\ 0 & 0 & 0 & 0 \end{bmatrix} \begin{bmatrix} x_0 \\ \dot{x}_0 \\ \theta \\ \dot{\theta} \end{bmatrix} + \begin{bmatrix} 0 & 0 \\ \frac{1}{m} & \frac{1}{m} \\ 0 & 0 \\ -\frac{1}{I_0(\frac{L}{2}-l)} & \frac{1}{I_0(\frac{L}{2}-l)} \end{bmatrix} \begin{bmatrix} F_1 \\ F_2 \end{bmatrix}$$

is derived from equations 3.20 and 3.21

$$\ddot{\chi}_0 = \frac{F_1}{m} + \frac{F_2}{m}$$

Equation 3.20

$$\ddot{\theta} = \frac{F_2(\frac{L}{2} - l)}{I_0} - \frac{F_1(\frac{L}{2} - l)}{I_0} = -\frac{1}{I_0}(\frac{L}{2} - l)F_1 + \frac{1}{I_0}(\frac{L}{2} - l)F_2$$

Equation 3.21

7. Equation 3.25

$$\begin{bmatrix} X_1 \\ X_2 \end{bmatrix} = \begin{bmatrix} 1 & 0 & -(\frac{l}{2} - l_2) & 0 \\ 1 & 0 & (\frac{l}{2} - l_2) & 0 \end{bmatrix} \begin{bmatrix} x_0 \\ \dot{x}_0 \\ \theta \\ \dot{\theta} \end{bmatrix}$$

is derived from equations 3.22 and 3.23

$$X_1 = x_0 - (\tfrac{L}{2} - l_2)\theta$$

Equation 3.22

$$X_2 = x_0 + (\tfrac{L}{2} - l_2)\theta$$

Equation 3.23

8. Equation 3.28

$$\frac{\partial F_i}{\partial x_i} = k\left(\frac{-2(i_{controli} + 0.5)^2}{(x_i - 0.0004)^3} - \frac{-2(i_{controli} - 0.5)^2}{(x_i + 0.0004)^3} \right)$$

Is derived from equation 3.27

$$F_i = k\frac{(i_{control_i} + 0.5)^2}{(x_i - 0.0004)^2} - k\frac{(i_{control_i} - 0.5)^2}{(x_i + 0.0004)^2}$$

9. Equations 3.32 and 3.33

$$F_1 = 4375x_1 + 3.5i_{control1}$$

Equation 3.32

$$F_2 = 4375x_2 + 3.5i_{control2}$$

Equation 3.33

are derived from equations 3.26, 3.29 and 3.31

$$F_i(x_i, i_{controli}) = F_i(0,0) + \left[\frac{\partial F_i}{\partial x_i}(0,0) \right](x_i - 0) + \left[\frac{\partial F_i}{\partial i_{controli}}(0,0) \right](i_{controli} - 0)$$

Equation 3.26

$$\left.\frac{\partial F_i}{\partial x_i}\right|_{(0,0)} = 4375$$

Equation 3.29

$$\left.\frac{\partial F_i}{\partial i_{controli}}\right|_{(0,0)} = 3.5$$

Equation 3.31

10. Equation 3.34

$$F_1 = 4375x_0 - 4375(\tfrac{L}{2} - l)\theta + 3.5i_{control1}$$

is derived from equations 3.7 and 3.32

$$x_1 = x_0 - (\tfrac{L}{2} - l)\sin\theta$$

Equation 3.7

$$F_1 = 4375x_1 + 3.5i_{control1}$$

Equation 3.32

11. Equation 3.35

$$F_2 = 4375x_0 + 4375(\tfrac{L}{2} - l)\theta + 3.5i_{control2}$$

is derived from equations 3.8 and 3.33

$$x_2 = x_0 + (\tfrac{L}{2} - l)\sin\theta$$

Equation 3.8

$$F_2 = 4375x_2 + 3.5i_{control2}$$

Equation 3.33

12. Equation 3.36

$$\ddot{x}_0 = \frac{4375x_0 - 4375(\frac{L}{2} - l)\theta + 3.5i_{control1}}{m} + \frac{4375x_0 + 4375(\frac{L}{2} - l)\theta + 3.5i_{control2}}{m}$$

$$\ddot{x}_0 = \frac{8750}{m}x_0 + \frac{3.5i_{control1}}{m} + \frac{3.5i_{control2}}{m}$$

is derived from equations 3.20, 3.34 and 3.35

$$\ddot{\chi}_0 = \frac{F_1}{m} + \frac{F_2}{m}$$

Equation 3.20

$$F_1 = 4375x_0 - 4375(\frac{L}{2} - l)\theta + 3.5i_{control1}$$

Equation 3.34

$$F_2 = 4375x_0 + 4375(\frac{L}{2} - l)\theta + 3.5i_{control2}$$

Equation 3.35

13. Equation 3.37

$$\ddot{\theta} = 8750\frac{(\frac{L}{2} - l)^2\theta}{I_0} - 3.5\frac{(\frac{L}{2} - l)\theta}{I_0}i_{control1} + 3.5\frac{(\frac{L}{2} - l)\theta}{I_0}i_{control2}$$

is derived from equations 3.21 ; 3.34 and 3.35

$$\ddot{\theta} = \frac{F_2(\frac{L}{2} - l)}{I_0} - \frac{F_1(\frac{L}{2} - l)}{I_0} = -\frac{1}{I_0}(\frac{L}{2} - l)F_1 + \frac{1}{I_0}(\frac{L}{2} - l)F_2$$

Equation 3.21

$$F_1 = 4375x_0 - 4375(\frac{L}{2} - l)\theta + 3.5i_{control1}$$

Equation 3.34

$$F_2 = 4375x_0 + 4375(\tfrac{L}{2} - l)\theta + 3.5i_{control2}$$

Equation 3.35

14. Equation 3.38

$$\begin{bmatrix} \dot{x}_0 \\ \ddot{x}_0 \\ \dot{\theta} \\ \ddot{\theta} \end{bmatrix} = \begin{bmatrix} 0 & 1 & 0 & 0 \\ \frac{8750}{m} & 0 & 0 & 0 \\ 0 & 0 & 0 & 1 \\ 0 & 0 & \frac{8750(\frac{L}{2}-l)^2}{I_0} & 0 \end{bmatrix} \begin{bmatrix} x_0 \\ \dot{x}_0 \\ \theta \\ \dot{\theta} \end{bmatrix} + \begin{bmatrix} 0 & 0 \\ \frac{3.5}{m} & \frac{3.5}{m} \\ 0 & 0 \\ -\frac{3.5}{I_0}(\frac{L}{2}-l) & \frac{3.5}{I_0}(\frac{L}{2}-l) \end{bmatrix} \begin{bmatrix} i_{control1} \\ i_{control2} \end{bmatrix}$$

is derived from equations 3.36 and 3.37

$$\ddot{x}_0 = \frac{8750}{m}x_0 + \frac{3.5i_{control1}}{m} + \frac{3.5i_{control2}}{m}$$

Equation 3.36

$$\ddot{\theta} = 8750\frac{(\frac{L}{2}-l)^2\theta}{I_0} - 3.5\frac{(\frac{L}{2}-l)\theta}{I_0}i_{control1} + 3.5\frac{(\frac{L}{2}-l)\theta}{I_0}i_{control2}$$

Equation 3.37

15. Equation 3.39

$$\begin{bmatrix} X_1 \\ X_2 \end{bmatrix} = \begin{bmatrix} 1 & 0 & -(\frac{L}{2}-l_2) & 0 \\ 1 & 0 & (\frac{L}{2}-l_2) & 0 \end{bmatrix} \begin{bmatrix} x_0 \\ \dot{x}_0 \\ \theta \\ \dot{\theta} \end{bmatrix}$$

is derived from equations 3.22 and 3.23

$$X_1 = x_0 - (\tfrac{L}{2} - l_2)\theta$$

Equation 3.22

$$X_2 = x_0 + (\tfrac{L}{2} - l_2)\theta$$

Equation 3.23

16. Equation 3.45

$$\begin{bmatrix} V_{sense1} \\ V_{sense2} \end{bmatrix} = 5000 \begin{bmatrix} 1 & 0 & -(\tfrac{L}{2} - l_2) & 0 \\ 1 & 0 & (\tfrac{L}{2} - l_2) & 0 \end{bmatrix} x_r$$

is derived from equations 3.22, 3.23 and 3.43

$$X_1 = x_0 - (\tfrac{L}{2} - l_2)\theta$$

Equation 3.22

$$X_2 = x_0 + (\tfrac{L}{2} - l_2)\theta$$

Equation 3.23

$$\left.\frac{\partial V_{sensei}}{\partial X_i}\right|_{(0)} = 5000$$

Equation 3.43

17. Equation 3.47

$$\begin{bmatrix} V_{sense1} \\ V_{sense2} \end{bmatrix} = 5000 \begin{bmatrix} 1 & 0 & -(\tfrac{L}{2} - l_2) & 0 & 0 & 0 \\ 1 & 0 & (\tfrac{L}{2} - l_2) & 0 & 0 & 0 \end{bmatrix} x_r$$

is derived from equations 3.36, 3.37 and 3.46

$$\ddot{x}_0 = \frac{8750}{m} x_0 + \frac{3.5 i_{control1}}{m} + \frac{3.5 i_{control2}}{m}$$

Equation 3.36

$$\ddot{\theta} = 8750\frac{(\frac{L}{2}-l)^2\theta}{I_0} - 3.5\frac{(\frac{L}{2}-l)\theta}{I_0}i_{control1} + 3.5\frac{(\frac{L}{2}-l)\theta}{I_0}i_{control2}$$

Equation 3.37

$$\dot{x}_r = \begin{bmatrix} 0 & 1 & 0 & 0 & 0 & 0 \\ \frac{8750}{m} & 0 & 0 & 0 & \frac{3.5}{m} & \frac{3.5}{m} \\ 0 & 0 & 0 & 1 & 0 & 0 \\ 0 & 0 & \frac{8750(\frac{L}{2}-l)^2}{I_o} & 0 & -\frac{3.5}{I_0}(\frac{L}{2}-l) & \frac{3.5}{I_0}(\frac{L}{2}-l) \\ 0 & 0 & 0 & 0 & \frac{-1}{2.2\times10^{-4}} & 0 \\ 0 & 0 & 0 & 0 & 0 & \frac{-1}{2.2\times10^{-4}} \end{bmatrix} x_r + \begin{bmatrix} 0 & 0 \\ 0 & 0 \\ 0 & 0 \\ 0 & 0 \\ \frac{0.25}{2.2\times10^{-4}} & 0 \\ 0 & \frac{0.25}{2.2\times10^{-4}} \end{bmatrix} \begin{bmatrix} V_{control1} \\ V_{control2} \end{bmatrix}$$

Equation 3.46

18. Equation 3.48

$$a \equiv \begin{bmatrix} a_1 \\ a_2 \end{bmatrix}$$

is derived from equations 3.22, 3.23 and 3.43

$$X_1 = x_0 - (\tfrac{L}{2} - l_2)\theta$$

Equation 3.22

$$X_2 = x_0 + (\tfrac{L}{2} - l_2)\theta$$

Equation 3.23

$$\left.\frac{\partial V_{sensei}}{\partial X_i}\right|_{(0)} = 5000$$

Equation 3.43

19. Equation 3.55

$$\dot{x}_f = \begin{bmatrix} 0 & 0 & 1 & 0 \\ 0 & 0 & 0 & 1 \\ \frac{-6.05762e6}{0.272146} & 0 & 0 & 0 \\ 0 & \frac{-4.4363e7}{0.262297} & 0 & 0 \end{bmatrix} x_f + \begin{bmatrix} 0 & 0 \\ 0 & 0 \\ \frac{-1.19029}{0.272146} & \frac{-1.19029}{0.272146} \\ \frac{-0.608354}{0.262297} & \frac{0.608354}{0.262297} \end{bmatrix} \begin{bmatrix} F_1 \\ F_2 \end{bmatrix}$$

is derived from equations 3.51, 3.52, 3.53 and 3.54

$$M = \begin{bmatrix} 2.72146e-01 & 0 \\ 0 & 2.62297e-01 \end{bmatrix}$$

Equation 3.51

$$K = \begin{bmatrix} 6.05762e+06 & 0 \\ 0 & 4.4363e+07 \end{bmatrix}$$

Equation 3.52

$$P = \begin{bmatrix} -1.19029e+00 & -1.19029e+00 \\ -6.08354e-01 & 6.08354e-01 \end{bmatrix} \begin{bmatrix} F_1 \\ F_2 \end{bmatrix}$$

Equation 3.53

$$M\ddot{a} + Ka = P$$

Equation 3.54

20. Equation 3.56

$$\begin{bmatrix} X_1 \\ X_2 \end{bmatrix} = \begin{bmatrix} -1.93745 & -1.83546 & 0 & 0 \\ -1.93745 & 1.83546 & 0 & 0 \end{bmatrix} x_f$$

is derived from equation 3.49

$$\begin{bmatrix} X_1 \\ X_2 \end{bmatrix} = \begin{bmatrix} -1.93745e+00 & -1.83546e+00 \\ -1.93745e+00 & 1.83546e+00 \end{bmatrix} \text{a}$$

21. Equation 3.57

$$\dot{x}_{total} = \begin{bmatrix} 0 & 1 & 0 & 0 & 0 & 0 & 0 & 0 \\ 0 & 0 & 0 & 0 & 0 & 0 & 0 & 0 \\ 0 & 0 & 0 & 1 & 0 & 0 & 0 & 0 \\ 0 & 0 & 0 & 0 & 0 & 0 & 0 & 0 \\ 0 & 0 & 0 & 0 & 0 & 0 & 1 & 0 \\ 0 & 0 & 0 & 0 & 0 & 0 & 0 & 1 \\ 0 & 0 & 0 & 0 & -2.226e7 & 0 & 0 & 0 \\ 0 & 0 & 0 & 0 & 0 & -1.6913e8 & 0 & 0 \end{bmatrix} x_{total} + \begin{bmatrix} 0 & 0 \\ 3.8037 & 3.8037 \\ 0 & 0 \\ -69.5669 & 69.5669 \\ 0 & 0 \\ 0 & 0 \\ -4.3737 & -4.3737 \\ -2.3193 & 2.3193 \end{bmatrix} \begin{bmatrix} F_1 \\ F_2 \end{bmatrix}$$

is derived from equations 3.50, 3.51, 3.52 and 3.53

$$\begin{bmatrix} x_1 \\ x_2 \end{bmatrix} = \begin{bmatrix} -1.19029e+00 & -6.08354e-01 \\ -1.19029e+00 & -6.08354e-01 \end{bmatrix} \text{a}$$

Equation 3.50

$$M = \begin{bmatrix} 2.72146e-01 & 0 \\ 0 & 2.62297e-01 \end{bmatrix}$$

Equation 3.51

$$K = \begin{bmatrix} 6.05762e+06 & 0 \\ 0 & 4.4363e+07 \end{bmatrix}$$

Equation 3.52

$$P = \begin{bmatrix} -1.19029e+00 & -1.19029e+00 \\ -6.08354e-01 & 6.08354e-01 \end{bmatrix} \begin{bmatrix} F_1 \\ F_2 \end{bmatrix}$$

Equation 3.53

APPENDIX E

Fuzzy Theory

Fuzzy Theory

Fuzzy Set

Fuzzy logic is designed for situations where information is inexact and the traditional binary logic based on "true" (or "1") and "false" (or "0") are not possible. Fuzzy logic is a form of logic in which variables can have degrees of truth or falsehood. Fuzzy logic starts with the concept of a fuzzy set. Fuzzy set consists of elements with only a partial degree of membership.

A fuzzy set F in a universe of discourse U is characterised by a membership function μ which takes values in the interval [0,1] namely, μ_F: $U \rightarrow [0,1]$.

Membership Function (MF)

A membership function (MF) is a curve that defines how to map every point in the input to a membership value or degree of membership between 0 and 1. The input is referred to as the universe of discourse. Figure 1 shows some typical membership functions (Passino and Yurkovich 1998). The typical membership functions may include triangular membership function, trapezoidal membership function, a simple Gaussian membership function, a two-sided composite of two different Gaussian curves, generalised bell shape membership function, sigmoidal membership functions, a singleton membership function, etc (A Zadeh 1995).

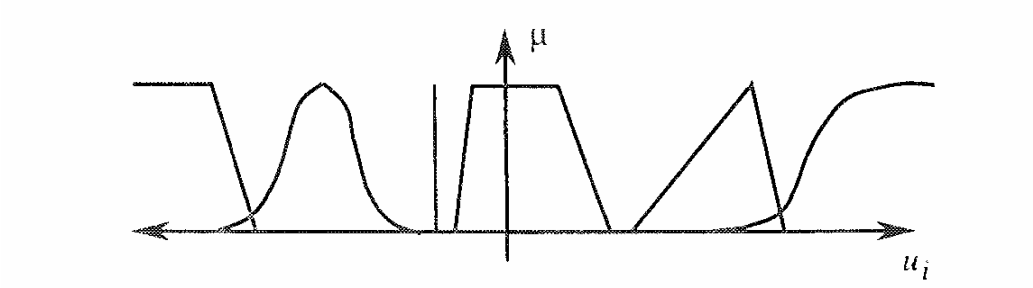

Figure1 Some typical membership functions
Source : (Passino and Yurkovich 1998; Mukaidono 2001)

The triangular membership function is commonly used due to its simplicity. Because of the smoothness and concise notation of the Gaussian membership function, it is also often used for specifying fuzzy sets. The mathematical descriptions of the triangular and Gaussian membership functions are provided in Tables 1 and 2 (Reznik 1997; Passino and Yurkovich 1998).

Additional concepts related to membership functions and fuzzy sets such as *support of a fuzzy set, α-cut, height of a fuzzy set or membership function, normal fuzzy sets, convex fuzzy sets, extension principle* can be found in (Reznik 1997; Passino and Yurkovich 1998).

	Triangular Membership Function
Left	$\mu^L(u) = \begin{cases} 1 & if \quad u \le c^L \\ \max\left\{0, 1 + \frac{c^L - u}{0.5\omega^L}\right\} & otherwise \end{cases}$
Centres	$\mu^C(u) = \begin{cases} \max\left\{0, 1 + \frac{u - c}{0.5\omega}\right\} & if \quad u \le c \\ \max\left\{0, 1 + \frac{c - u}{0.5\omega}\right\} & otherwise \end{cases}$
Right	$\mu^R(u) = \begin{cases} \max\left\{0, 1 + \frac{u - c^R}{0.5\omega^R}\right\} & if \quad u \le c^R \\ 1 & otherwise \end{cases}$

Table 1 Mathematical characterisation of triangular membership function
Source: (Reznik 1997; Passino and Yurkovich 1998)

	Gaussian Membership Function
Left	$\mu^L(u) = \begin{cases} 1 & if \quad u \le c^L \\ \exp\left(-\frac{1}{2}\left(\frac{u-c^L}{\sigma^L}\right)^2\right) & otherwise \end{cases}$
Centres	$\mu(u) = \exp\left(-\frac{1}{2}\left(\frac{u-c}{\sigma}\right)^2\right)$
Right	$\mu^R(u) = \begin{cases} \exp\left(-\frac{1}{2}\left(\frac{u-c^R}{\sigma^R}\right)^2\right) & if \quad u \le c^R \\ 1 & otherwise \end{cases}$

Table 2 Mathematical characterisation of Gaussian membership function
Source: (Reznik 1997; Passino and Yurkovich 1998)

Linguistic Variables and Hedges

A linguistic variable is a variable with its values represented by either using words or sentences of a natural language or by using numerical expression. Figure 2 illustrates the definition of the linguistic variable (Reznik 1997).

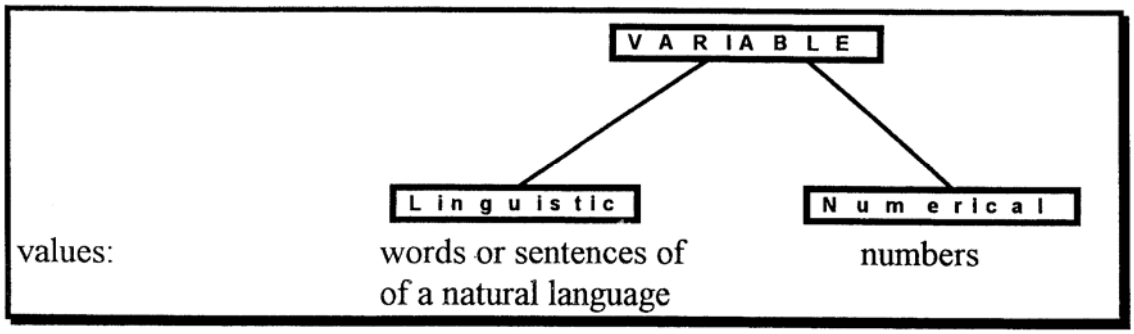

Figure 2 Linguistic variable
Source : (Reznik 1997; Mukaidono 2001)

In general, a linguistic variable is a composite term. It normally consists of primary terms and hedges. A primary term is just a name or a label of a fuzzy set. For example, 'slow', medium' and 'fast' are the primary terms of the linguistic variables that can be used to describe the variable speed (see Figure 3). Hedges represent words and

expression of the natural language and a vocabulary of the natural language. Typical hedges are ‘very’, ‘most’, ‘rather’, ‘slightly’, ‘more or less’, etc. Some widely used hedges and their meanings are shown in Table 3 (Reznik 1997; Mukaidono 2001).

Hedge	Meaning
About, around, near, roughly	Approximate a scalar
Above, more than	Restrict a fuzzy region
Almost, definitely, positively	Contrast intensification
Below, less than	Restrict a fuzzy region
Vicinity of	Approximate broadly
Generally, usually	Contrast diffusion
Neighbouring, close to	Approximately narrowly
Not	Negation or complement
Quite, rather, somewhat	Dilute a fuzzy region
Very, extremely	Intensify a fuzzy region

Table 3 Some widely used hedges
Source: (Reznik 1997; Mukaidono 2001)

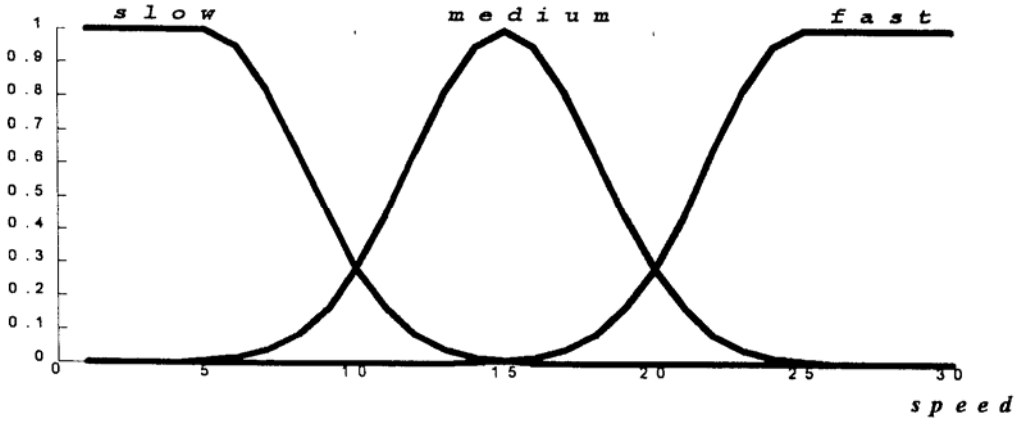

Figure 3 Membership functions for linguistic values
Source: (Reznik 1997; Passino and Yurkovich 1998)

Figure 4 shows the application of different hedges to describe 'medium' speed.

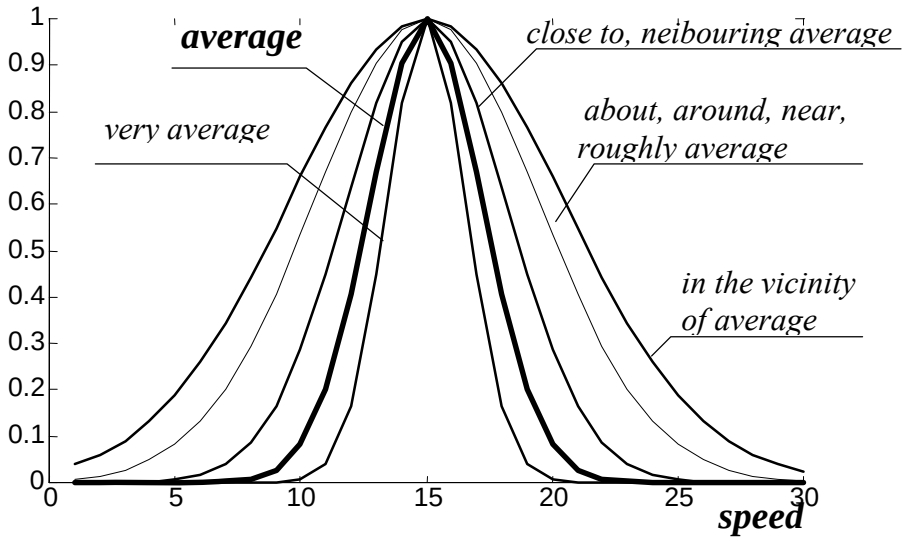

Figure 4 Application of different hedges
Source: (Reznik 1997; Mukaidono 2001)

Operations on Fuzzy sets

Fuzzy Complement:

The complement of a fuzzy set *A* has a membership function which is pointwise defined for all $u \in U$ by:

$$\mu_A(u) = 1 - \mu_A(u).$$

This corresponds to the logic NOT operation.

Fuzzy Intersection:

The intersection of two fuzzy sets $C = A \cap B$ has the membership function:

$$\mu_{A \cap B}(u) = \mu_A(u) \; t \; \mu_B(u) \leq Min(\mu_A(u), \mu_B(u))$$

where ***t*** is a triangular norm (or measure) defined as follows:

The ***t*** norm or triangular norm is a two place function from [0,1] * [0,1] to [0,1], i.e. ***t***: [0,1] * [0,1] $\rightarrow$ [0,1] which is non-decreasing in each element $x \; t \; w \leq y \; t \; z$ if $x \leq y$,

w ≤ z. It is commutative, associative and satisfies boundary conditions x ***t*** 0 = 0, and x ***t*** 1 = x; for any x,y,z,w ∈ [0,1].

Figure 5 displays two different ways for calculating t-norm operations. One method uses *minimum* operation and the other method uses *product* operation.

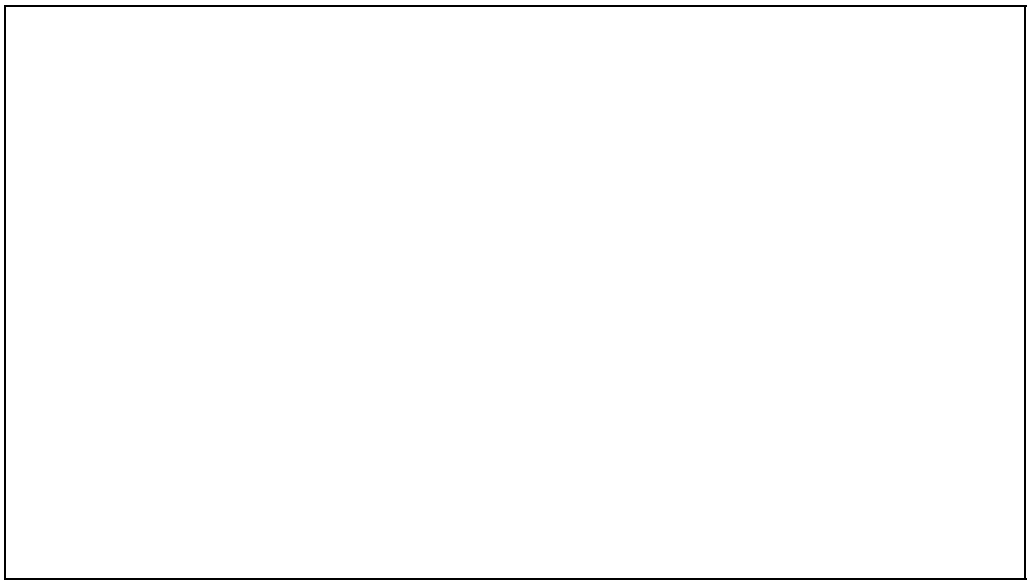

Figure 5 Two different ways (minimum and product) for calculating t-norm operations
Source: (Reznik 1997; Passino and Yurkovich 1998)

Fuzzy Union

The union (or disjunction) of two fuzzy sets $\boldsymbol{C = A \cup B}$ has the membership function:

$$\mu_{A \cup B}(u) = \mu_A(u) \; s \; \mu_B(u) \geq Max(\mu_A(u), \mu_B(u))$$

where ***s*** is a triangular co-norm (or measure, or ***s*** -norm) defined as follows:

The ***s*** norm or triangular co-norm is a two place function from [0,1] * [0,1] to [0,1], i.e. ***s***: [0,1] * [0,1] → [0,1] which is non-decreasing in each element, commutative, associative and satisfies boundary conditions x ***s*** 0 = x, and x ***s*** 1 = 1; for all x ∈ [0,1].

Some classes of fuzzy set unions and intersections are shown in Table 4.

SOME CLASSES OF FUZZY SET UNIONS AND INTERSECTIONS

Reference	Fuzzy Unions	Fuzzy Intersections	Range of Parameter
	Max (a,b)	**Min (a,b)**	
	a + b - ab	**ab**	
Schweizer & Sklar [1961]	$1 - \max[0, (1 - a)^{-p} + (1 + b)^{-p} - 1)]^{1/p}$	$\max(0, a^{-p} + b^{-p} - 1)^{-1/p}$	$p \in (-\infty, \infty)$
Hamacher [1978]	$(a + b - (2 - g)\,ab)/(1 - (1 - g)ab)$	$ab/(g + (1-g)(a + b - ab))$	$g \in (0, \infty)$
Frank [1979]	$1 - \log_s [1 + (s^{1-a} - 1)(s^{1-b} - 1)/(s - 1)]$	$\log_s [1 + (s^a - 1)(s^b - 1)/(s - 1)]$	$s \in (0, \infty)$
Yager [1980]	$\min[1, (a^w + b^w)^{1/w}]$	$1 - \min[1, (1-a)^w + (1-b)^w)^{1/w}]$	$w \in (0, \infty)$
Dubois & Prade [1980]	$\dfrac{a + b - ab - \min(a, b, 1 - \alpha)}{\max(1-a, 1-b, \alpha)}$	$ab/\max(a, b, \alpha)$	$\alpha \in (0,1)$
Dombi [1982]	$\dfrac{1}{1 + [(1/a - 1)^{-\lambda} + (1/b - 1)^{-\lambda}]^{-1/\lambda}}$	$\dfrac{1}{1 + [(1/a - 1)^{\lambda} + (1/b - 1)^{\lambda}]^{1/\lambda}}$	$\lambda \in (0, \infty)$

Table 4 Some classes of fuzzy set unions and intersections

Source: (Reznik 1997; Passino and Yurkovich 1998)

The Rule Base

Most of the fuzzy logic applications involve fuzzy rules construction and processing. Fuzzy rules are used to describe qualitative dependencies between two or more variables in linguistic terms. Fuzzy rules processing or reasoning provides a mechanism for using fuzzy rules to compute the response to a given fuzzy input. The *If-Then* rule statements are used to formulate the conditional statements that represent fuzzy logic. The general form of the linguistic rules is:

If premise **Then** consequent

The premises are sometimes called antecedents, they are associated with the fuzzy inputs and are put on the left-hand-side of the rules, while the consequents which are sometimes called different names such as conclusions or actions are associated with the fuzzy outputs and are put on the right-hand-side of the rules (Reznik 1997; Passino and Yurkovich 1998). For example one of the rules developed for the fuzzy logic controller for the magnetic bearing system can be represented as:

If error is negative big **and** change-in-error is negative big **Then** force is negative big.

Some important properties for a set of rules are (Reznik 1997; Passino and Yurkovich 1998):

- Completeness

  A set of if-then rules is complete if any combination of input values results in an appropriate output value.

- Consistency

  A set of *if-then* rules is inconsistent if there are two rules with the same rules-antecedent but different rule-consequent.

- Continuity

  A set of if-then rules is continuous if it does not have neighbouring rules with output fuzzy sets that have empty intersections.

Fuzzy Cartesian Product

The intersection and union described previously are both defined for fuzzy sets that lie on the same universe of discourse. The fuzzy Cartesian product is used to quantify operations on many universes of discourse. If $A_1, \ldots, A_n$ are fuzzy sets in the universes of discourse $U_1, \ldots, U_n$ then the Cartesian product of $A_1, \ldots, A_n$ is a fuzzy set in the product space $U_1 * \ldots * U_n$ with the membership function:

$$\mu_{A1*\ldots*An}(u_1,\ldots,u_n) = \mu_{A1}(u_1) \; t \; \mu_{A2}(u_2) \; t \ldots t \; \mu_{An}(u_n)$$

The ***t*** norm used in the Cartesian product represents the "ands" used in the rule antecedent as each of the terms in an antecedent comes from a different universe of discourse (Reznik 1997; Passino and Yurkovich 1998).

Fuzzy Quantification of Rules: Fuzzy Implications

Fuzzy implication is used to quantify the linguistic elements in the antecedent and the consequent of the linguistic If-Then rule with fuzzy sets.

Fuzzification

Fuzzification is the process of converting numeric inputs into fuzzy sets. These fuzzy sets are used to quantify the information in the rule base. The inference mechanism operates on the fuzzy sets in the rule base to produce fuzzy sets.

The Inference Mechanism

The inference mechanism is used to produce fuzzy sets representing the conclusions that it reaches using the current inputs and the rule base. The inference mechanism has two basic tasks. The first task is called *matching* and the second is called *inference*. In the first task, the extent to which a rule is relevant to the current situation as characterised by the inputs is determined. The antecedents of all the rules are compared to the controller inputs in order to determine which rules apply to the current situation. The "matching" process involves determining the certainty that each rule applies, and recommending certain rules to be applied to the current situation. Matching involves two basic steps. The first step of the matching combines the fuzzy sets from fuzzification with the fuzzy sets used in each of the terms in the antecedents of the rule. The second step of matching determines which rules are on. Membership values represent the certainty of an antecedent of a rule is determined in that particular step. In the *inference* step, conclusions are drawn from the current inputs and the information in the rule-base. There are two standard alternatives in this step. One method uses the *implied fuzzy sets*. The *implied fuzzy set* specifies the certainty level that the output should be a specific crisp output with the output universe of discourse, taking into consideration one rule at a time. Another inference method computes the *overall implied fuzzy set* considering all the rules in the rule base at the same time (A Zadeh 1995; Passino and Yurkovich 1998).

Defuzzification

The defuzzification process converts the fuzzy set quantifications of the conclusions obtained in the inference step to a numeric value that can be applied to the plant.

There are many defuzzification methods. Each method produces a single output based on either the implied fuzzy sets or the overall implied fuzzy set.

Drawing on (A Zadeh 1995; Reznik 1997), some of the defuzzification methods are listed below:

- Centre of Area / Gravity (CoA)
- Centre average
- Centre of Largest Area (CLA)
- First of Maxima (FoM) /Last of Maxima
- Middle of Maxima (MoM)
- Mean of maxima
- Height of defuzzification (HM)

Comparison of different defuzzification procedures uses the following four characteristics:

- Continuity

A small change in an input of a fuzzy controller should not result in a large change in the output.

- Disambiguity

A deffuzzification method should work in any situation. The centre of largest area method does not allow a choice when there are two equal areas.

- Plausibility

A procedure produces a defuzzified output that lies approximately in the middle of the support of the resulting membership function and has a high degree of membership.

- Computational Complexity

This is important in practical applications. It depends on the shape of the output membership function and the max-min composition or the scaled composition.

Table 5 compares a few different defuzzification methods using the above characteristic descriptions.

	CoA	MoM	FoM	HM	CLA
Continuity	Yes	No	No	Yes	No
Disambiguity	Yes	Yes	Yes	Yes	No
Plausibility	Yes	No*	No	Yes	Yes
Computational Complexity	Bad	Good	Good	Good	Bad

Table 5 Comparison of deffuzzification methods
Source: (Reznik 1997; Passino and Yurkovich 1998)

CoA= Centre of Area

MoM=Middle of Maxima

FoM=First of Maxima

HM=Height and Mean of maxima

CLA=Centre of Largest Area

No*=only in the case of scaled inference

The fuzzy system described above is either called a standard fuzzy system or referred to as the Mamdani method. Alternatively, another method of fuzzy processing is defined as a functional fuzzy system which is referred to as the Sugeno method. In the Sugeno method, the antecedent part of the rule is similar to that of the Mamdani method. However, the consequent parts of the rules are different. The consequent part uses a mathematical function of the input variables instead of a linguistic term with an associate membership function (Passino and Yurkovich 1998).

Table 6 shows some similarities and differences between these two methods.

	Mamdani	**Takagi-Sugeno**
Similarity	The antecedent parts of the rules are the same.	
Difference	The consequent parts are fuzzy sets.	The consequent parts are singletons (single spikes) or mathematical functions of them.
Advantages	It is very understandable by human experts. It is simpler to formulate rules. This method was proposed earlier and commonly used.	It is more effective computationally. It is more convenient in mathematical and system analysis. It guarantees continuity of the output surface.

Table 6 Comparison of Mamdani and Takagi-Sugeno Methods

Sources: (Reznik 1997; Passino and Yurkovich 1998; Mukaidono 2001)

Figure 6 shows an example illustrating the fuzzy processing described in this section using the Mamdani and Sugeno methods (Reznik 1997).

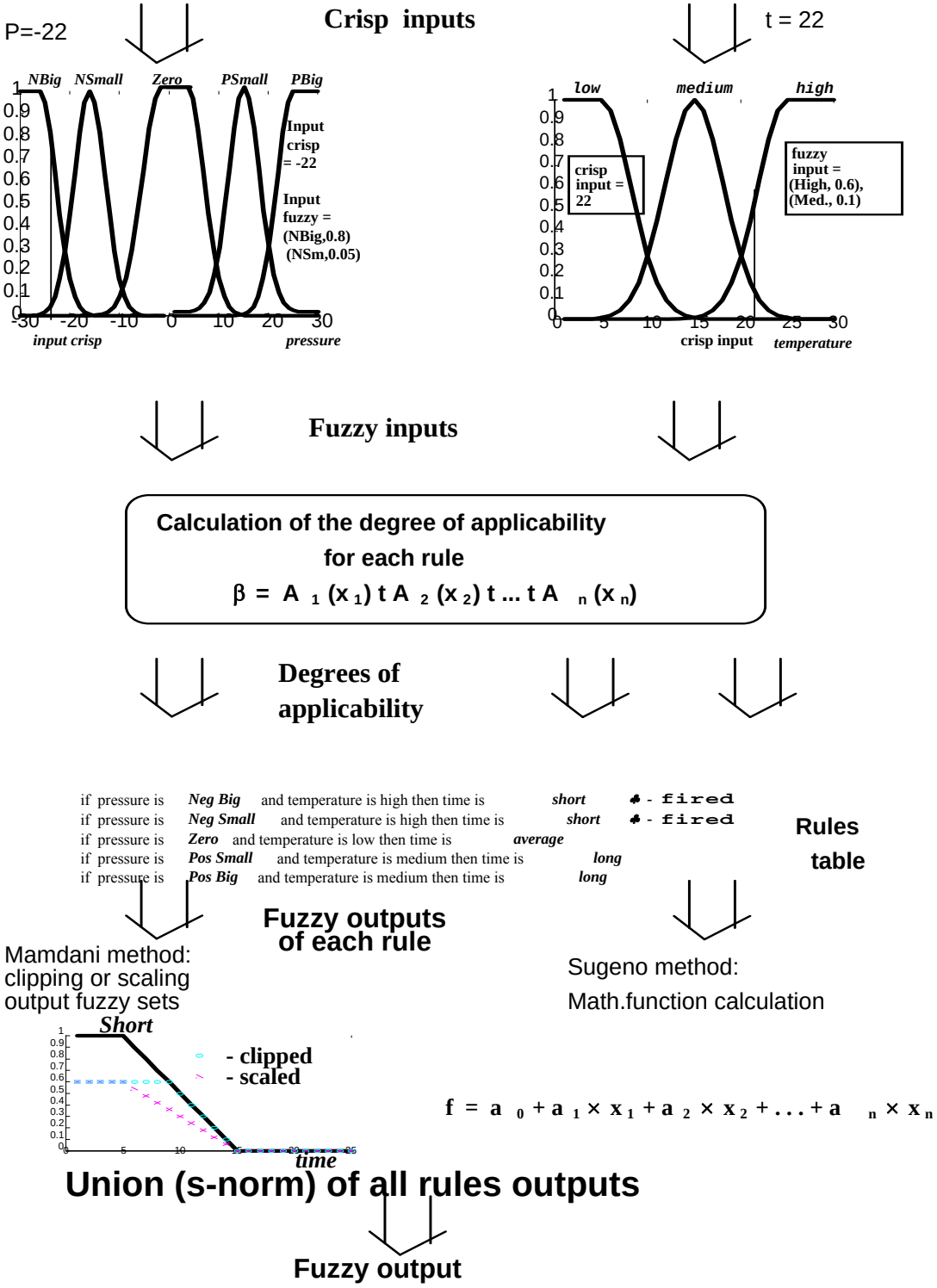

Figure 6 An example of fuzzy processing using Mamdani and Takagi-Sugeno methods

Source: (Reznik 1997; Passino and Yurkovich 1998)